University of Tennessee, Knoxville
Trace: Tennessee Research and Creative Exchange

Doctoral Dissertations | Graduate School

5-2010

Development of Nanomechanical Sensors for Environmental Contaminate Screening Using Protein Functionalized Microcantilevers

Kasey L. Hill
University of Tennessee - Knoxville, khill9@utk.edu

Recommended Citation
Hill, Kasey L., "Development of Nanomechanical Sensors for Environmental Contaminate Screening Using Protein Functionalized Microcantilevers. " PhD diss., University of Tennessee, 2010.
http://trace.tennessee.edu/utk_graddiss/700

This Dissertation is brought to you for free and open access by the Graduate School at Trace: Tennessee Research and Creative Exchange. It has been accepted for inclusion in Doctoral Dissertations by an authorized administrator of Trace: Tennessee Research and Creative Exchange. For more information, please contact trace@utk.edu.

To the Graduate Council:

I am submitting herewith a dissertation written by Kasey L. Hill entitled "Development of Nanomechanical Sensors for Environmental Contaminate Screening Using Protein Functionalized Microcantilevers." I have examined the final electronic copy of this dissertation for form and content and recommend that it be accepted in partial fulfillment of the requirements for the degree of Doctor of Philosophy, with a major in Chemistry.

Michael J. Sepaniak, Major Professor

We have read this dissertation and recommend its acceptance:

Michael Best, Panos Datskos, Frank Vogt

Accepted for the Council:
Dixie L. Thompson

Vice Provost and Dean of the Graduate School

(Original signatures are on file with official student records.)

To the Graduate Council:

I am submitting herewith a dissertation written by Kasey L. Hill entitled "Development of Nanomechanical Sensors for Environmental Contaminate Screening Using Protein Functionalized Microcantilevers." I have examined the final electronic copy of this dissertation for form and content and recommend that it be accepted in partial fulfillment of the requirements for the degree of Doctor of Philosophy, with a major in Chemistry.

Michael J. Sepaniak, Major Professor

We have read this dissertation
and recommend its acceptance:

Michael D. Best

Panos G. Datskos

Frank Vogt

Accepted for the Council:

Carolyn R. Hodges
Vice Provost and Dean of the Graduate School

(Original signatures are on file with official student records.)

Development of Nanomechanical Sensors for Environmental Contaminate Screening Using Protein Functionalized Microcantilevers

A Dissertation
Presented for the
Doctor of Philosophy Degree
The University of Tennessee, Knoxville

Kasey L. Hill
May 2010

Acknowledgements

First, I would like to thank Dr. Sepaniak for all your help. I have learned so much from you. I would like to thank the members of the Sepaniak group for all their help with my research and making my days something to look forward to. I would like to thank previous members of the group: Maggie Connatser for all your guidance and training, Pampa Dutta for teaching me about the world of microcantilevers, Jenny Oran for being first a great friend and second a secretary, Amber Wellman for all the great times and explaining antibodies to me a million times, Nahla Abu Hatab for all her support, and Pete Chapman for being a good friend and always lending a helping hand. I would also like to thank the all the current members and in particular: Sabrina Wells for always listening, Lisa Taylor for all her help, Deepak Bhandari for always listening to me complain, Zhou Long for his willingness to help me and others, and Matt Walworth for so many hilarious stories and help with my antibody figure. I would like to thank Royce Dansby-Sparks for his endless knowledge and help. I appreciate all of Melanie Eldridge's help in deciphering biology terminology and Gary Wynn's help in all my electronic problems. I want to extend my thanks to all the support staff in the stock room for all their help. I would also like to thank my committee members: Dr. Best, Dr. Datskos, and Dr. Vogt. Thank you for taking the time to serve on my committee.

I want to extend my sincere appreciation and love to my family because without them I would have never made it this far.

Abstract

The development of real time, label-free biosensors based on ligand-induced nanomechanical responses of microcantilevers (MCs) allows for sensitive and selective detection. High sensitivity is afforded by the MCs small dimensions. Immobilizing biomolecular recognition phases imparts selectivity from bioaffinity interactions. Biological sensors on a MC platform utilize various proteins, such as antibodies and nuclear receptors, which can be used to detect and screen for potential environmental contaminants.

The interaction between contaminants and immobilized receptors induces an apparent surface stress that leads to static bending of the MC, which is monitored by an optical beam bending technique. Biofunctionalized MCs can provide high sensitivity and selectivity on a relatively inexpensive platform that requires small amounts of analyte. The goal of this research is to develop and optimize MCs as biosensors to detect low concentrations of contaminants.

Initially, the research utilized specific receptors and antibodies to detect and screen for contaminants that are deemed endocrine disrupting chemicals (EDCs). Immobilizing estrogen receptors and specific antibodies on the MC surface may provide information on the ever expanding list of EDCs, along with fundamental endocrine studies.

Then, the MC surface was morphologically and chemically optimized. This optimization included the thickness and metal ratio of the dealloyed surface. The concentration, reaction time, and pH of chemical immobilization reagents, which include aminoethanethiol and glutaraldehyde, were optimized by using an anti-body test system. Antibody and protein functionalization conditions, which are incubation time and

concentration, were optimized using the anti-immunoglobulin G (anti-IgG) receptor: IgG and an anti-biotin:biotin test systems. The optimized immobilization conditions were applied to the detection of thyroid disrupting chemicals (TDCs) using MCs functionalized with the transport protein thyroxine-binding globulin.

The final project involved developing a nanomechanical transducer to study xenobiotic and EDC interactions with the bioreceptor PXR's ligand binding domain (LBD). The combination of immobilized LBD PXR with a nanostructured microcantilever (MC) platform allows for the study of ligand interaction with the receptor's binding domain. PXR shows real-time, reversible responses when exposed to specific pharmaceutical, EDC, and xenobiotic ligands. Three binding interactions that involve EDCs are tested, which include phthalic acid, nonylphenol, and bisphenol A, with PXR.

Table of Contents

Chapter 1 Introduction to Microcantilevers as Biosensors 1
1.1 Microcantilevers (MCs) 1
1.1.1 Microcantilever Background 1
1.1.2 Comparative Sensors 3
1.1.3 MC Measurement Modes 3
1.1.4 Static Mode Instrumentation 6
1.2 Molecular Recognition Phases 11
1.3 Biosensor Overview 12
1.3.1 Biosensor Capabilities 12
1.3.2 Types of Biosensors 13
1.4 Protein and Antibody Significance 15
1.5 Immobilization of Bioreceptors on the MC Surface 19
1.5.1 Nanostructured MC Surface 19
1.5.2 Chemical Immobilization 21
1.6 Ligands and Analytes 22
1.7 Estrogen Receptors and Thyroid Proteins 25
1.7.1 Estrogen Receptors 25
1.7.2 Endocrine Disrupting Chemicals (EDCs) 27
1.7.3 Thyroid Transport Proteins 29
1.7.4 Thyroid Disrupting Chemicals (TDCs) 30
1.8 Pregnane X Receptor (PXR) 30
1.8.1 Nuclear Receptors 30
1.8.2 PXR Significance 31
1.8.3 PXR and Pharmaceuticals 32
Chapter 2 Development of a Nanomechanical Biosensor for Analysis of Endocrine Disrupting Chemicals 34
2.1 Introduction 34
2.2 Experimental 37
2.3 Results and Discussion 41
2.3 Conclusions 54
Chapter 3 Morphological and Chemical Optimization of Microcantilever Surfaces for Thyroid System Biosensing and Beyond 56
3.1 Introduction 56
3.2 Experimental 59
3.3 Results and Discussion 63
Chapter 4 Microcantilever-based Nanomechanical Studies of the Orphan Nuclear Receptor PXR 79
4.1 Introduction 79
4.2 Experimental 82
4.3 Results and Discussion 86
Chapter 5 Summary 97
References 101

Appendix: Development of a Nanomechanical Biosensor for Analysis of Endocrine Disrupting Chemicals 108
Experimental 109
Results and Discussion 110
Response characteristics of nanostructured MCs 110
Random and Oriented functionalization of antibody and antigen 112
Vita 116

List of Figures

Figure **Page**

Fig. 1 The static bending of the MC 7

Fig. 2 MC static bending mode setup 8

Fig. 3 Beam bending optical readout method 9

Fig. 4 Basic IgG antibody structure 16

Fig. 5 Depositing dealloyed 20

Fig. 6 Protein chemical immobilization 23

Fig. 7 Common EDC structures 28

Fig. 8 (A) Micrograph of silicon cantilevers with schematic depiction of optical detection system and surface immobilized receptor proteins. (B) Photograph of delrin flow cell. .40

Fig. 9 (A) Comparison of nanomechanical responses of ER-β functionalized MC on exposure to $1x10^{-7}$ M and $1x10^{-9}$ M of several different potential EDCs in PBS illustrating selectivity. (B) Comparison of ER-β to BSA (blank) functionalized MC on exposure to $1x10^{-7}$ M of 17-β-ES in PBS. 44

Fig. 10 (A) Comparison of nanomechanical responses of ER-α and ER-β functionalized MCs on exposure to $1x10^{-9}$ M of 2-OH-estrone, 17-α-ES, and 17−β-ES in PBS. (B) Response of ER-β functionalized MC to $1x10^{-9}$ M of 17−β-ES; (a) absence and (b) presence of $1x10^{-8}$ M of $CdCl_2$. 46

Fig. 11 Nanomechanical responses of an anti-17-β-ES antibody (Ab) functionalized MC to $1x10^{-8}$ M of 17-β-ES in comparison no responses to non-specific analytes 17-α-ES and BSA at higher concentration of $1x10^{-7}$ M. 49

Fig. 12 Concentration based nanomechanical responses of ER-β protein and anti-17-β-ES Ab functionalized MC to different concentrations of 17−β-ES. 51

Fig. 13 Nanomechanical responses of ER-β functionalized MC on exposure to $1x10^{-10}$ M 17-β-ES for three replicate injections demonstrating reproducibility in nanomechanical responses where the inset shows the response and CV for three replicate measurements of this EDC using both the receptor protein and the antibody functionalized MCs. 53

Fig. 14 Comparison of responses of anti-hIgG Ab functionalized DA MCs with different thicknesses of the DA layers on exposure to 0.05 mg/mL of hIgG. 65

Fig. 15 Nanomechanical responses of anti-hIgG Ab functionalized 150 nm DA MCs on exposure to 0.05mg/mL hIgG in PBS. The concentration and time of incubation with AET solution were varied. 67

Fig. 16 Comparison of responses of anti-hIgG Ab functionalized 150 nm DA MCs on exposure to 0.05 mg/mL hIgG in PBS at different conditions of GA functionalization. The concentration, pH and time of incubation with GA solution were varied. 69

Fig. 17 Comparison of responses of anti-hIgG and anti-biotin functionalized 150 nm DA MCs on exposure to 0.05 mg/mL hIgG in PBS and 0.05 mg/mL biotin D in PBS. The concentration of protein and incubation time were varied. 72

Fig. 18 Schematic of 0.5 mg/mL hIgG (Ag) immobilized in random (no protein A attached) and oriented (0.5 mg/mL protein A) manner and 0.5 mg/mL anti-hIgG (Ab) immobilized (functionalized) in random (no protein A attached) and oriented (0.5 mg/mL protein A) manner on 150 nm DA MCs. 74

Fig. 19 (A) Comparison of responses of TBG functionalized DA MCs on exposure to $1x10^{-6}$ M solutions of four different potential TDCs in 10 mM pH 8.5 PBS. (B)

Concentration-based nanomechanical responses of TBG protein functionalized MC to different concentrations of T4.....76

Fig. 20 Comparison of nanomechanical responses of PXR functionalized MC on exposure to $1x10^{-6}$ M of Rifampicin, PCN, and 3-MC in PBS.....88

Fig. 21 Comparison of nanomechanical responses of PXR and ovalbumin functionalized MCs exposed to $1x10^{-6}$ M Rifampicin, PCN, and 3-MC in PBS. 90

Fig. 22 Comparison of response magnitudes in 8.5 min of PXR functionalized MC on exposure to $1x10^{-6}$ M analytes in PBS, which include three EDCs. 91

Fig. 23 (A) Concentration-based nanomechanical responses of PXR functionalized MC to different concentrations of rifampicin in PBS over the range $1x10^{-10}$ to $1x10^{-6}$ M. (B) Responses to rifampicin at 6.7 min for PXR are plotted over a concentration range from $1x10^{-10}$ M to $1x10^{-6}$ M, respectively. 93

Fig. 24 (A) Comparison of 6-HIS tagged PXR LBD (AZ) and GST tagged PXR LBD (Invitrogen) on exposure to $1x10^{-6}$ M Rifampicin in PBS. (B) Schematic depiction of 6-HIS tagged PXR and GST tagged PXR immobilized on DA MC surface. 95

Fig. Appendix 1 Comparison of bending signals of anti human IgG antibody functionalized nanostructured (dealloyed) MC to similarly functionalized smooth gold MC. 111

Fig. Appendix 2 Response of anti human IgG antibody functionalized nanostructured (dealloyed) MC with different thicknesses of the dealloyed surfaces on exposure to 0.05 mg/mL of human IgG in 10 mM pH 7 PBS. 113

Abbreviations and Symbols

Ab: antibody

AET: 2-aminoethanethiol hydrochloride

AFM: atomic force microscopy

Ag: antigen

ALB: serum albumin

ATP: 4-aminothiophenol

Bis A: bisphenol A

BSA: bovine serum albumin

CYP3A4: cytochrome P4503A4

Δm: mass changes

DES: diethylstilbestrol

EDC: endocrine disrupting chemical

ELISA: enzyme-linked immunosorbent assay

EPA: Environmental Protection Agency

ER-α: estrogen receptor alpha

ER-β: estrogen receptor beta

f: resonance frequency

GA: glutaraldehyde

IgG: immunoglobulin G

kD: kiloDalton

LBD: ligand binding domain

LOD: limit of detection

LPCVD: low pressure chemical vapor deposition

m^*: effective MC mass

MAbs: monoclonal antibodies

m_b: beam mass

MCAs: Microcantilever arrays

MCs: microcantilevers

MEMS: microelectromechanical systems

MRP: molecular recognition phase

PAbs: polyclonal antibodies

PAR: pregnane activated receptor

PBS: phosphate buffered saline

PCB: polychlorinated hydroxybiphenyl

PECVD: plasma-enhanced chemical vapor deposition

p,p'-DDE: dichlorodiphenyldichloroethylene

PSD: position sensitive detector

PVD: physical vapor deposition

PXR: pregnane X receptor

QCM: quartz crystal microbalance

RIE: reactive ion etch

RNA: ribonucleic acid

SAM: self assembled monolayer

SAW: surface acoustic wave transducers

SXR: steroid and xenobiotic receptor

T4: L-thyroxine

TBG: thyroxine-binding globulin

TDC: thyroid disrupting chemical

TTR: transthyretin

VCSELs: vertical cavity surface emitting lasers

Chapter 1 Introduction to Microcantilevers as Biosensors

1.1 Microcantilevers (MCs)

1.1.1 Microcantilever Background

Microcantilever (MC) popularity grows as chemical and biological sensors as advances are made in microfabrication. Atomic force microscopy (AFM) cantilever probes paved the way for the production and use of MCs as sensors. AFM cantilever probes can vary in response characteristics with environmental changes. Humidity, pressure, temperature, and acoustic noise can all contribute to changes on cantilever probes in AFM (1). In AFM, a flexible cantilever with a tip is scanned in a raster pattern over a surface where the force between the tip and the surface causes deflection of the cantilever. This deflection is measured and the topography of the surface can be mapped (2). The need for micromachined AFM cantilevers pushed forward advances in microfabrication technology.

In 1994, researchers began to take advantage of AFM cantilevers and utilize them as sensors (3,4). This ushered in MCs, AFM cantilevers without the tip, as a new physical and/or chemical sensor with excellent sensitivity. MCs are simple mechanical devices that can be bulk fabricated and are typically 0.2-1 μm thick, 20-100 μm wide, and 100-500 μm long. MC chips can be fabricated using routine photolithographic patterning and a combination of bulk and surface micromachining (5). Bulk micromachining removes a large portion of the substrate. It is often utilized when fabricating suspended structures. Surface micromachining keeps much of the original

substrate intact and is used as the base for devices created through deposition and etching processes. Single crystal silicon is the preferred material for MC fabrication. Usually, MC fabrication consists of deposition, patterning, and etching steps. These steps define the MC thickness, lateral size, and surrounding lever area. MC fabrication commonly begins with the deposition of a sacrificial layer on a prepatterned substrate. Then, a silicon nitride or a polysilicon structural layer is deposited using low pressure chemical vapor deposition (LPCVD) or plasma-enhanced chemical vapor deposition (PECVD) on the sacrificial layer. Cantilevers shapes can be patterned by photolithography on the silicon nitride film followed by reactive ion etching (RIE). The silicon substrate is then etched away leaving free-standing cantilevers (6). The promise of MCs as sensors not only lies in it's small size, but also it's relatively low cost, disposable platform, easy integration or coupling with other methodologies (separations, spectroscopy), generally quick response time, and array capabilities. MCs are one part of microelectromechanical systems (MEMS), which involve transduction of mechanical energy in sensors. MEMS sensors rely on mechanical movements and deformations of their micromachined parts, which can include single-clamped suspended beams (cantilevers). MEMS sensors as micromechanical transducers can be affected by physical, chemical, or biological stimuli that can induce changes, which can be measured electronically, optically, or by other means. MCs can detect changes in surface stress, small mechanical forces, charges, temperature, and IR photons (6).

1.1.2 Comparative Sensors

Comparing MCs to traditional sensors, like quartz crystal microbalance (QCM) and surface acoustic wave (SAW) transducers, demonstrates their excellent sensitivity (5). QCMs are mass sensitive sensors that utilize the change in frequency of the quartz crystal resonator when material is deposited on the surface (7). SAWs are also mass sensors that use alternating voltage on two interdigital transducers. This creates a surface wave on the piezoelectric substrate such that the amount of material deposited between the transducers can be measured due to the change in the surface wave velocity and therefore frequency (8). QCM sensors are limited when placed in viscous liquids, whereas SAW sensors are constrained when placed in any liquid. These limitations are both related to frequency dampening. Compared to QCM and SAW, MCs have much better sensitivity to minute quantities of adsorbates (5).

1.1.3 MC Measurement Modes

MC sensing can be measured in two modes: dynamic and static. Each mode has it's own advantages and should be chosen depending on the medium it will be used in and what response mechanism is involved. Resonant or dynamic mode can use oscillation dampening to measure mass changes on the MC surface (6). Measuring the change in resonance frequency may indicate analyte binding to a molecular recognition phase (MRP) on the MC surface. Resonance frequency, f, of an oscillating cantilever can be expressed as equation 1 (9)

$$f = 1/(2\pi) \times \sqrt{(K / m*)} \qquad (1)$$

where K is the MC spring constant, m^* is the effective MC mass. Effective MC mass is related to the beam or lever mass, m_b, through equation 2 (9)

$$m^* = nm_b \qquad (2)$$

where n is the geometric parameter. Resonance frequency changes, from f_0 to f_1, due to mass changes, Δm, can be expressed through equation 3 (5)

$$1/f_1^2 - 1/f_0^2 = \Delta m/(4\pi^2 K) \qquad (3)$$

where K is the MC spring constant. Dynamic or resonant mode has low sensitivity, which has been used to detect bacteria and single cell virus particles (10, 11). Resonant mode of MCs consists of three mechanisms, adsorbate-induced mass-loading, chemical changes of cantilever stiffness, and dampening by the viscous medium (6). A disadvantage of dynamic mode is the dampening that can occur in liquid media, which may reduce sensitivity (9). Dynamic mode is still used in liquid or aqueous media depending on the mechanism being studied. Dareing, et al. have demonstrated that the frequency shift due to dampening is small compared to the frequency shift induced by changes in effective mass (12).

Static mode measures the deflection of the MC tip or simply the bending of the MC. Cantilever deflections may be caused by either external forces on the surface or stresses generated on or in the lever (6). One must establish asymmetry on the MC by creating two sides to the lever, an active and passive side, to measure the deflection or bending due to analyte binding. The active side is functionalized with a MRP that has some degree of affinity for the analyte, whereas the passive side does not have affinity for the analyte molecule. There are various models to consider on how different coatings

provide chemical responses on MC sensors working in static bending mode. When interactions between the MC and its environment are purely surface confined, an example being chemisorption of straight-chain thiol molecules on a gold-coated cantilever, the spontaneous adsorption processes are driven by an excess of interfacial free energy. This is typically accompanied by a reduction of interfacial stress. The surfaces usually expand as a result of adsorptive processes. This type of surface stress change is defined as compressive, referring to the possibility that the surface may return to its original compressed state. When a MC is modified with an analyte-permeable coating that is much thicker than a monolayer, the interactions of the analyte molecules with the bulk of the responsive phase are taken into account. A predominant mechanism of cantilever deflection in this case is described as analyte-induced swelling of the coating. Such swelling processes can be quantified by evaluating molecular forces acting in the coating and between the coating and the analyte species. In general, dispersion, electrostatic, steric, osmotic, and salvation forces acting within the coating can be altered by absorbed analytes (13). The changes of these forces within the coating can cause stress changes which are imparted on the cantilever causing deflection. When nanostructured interfaces and coatings are used, analyte-induced deflections of cantilevers combine mechanisms of bulk, surface, and intersurface interactions. A combination of these mechanisms facilitates efficient conversion of the energy of receptor-analyte interactions into mechanical energy of cantilever bending (5). Regardless of the active side MRP surface stress method, the static bending or tip deflection, z_{max}, of the MC varies depending on the preferential binding of analyte molecules to the active, functionalized side of the lever and is governed by Stoney's equation (14)

$$z_{\max} = 3l^2(1-\nu)\Delta\sigma / Et^2 \qquad (4)$$

where ν and E are, respectively, the Poisson ratio and Young's modulus for the cantilever, t is the MC thickness, l is the MC effective length, and Δσ is the analyte-induced differential surface stress ($\Delta\sigma_{\text{active side}} - \Delta\sigma_{\text{passive side}}$) (Fig. 1). This deflection measuring method is commonly used in AFM. The MC static bending mode functions well in both liquid and gas media, since it has no dependence on the resonant frequency of the MC. In the research presented herein, the static bending mode is used with MCs that are nanostructured for increased sensitivity and functionalized with MRP for selectivity. Static mode is preferred since all measurements were made in liquid phase which leads to significant damping of MC oscillations and hampers dynamic mode monitoring. Furthermore, mass changes are many times miniscule due to the use of very large immobilized bioreceptors with very small ligands.

1.1.4 Static Mode Instrumentation

Typically, a MC static bending mode or tip deflection instrumental setup consists of seven main parts: a diode laser, lenses, a neutral density filter, a position sensitive detector (PSD), a microfluidic cell, the MC chip and an output device or recorder, as seen in Fig. 2. We have extensively studied our single laser static bending mode setup using MCs that are 400 μm in length, 100 μm in width, and 1 μm thick and determined that a 1 mV response corresponds to approximately 1 nm of MC bending. The microfluidic cell is designed to flow background and analyte solutions past the MCs. A well designed flow cell requires low volumes and has a thorough, quick washout of analyte solution and can be utilized with a pump or gravity flow. Static bending mode can utilize the optical

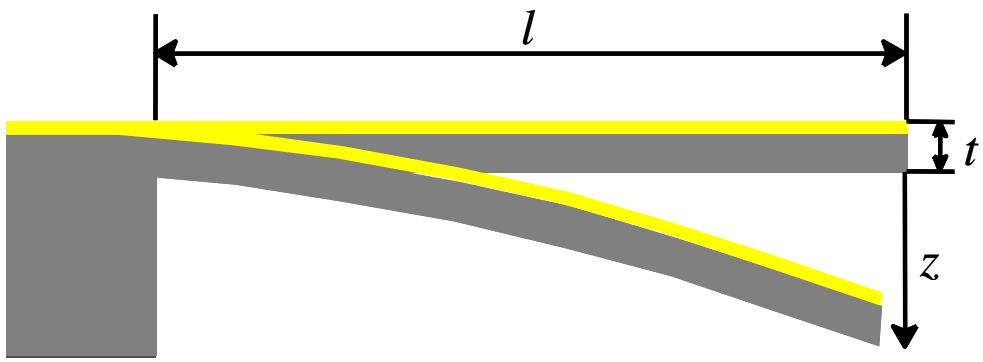

Fig. 1. The static bending of the MC. Tip deflection or bending is illustrated.

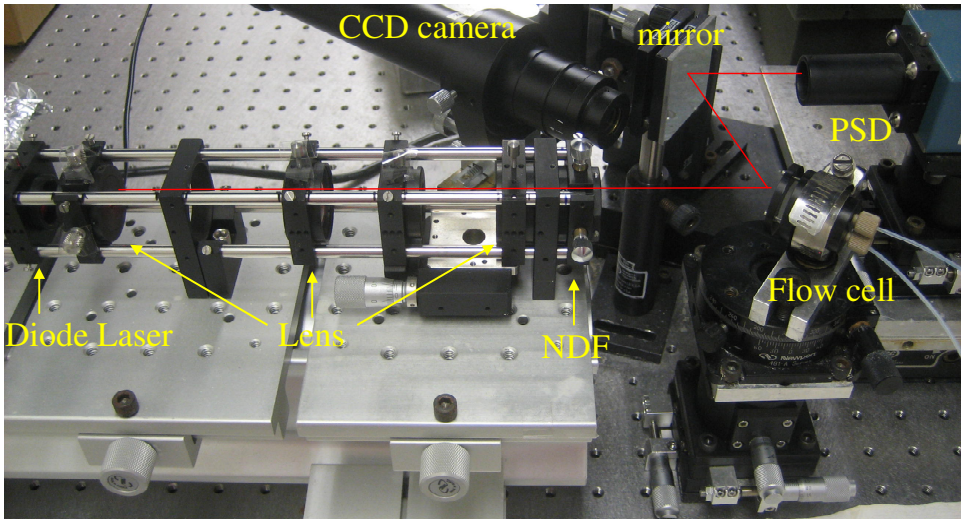

Fig. 2. MC static bending mode setup: The diode laser passes through a series of lenses and a neutral density filter then onto the MC tip in the flow cell. The reflected laser light goes onto a mirror and into a PSD.

beam deflection technique. This optical readout method focuses a laser beam on the tip of the lever which is reflected onto a PSD as illustrated in Fig. 3. The PSD quantifies the MC deflection or bending. The optical lever readout scheme is commonly used in AFM instruments. The absence of electrical connections to the cantilever, linear response, simplicity, and reliability are important advantages of the optical lever method. This method is used in the vast majority of the work on cantilever sensors, so its limitations are well recognized. For instance, changes in the optical properties of the medium surrounding the cantilever may interfere with the output signal. This interference can be avoided with the proper orientation of MCs relative to the optical components of the setup. Refractive index changes can affect the output signal as well. Using differential pairs or arrays of cantilevers can suppress the refractive index changes as well as other interfering factors (6). Microcantilever arrays (MCAs), which differentially functionalize individual levers on the same chip with various MRPs, use slightly different optical system instrumentation (19). A beam of laser light from an array of vertical cavity surface emitting lasers (VCSELs) is focused onto the tip of each MC, and the reflected beam is captured and monitored by a single PSD. A single lens is used to focus the VCSELs so that the beam from each VCSEL is focused onto a single corresponding cantilever (12 VCSELs onto 12 cantilevers). The deflection of the cantilever results in a corresponding motion of the reflected beam as monitored by the PSD. The entire cycle of measuring and recording all 12 MCs can take less than one second. This allows all MRPs on different levers to be monitored within a second.

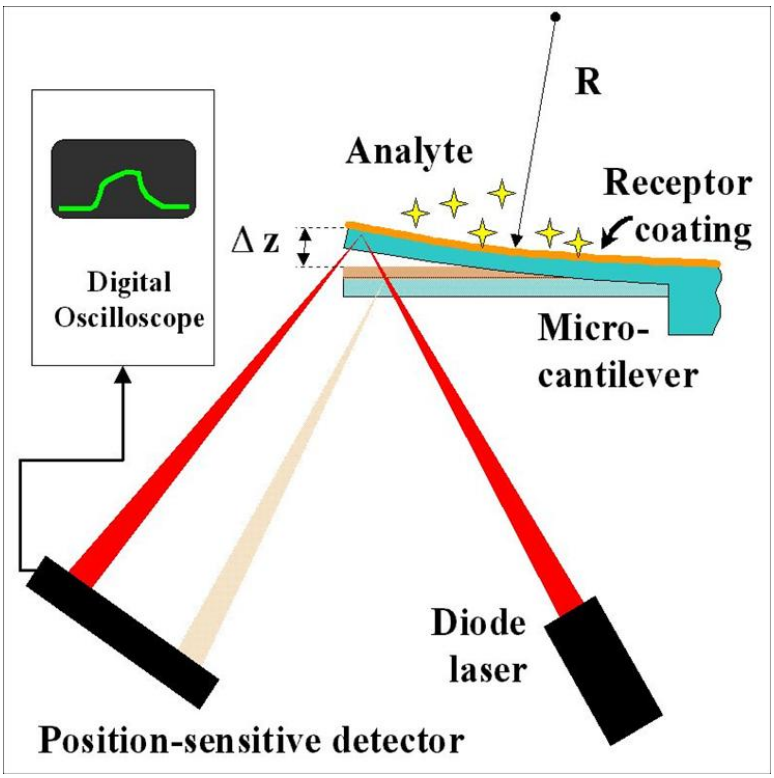

Fig. 3. Beam bending optical readout method: The PSD measures the movement of the reflected laser light when the MC bends upon analyte binding to the molecular receptor phase.

1.2 Molecular Recognition Phases

Molecular recognition phases can include a variety of compounds, including but not limited to polymers, cyclodextrins, proteins, antibodies, metals, and sol-gels (5, 6, 9, 15-18). The use of MRPs promotes selectivity that is not inherent to MCs. Spectroscopy provides a vibrational fingerprint to chemicals and compounds, where MC responses do not provide that characterization. The use of an appropriate MRP responds to an injected analyte with a unique response signature, but this does not impart the characteristic vibrational bands for analytes that is present in spectroscopy. This necessitates the need for selective MRPs. There are two methods for utilizing MRPs to impart selectivity: moderately selective MRPs for distributed selectivity and bioaffinity or high affinity MRPs. Distributed selectivity functions in an array platform (see above) providing response patterns for analytes. Chemical selectivity may be demonstrated by using a large number of moderately selective MRPs and pattern recognition algorithms to examine the unique analyte responses (19). Disadvantages of the distributed selectivity method may arise with the complicated data sets if there is not enough contrast between the response profiles or the amount of time and difficulty that surrounds creating arrays with many MRPs. Bioaffinity or high selectivity MRPs (biosensors) provide selectivity by exploiting the high affinity interaction or binding that is inherent to many biological receptors to specific analytes (15, 20, 21). Disadvantages of the bioaffinity method may include reversibility issues and the robustness of the immobilized bioreceptor.

1.3 Biosensor Overview

1.3.1 Biosensor Capabilities

Chemical sensors and biosensors are defined as *measurement devices which utilize chemical or biological reactions to detect and quantify a specific analyte or event* (22). A sensor converts physical dimension changes to an electrical component that can be processed or electrically transmitted (23). Components of a sensor include an active surface, physical transducer, and an output of the signal. The active surface contains the immobilized receptor and the interaction between the receptor and the analyte is detected by a transducer. The interaction causes a change, usually a binding event, that the transducer expresses as a signal or response, which can include changes in impedance, frequency, voltage, reflectance, or weight (22).

Chemical and biosensor development began over 90 years ago. In 1916, Nelson and Griffin first reported the immobilization of proteins on activated charcoal (24) and six years later the first glass pH electrode was developed by Hughes (25). A sensor's purpose is to provide information about the physical, chemical, and biological aspects of the environment. The demand for more information has motivated the expansion of chemical and biosensors. In general, sensing consists of two steps, which are recognition and amplification (26). The central component to any chemical sensor is selectivity or recognition with biological components being one of the most prevalent sources (27). A sensor requires some fundamental properties which include sensitivity and reversibility and for many applications a quick response time is also important. Sensors should also possess some general requirements to be useful to the user. These may include good

reproducibility, dynamic range, stability, and a long life or problem free sensor replacement (23). "Good" is a relative term that often depends on the type of sensor and the analyte in question. Often it is the physical transducer that imposes limits on the figures of merit that can be achieved by a specific sensor (6).

1.3.2 Types of Biosensors

Biosensors are a constantly expanding field that is needed for many applications, which can include medical and pharmaceutical applications, as well as environmental research. There is a broad spectrum of biosensor types depending on the specific function or purpose. This can include many popular and well established biological sensing methodologies. Enantioselective sensors are used to determine the presence of enantiomers of chiral compounds (21, 28-30). This is of crucial importance to pharmaceutical companies since many of the drugs in development are chiral. Enantiomers of a chiral pharmaceutical agent can have very different effects on the body, some of which can be detrimental.

Enzyme-linked immunosorbent assay (ELISA) is a biochemical technique used to detect binding of biochemicals or bioreagents which can be quantified by determining the amount of color change or generated color that occurs upon ligand binding. This requires an enzyme to be chemically attached to a labeled antibody before ligand binding. This is a very common assay for determining binding events for a specific receptor. It can be used for various applications, which include detecting environmental contaminants with bioreceptors, screening for drugs of abuse, and detection of hormones in various

chemicals (31-35). ELISA can be used to determine equilibrium disassociation constant for receptor and ligand interactions (36). Drawbacks of ELISA based methods can include long, multistep assay preparation with labels and multi-step enzyme-ligand-receptor interactions, which may not provide real-time results and may not measure trace concentrations of ligands.

Radioligand binding assays are another well established method for detecting binding events for biological entities (37-41). In this type of assay the antibody is labeled with a radioactive isotope. This radioactively labeled antibody or protein is commonly termed a tracer. Equilibrium constants for binding of analyte and receptor can be determined with radioligand binding assays. In one assay method, the radioligand is displaced from the receptor by a higher affinity analyte and the radioactive decay is measured. This method is considered to be very sensitive utilizing high-affinity interactions and may require small concentrations of ligand or analyte (36). Radioligand binding assays require labeling with radioisotopes, which require special protocols for handing and stringent disposal regulation (22).

Competitive binding immunoassays usually require antigens (see below) to compete for a limited number of antibody binding sites. A determined concentration of labeled antigen competes with unlabeled antigens for the antibody binding sites. In this method, competitive assays are reagent limited. The signal produced by the labeled antigen is inversely proportional to the concentration of the unlabeled antigen. There are many experimentally specific variations to this assay. Competitive assays can be used for various applications, which include detecting small molecules, exogenous chemicals, and

contaminants binding with bioreceptors (41-45). A good review of biosensing methods can be found in *The Immunoassay Handbook* edited by David Wild (46).

1.4 Protein and Antibody Significance

Proteins and antibodies (Abs) can be considered ideal receptors in producing sensor selectivity. This is in part due to the stereospecificity of their ligand binding site which can be specific to certain antigens and haptens (26). A protein is defined as *a macromolecule composed of one or more polypeptide chains, each with a characteristic sequence of amino acids linked by peptide bonds* (47). Proteins encompass a large group of biological compounds, which include antibodies and enzymes and may be the most adaptable of all biomolecules.

Antibodies are key elements for studying many biological processes. An antibody is a serum protein that is part of the immunoglobulin family. Their molecular weights range from 140 kD to 970 kD (26). It is produced by humans and animals in an immune response to foreign substances or antigens (Ags). The immunoglobulin family is made up of many subclasses which include immunoglobulin A (IgA), IgD, IgE, IgG, and IgM. The class that is responsible for the majority of antibody immune response is IgG. IgG is one of the most commonly used antibodies in immunoassay and biosensor development due to it's widespread availability and large research literature base. IgG is a Y-shaped biomolecule comprised of four polypeptide chains, two identical heavy chains and two identical light chains that are connected by disulfide linkages (Fig. 4). The molecular weight of IgG is approximately 150,000 Daltons, where each heavy chain is 50,000 Da and each light chain is 25,000 Da. Antibodies can be digested to three portions or

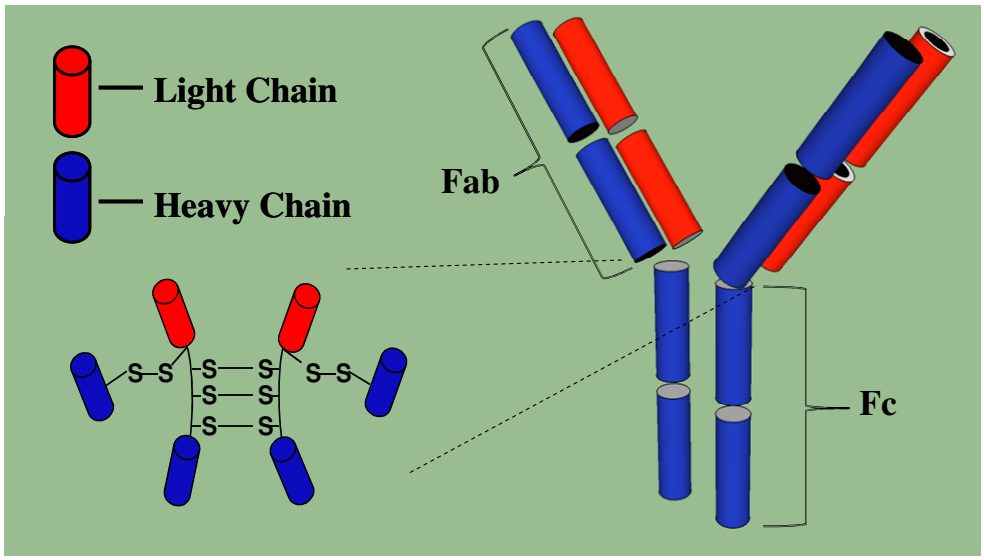

Fig. 4. Basic IgG antibody structure.

fragments, which are Fab, $F(ab')_2$ and Fc. The Fab and $F(ab')_2$ fragments are responsible for antigen binding. Antibody production is universal and relatively inexpensive. An immune response to almost any antigen can illicit antibodies, regardless of the shape or chemical makeup of the antigen. Antigen size is the only limitation that has to be overcome. Antigens with a molecular weight of less than 2000 Da is defined as a hapten and does not normally produce an immune response on it's own. To induce an immune response and generate antibodies the hapten is linked to a larger carrier, which can be a high molecular weight polymeric carrier (26). The generated antibodies provide specificity to the hapten and the carrier molecule, so the hapten specific antibodies need to be filtered out of the carrier specific antibodies. This allows antibodies to be produced to substances, like haptens, that are normally unrecognizable to the immune system. Once the antibody response occurs the IgG can be isolated from the whole serum. Later in this chapter and in Chapter 4, I discuss a class of proteins that do respond to and eliminate small foreign molecules.

Antibodies can be either monoclonal or polyclonal. Both types are useful depending on their application. Polyclonal antibodies (PAbs) result from an injected antigen stimulating production of many antibodies, recognizing several epitopes on the antigen. Due to the heterogeneity of the PAbs, the effect of small changes in an antigen epitope is less likely to be significant. PAbs are produced by a large number of B cells in response to the antigen and are therefore a combination of antibodies with unique specificities. Kohler and Milstein first developed monoclonal antibodies (MAbs) by fusing single B-cells with immortal myeloma cells producing a hybridoma that can yield multiple copies of the exact same antibody (48). MAbs are homogenous and consistent

making them useful when evaluating conformational changes or protein interactions. This homogeneity makes them more susceptible to small changes in epitope structure. MAbs are constantly generated once a hybridoma is successfully created and are generated at a higher concentration and purity for a given antibody than PAbs. MAb generation is expensive, time consuming, and requires considerable technical skill compared to PAbs. Generally, PAbs are more robust, can be generated by a variety of species, and are more tolerant of small conformational changes in the antigen. MAbs are excellent primary antibodies due to their specificity and yield reproducible results because of their homogeneity.

Antibody specificity for a target antigen is better than most MRPs. Antibodies should be able to bind to a small concentration of analyte even in the presence of other similar compounds. The average binding of PAbs and an antigen is termed avidity and the binding equilibrium is called affinity. For MAbs avidity and affinity are the same due to their inherent homogeneity. The most common interactions in immunochemical reactions between an antibody and an antigen are coulombic and van der Waals interactions. Typical affinity constants or equilibrium constant values for IgG are 10^5-10^9 L/mol. At equilibrium, the antibody –antigen binding can be shown as

$$Ab + Ag \underset{k_r}{\overset{k_f}{\Leftrightarrow}} [Ab.Ag] \qquad (5)$$

where the binding constant K is defined by the forward and reverse rate constants. The forward rate constant range is 10^7-10^9 L mol^{-1} s^{-1} and the reverse rate constant range is 10^{-2}-10^4 s^{-1} (26).

1.5 Immobilization of Bioreceptors on the MC Surface

1.5.1 Nanostructured MC Surface

The key approach to enhance the sensitivity of chemi-mechanical responses is to employ nanostructured gold MC surfaces. The active side of the MC is nanostructured to increase surface area, which in turn inherently increases sensitivity. Nanostructured responsive phases increase the amount of binding sites per cantilever, but still allow analyte accessibility (6). To create the nanostructured surface in our approach, gold and silver are co-deposited in a physical vapor deposition (PVD) chamber. The alloy is chemically altered to remove the silver via oxidation using $HAuCl_4$, leaving a granular, porous dealloyed gold surface. This process is illustrated in Fig. 5. The PVD instrument operates under high vacuum ($1x10^{-3}$-$1x10^{-9}$ Torr) using a mechanical pump and a diffusion pump. The mechanical pump initially pumps down the system from atmospheric pressure to ~$1x10^{-3}$ Torr, and then the diffusion pump pulls the system down to ~$1x10^{-6}$ Torr. The metals to be deposited (chromium, gold, and silver) reside in small tungsten boats that are held in electrodes. The metals are electrically heated causing evaporation and metal deposition onto the MC surface. The rate of deposition and metal thickness on the MC are measured by a QCM, respectively. The PVD creates an alloy surface that is then chemically altered to dealloyed, as described above. In some cases, utilizing dealloyed MCs provides a two order of magnitude response enhancement (16, 49). The dealloyed surface enhances the transduction of molecular recognition interactions into MC responses, increases MC surface area, increases sensitivity, and provides for film stability for thicker MRPs (17). When an unfunctionalized

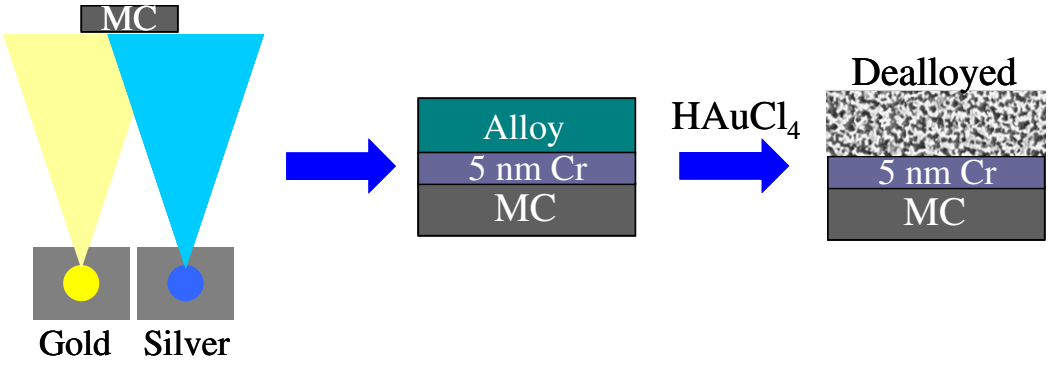

Fig. 5. Depositing dealloyed: Co-deposition of gold and silver in the physical vapor deposition chamber creates a composite layer (alloy). The alloy chip is then placed in $HAuCl_4$ solution to remove the silver, leaving a nanostructured gold surface (dealloyed).

nanostructured MC surface is exposed to Abs, the resulting response from physical adsorption is large, reversible, and tensile, whereas the smooth gold MC surface response is much smaller, reversible, and compressive (expansive) (21). The advantages to using dealloyed MCs include much improved sensitivity and coating stability.

1.5.2 Chemical Immobilization

Chemically linking the bioreceptor to the MC surface provides for stability when flowing aqueous buffer background and when injecting analyte solutions. Concern arises that the active bioreceptor binding sites will be distorted or blocked when chemically immobilizing to the MC surface, which would not allow the analyte to interact with the receptor (see Chapter 3). Studies have shown that random chemical linkages leave an appreciable concentration of receptor sites active (15, 20, 21, 50). To chemically modify the dealloyed surface in our work, the MCs are immersed in 2-aminoethanethiol hydrochloride (AET) producing a self assembled monolayer (SAM). The use of SAMs to functionalize a solid support, like gold, has become important in the field of biotechnology, and in particular biosensor development due to the simplicity (51). In 1983, Nuzzo and Allara developed a structural understanding of thiol organization on a gold surface (52). Advancements have continued and today many useful modification agents have been used to form functioning surface coatings on solid supports.

The amino groups on the AET are derivatized with glutaraldehyde (GA), which is one of the most common crosslinkers for bio-immobilization. The GA is a linker for the bioreceptor to the AET nanostructured gold surface. Common crosslinking agents are glutaraldehyde, hexamethylene diisocyante, difluoro-dinitrobenzene, and dimethyl

suberimidate. Crosslinkers are used to polymerize a base layer and to anchor the bioreceptor molecule to the sensor surface. The anchoring is a result of intermolecular linkages between the surface and the receptor, which provides a more stable MRP on the sensor. The crosslinker and it's concentration are critical, so that it will not interfere with the bioreceptor's activity (22). GA's optimal concentration varies depending on experimental use, therefore the conditions must be determined on a case by case basis. The aldehyde in GA binds with the amine in the AET. A Schiff base reaction occurs between the carbonyl group of the GA and the lysine residues in the proteins, through the amines in the residue (53, 54). This results in the GA link between the AET and the protein (Fig. 6). GA is not thought to appreciably denature the proteins upon immobilization (55, 56). Studies have shown that the immobilization method into the MC surface does not significantly alter the ligand binding domain (LBD) of the bioreceptor (15, 20, 21, 50).

1.6 Ligands and Analytes

Analytes that are specific for protein functionalized MCs have a broad range, which can include antigens specific for antibodies, environmental contaminants, pharmaceuticals, metals, and various chemicals. Their size can range from small molecules (haptens) to large complexes, like many pharmaceutical compounds. Analytes or ligands stimulate the immobilized bioreceptor, usually by interacting with the LBD(s) of the protein or the Fab portion of antibodies. To translate this interaction to MC surface stress, which causes a measureable deflection, a conformational change of the immobilized protein maybe required. In some bioreceptors, the conformational change in

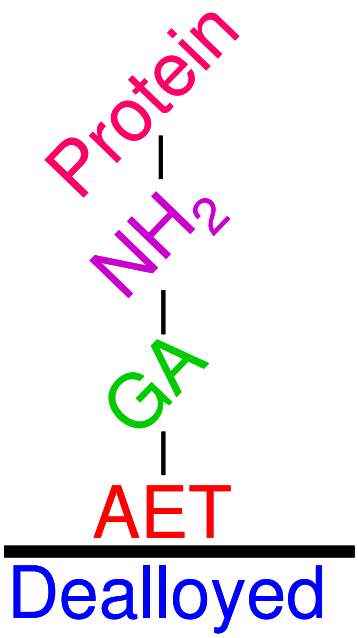

Fig. 6. Protein chemical immobilization.

the LBD upon analyte binding can cause changes in a DNA binding region of the receptor protein. This overall receptor conformational change may yield relatively large nanomechanical bending, especially if the immobilization occurs at the DNA binding site, making it a good candidate for MC sensing studies. Environmental contaminants, whether naturally occurring or synthetic, and pharmaceuticals are included as analytes or ligands for biosensors and bioassays with immobilized receptors. Contaminants can include organohalogenated hydrocarbons, polychlorinated hydroxybiphenyls (PCBs), insecticides, herbicides, plasticizers, and detergent byproducts. The human diet contains several nonsteroidal, weakly estrogenic compounds that are from plants and can act as contaminants within the body by inhibiting key system bioreceptors. These plant derived chemicals are phytoestrogens, which plants produce themselves, and mycoestrogens, which are from fungi that infect the plant. Phytoestrogens consist of three main groups: flavonoids, coumestans, and lignans. Mycoestrogens are mainly zearalenone and it's derivatives. Mycoestrogens are associated with estrogenizing syndromes in cattle that are fed fungi infected grain. Phytoestrogens and mycoestrogens have been linked to cell mitosis in breast cancer cells in vitro and compete with estrogens for their natural estrogen receptor. However, some studies show that phytoestrogen intake is linked to lower rates of prostate and breast cancer (40, 57). Phytoestrogen and mysoestrogen studies show that contaminate screening is an important and sometimes arduous task. Determining contaminates that have adverse health effects is not always an easy and straightforward task.

Hormones and pharmaceuticals are important ligands for our biosensors. This can include estrogens, steroids, antibiotics, and many other medications. Sometimes the line

can be blurred between drugs and contaminants. Medication that is widely prescribed can sometimes be considered a contaminant due to it's presence in the environment. People can ingest these pharmaceuticals/contaminants, from drinking water, etc., without their knowledge, which may alter receptors and transport proteins functions.

Some metals, like cadmium, bind to receptors and block binding by the natural ligand. Cadmium can be found in the air, water, and soil, therefore it can be inhaled or ingested. Once in the body, it may not be expelled, but can be stored in the lungs, liver, and kidneys. Cadmium has been shown to activate or bind to estrogen receptors, which could hinder it's natural activity, as presented in Chapter 2 (15, 58). Other metals, including lead, copper, and mercury, are considered contaminants that can cause adverse health effects. Therefore, some metals can be considered analytes for biosensors when studying environmental contaminates.

1.7 Estrogen Receptors and Thyroid Proteins

1.7.1 Estrogen Receptors

Estrogen receptors and thyroid proteins are both part of the endocrine system. The endocrine system includes glands throughout the body, which produce or transduce hormones, and the tissues and organs that respond to hormones. Major components include the ovaries, testes, and the pituitary, thyroid, and adrenal glands, but the effects of the endocrine system are throughout the entire body. The endocrine system processes include regulating metabolism, blood sugar levels, reproductive functions, and the brain and nervous system functions. An extremely wide range of biological processes are

influenced or controlled by the endocrine system, which include many bioreceptors like estrogen receptors and thyroid transport proteins.

Estrogen receptors, which exist in two forms, ER-α and ER-β, are part of the nuclear receptor family. They have similar affinities for most ligands, like estradiol, but can have different relative affinities for some synthetic and naturally occurring ligands. Some body tissues show a higher concentration of one subtype's ribonucleic acid (RNA). The kidney, uterus, pituitary, and epididymis contain more ER-α RNA than ER-β. ER-β is present in equal or greater quantities in the ovary and prostate. Estrogens, which are complementary hormones to estrogen receptors, have effects on the male and female reproductive systems, bone maintenance, and many other tissues throughout the body. Estrogen plays a role in many organs, including those of the cardiovascular, nervous, reproductive, and musculoskeletal systems (59). Estrogen is produced mainly in the ovaries and testes, where they are free to diffuse in and out of cells. They are retained by estrogen receptors due to their high affinity and specificity. Once estrogen- ER binding occurs the estrogen receptor undergoes a conformational change permitting the receptor to bind to chromatin within a cell's nucleus and control transcription of target genes (60). In the 1950's, pregnant women, who were deemed at risk, were given diethylstilbestrol (DES), a potent synthetic estrogen thought to prevent first trimester miscarriages, early during their gestational period. Their male offspring had increased incidence of undescended testes, urogenital tract abnormalities, and reduced semen quality compared to boys whose mothers did not take DES (61). This demonstrates one way synthetic estrogens can cause major health problems by disrupting the normal estrogen receptor

binding events and the transcription they stimulate. Many other pathways exist for exogenous compounds to cause adverse health issues that need to be studied.

1.7.2 Endocrine Disrupting Chemicals (EDCs)

Estrogen receptors can be impaired or inhibited by environmental contaminants, which can have sometimes detrimental effects on the endocrine and reproductive systems. These contaminants are called endocrine disrupting chemicals (EDCs). They comprise a wide and ever expanding range of naturally occurring and synthetic chemicals and their byproducts, which include pesticides, plasticizers, detergents, pharmaceuticals, and some biological compounds excreted by animals or plants (Fig. 7) (62, 63). EDCs like bisphenol A can leach from plastic into foods, as shown in canned foods which are lined with polycarbonate lacquers. Many workers who manufactured or sprayed large crops with insecticides have lower sperm counts, and some became impotent, due to the estrogenic activity of the insecticide (64). Humans, wildlife, and livestock are exposed to EDCs in many ways. EDCs can disrupt the endocrine system often resulting in chronic, debilitating health problems by mimicking or inhibiting the natural hormone (40, 58, 65). It is critical to identify potential EDCs so action can be taken to eliminate their effects. The Environmental Protection Agency (EPA) instituted the Endocrine Disruption Screening Program to screen and test chemicals to identify potential EDCs and assess and manage the risks of particular compounds (65). In Chapter 2, ER-α and ER-β are used to screen and detect for EDCs.

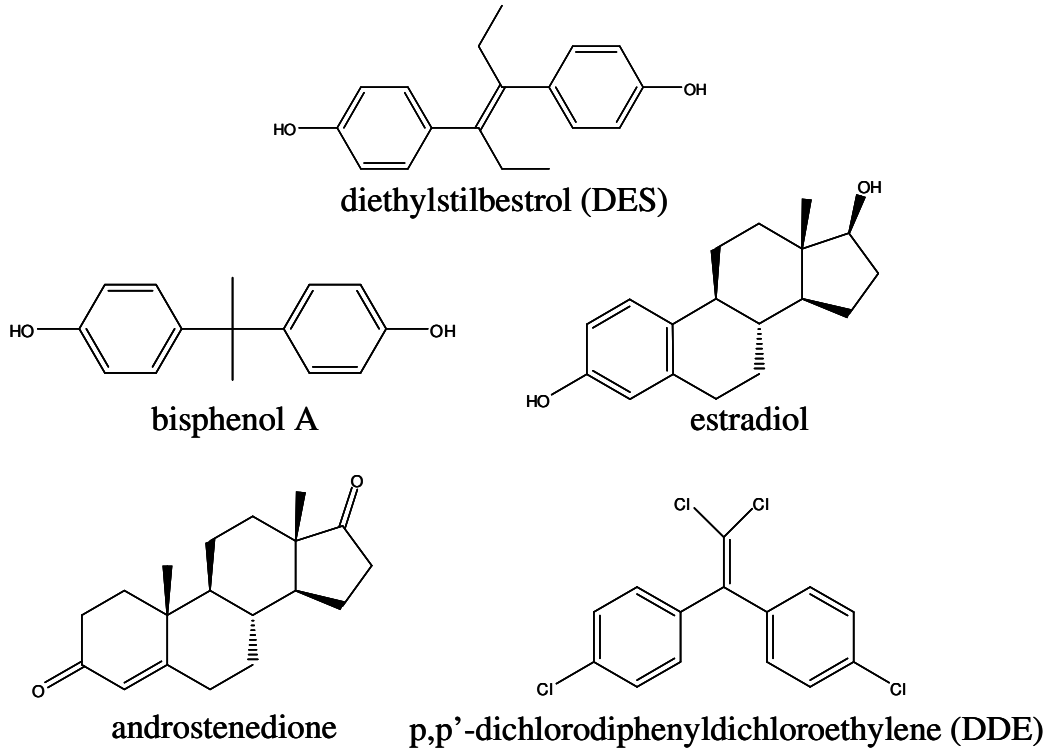

Fig. 7. Common EDC structures, including a pesticide breakdown product (DDE), a plastic component (bisphenol A), a synthetic steroid (androstenedione), and two synthetic estrogens (DES and estradiol).

1.7.3 Thyroid Transport Proteins

Thyroid proteins are another important component to the endocrine system. There are three main thyroid hormone binding proteins in the blood: thyroxine binding globulin (TBG), transthyretin (TTR), and serum albumin (ALB). These bind to and transport thyroid hormones in the blood. L-thyroxine (T4) is the main hormone of the thyroid system and a highly prescribed pharmaceutical in the United States. TBG, which is synthesized in the liver, is the main T4 transporter in human blood responsible for 75% of it's binding activity, while TTR only carries roughly 20% and ALB only 5% of T4. TBG is present in plasma at lower concentrations than other transport proteins, but carries the largest percentage of T4. This is due to TBG's high affinity to T4. TBG's affinity is 100-fold higher for T4 than the other two transport proteins (66). Although TBG has greater affinity to T4, TTR is crucial to T4 transport across the brain barrier and maternal to fetal delivery of thyroid hormones. TBG has one T4 binding site and TTR has two, each with different affinities for T4. TTR and TBG are similar in size (55 kDa and 54 kDa), but differ in their affinities for T4 and triiodothyronine (T3), which is a natural thyroid hormone in the body. T4 and T3 are two thyroid hormones, each containing multiple iodine atoms (four iodine atoms in T4 and three iodine atoms in T3), which makes them large in size and imparts important protein binding features due to the electronegativity of the iodine atoms (67). T4 and T3 appear to have an effect on nearly every organ and tissue of the body. These thyroid hormones are critical to normal growth and development and effect protein synthesis in many tissues (68). It has been suggested that hypothyroidism results in the displacement of T4 by contaminants when under

transport by TTR, therefore the study of thyroid hormone transport is an important aspect of thyroid disruption (69). TBG seems to be quantitatively more valuable than TTR for T4 transport, so Chapter 3 includes TBG screening and detection of contaminants.

1.7.4 Thyroid Disrupting Chemicals (TDCs)

Thyroid disrupting chemicals (TDCs) are a subclass of EDCs that have thyroid activity, which can include organohalogen compounds. Previous studies have demonstrated that organohalogen chemicals can have adverse affects on the thyroid gland morphology and hormonal balance in rats (70). The disruption or inhibition of the thyroid system may cause health problems and disease. They may have adverse affects on the thyroid gland, thyroid transport proteins, and/or thyroid hormone metabolism (37). Even trace concentrations of EDCs and TDCs may cause disruption of the endocrine system. A broad class of chemicals present thyroid activity, so screening for this growing list of TDCs is important. TDCs can disrupt the transport of thyroid hormones throughout the endocrine system.

1.8 Pregnane X Receptor (PXR)

1.8.1 Nuclear Receptors

Nuclear receptors are soluble, intracellular proteins that bind steroid and hormone ligands and other compounds. They bind to hormone ligands with high affinity and interact with specific DNA target elements. Nuclear receptors are responsible for regulating transcription of various genes making them crucial to many physiological processes. Lipophilic hormones, including steroids, retinoids, and thyroid hormones, are

able to move freely through cells. These hormones regulate development, cell differentiation, and organ physiology. Tracking hormone movement with radiolabeled ligands allowed the identification of binding proteins. The binding proteins were able to move from the cytoplasm to the cell nucleus. Steroids were proven to be tissue specific by the presence of high binding affinity receptors located in the tissue. Together this allowed the recognition of a steroid hormone signaling pathway. The identification of this pathway suggested that nuclear receptors when bound to hormones complexed with chromatin in the nucleus and regulated transcription. Nuclear receptors are characterized by a central DNA binding domain and the LBD located on the C-terminal half. The LBD assures specific hormone recognition and can morph the receptor into a transcriptionally active state. Nuclear receptors are part of a superfamily with hundreds of identified receptors. There are also many orphan nuclear receptors, which have no recognized specific ligand (71). Estrogen and thyroid receptors are members of the nuclear receptor superfamily.

1.8.2 PXR Significance

Pregnane X receptor (PXR) is a promiscuous, orphan nuclear hormone receptor that is activated by a wide range of exogenous compounds. It was isolated in 1998 by Bertilsson, et al., Blumberg, et al., and Kliewer et al. and called PXR, steroid and xenobiotic receptor (SXR), pregnane activated receptor (PAR), and NR1I2 (72-75). PXR is expressed mainly in the liver and intestine. Humans are exposed to a myriad of potentially toxic chemicals on a daily basis, so the body has developed a line of defense mechanisms. The main defender is the family of cytochrome P450 enzymes for

mammals, which includes cytochrome P450 monooxygenases: CYP1, CYP2, CYP3, and CYP4 (76). Cytochrome P4503A4 (CYP3A4) is a critical member of our defense system, which makes the removal of many unwanted exogenous compounds possible by metabolizing them from the body (77). PXR may be considered the first line of defense. When PXR binds with xenobiotic ligands this interaction causes transcriptional activation of CYP3A4, which may remove unwanted potentially toxic ligands (78). PXR is called a promiscuous receptor due to it's broad ligand specificity, which allows activation by a wide array of structurally diverse xenobiotics (79). This promiscuity makes it unlike most other types of hormone receptors, which are highly selective to their complementary hormone. This extremely wide ligand activation range is made possible by it's unique LBD, which has two β strands that are not present in other nuclear receptors and that allow it's expansion (80). Rifampicin, a potent PXR activator, is a macrolide antibiotic that is a commonly used treatment for tuberculosis. It is also one of the largest known ligands for PXR at 823 Da (81). Rifampicin's large size directly illustrates the structural flexibility of PXR's LBD. The flexible, hydrophobic LBD allows PXR activation by a diverse range of synthetic and naturally occurring chemicals making it an ideal candidate to serve as a xenobiotic sensor (82).

1.8.3 PXR and Pharmaceuticals

PXR could be a key nuclear receptor in pharmaceutical testing because it is activated by numerous pharmaceuticals with diverse properties, functions, and structures. PXR also controls the expression of genes that are vital to pharmaceutical and contaminate metabolism (81, 83). PXR activation mediates transcription of CYP

enzymes, including CYP3A, and many other enzymes and transporters within the body (82). CYP enzymes are considered drug metabolizing enzymes and are already involved in assays for drug development (76). Since, PXR activation allows for regulation and expression of CYP3A this interaction is critical to drug metabolism (77). Pharmaceutical metabolism and interaction is vital to monitor and prevent drug-drug interactions. Drug-drug interactions can occur when co-administered drugs alter the efficacy of one another. This usually occurs when one drug increases or decreases the metabolism of another (84, 85). Contaminants could modify drug concentrations in vivo and skew the prescribed therapeutic dose leading to fatal consequences. Drug-drug interactions can include common over-the-counter herbal and dietary supplements. Hyperforin, a compound in St. John's Wort, which is commonly used to treat depression, has been shown to be a powerful PXR activator (86). It is common practice to combine over-the-counter supplements with prescriptions, but since supplements may cause PXR activation, this could alter the efficacy of vital medications. Determining drug-drug and drug-contaminate interactions is critically important for human health and pharmaceutical development. In Chapter 4, we study PXR nanomechanical responses to exogenous chemicals, which include pharmaceuticals and EDCs.

Chapter 2 Development of a Nanomechanical Biosensor for Analysis of Endocrine Disrupting Chemicals

Chapter 2 is an adaptation of a research article *Lab on a Chip* **2007**, 7, 1184-1191. The article demonstrated that estrogen receptors and estradiol antibodies can be immobilized on the MC surface to detect potential EDCs.

2.1 Introduction

EDCs can adversely affect the health of human, domestic, and wildlife species by altering or inhibiting the function of the endocrine system (65). Due to the extremely wide range of biological processes EDCs can influence, often impairing, it is crucial to screen and detect for them. EDCs include a wide range of naturally occurring and synthetic chemicals. These chemicals and/or their byproducts include but are not limited to pesticides, plasticizers, detergents, pharmaceuticals, and biological compounds excreted by animals and plants (62, 63). Their interaction with hormone receptors, like estrogen receptors, often disrupt the normal function of the receptor causing chronic, debilitating health problems and disease (40, 58, 65). These contaminants cause undesirable effects to the endocrine system by mimicking or inhibiting a natural hormone (65). The Endocrine Disruption Screening Program of the Environmental Protection Agency (EPA) has mandated the screening and testing of chemicals to identify potential EDCs and their toxicity, then determine and manage the risk associated with the compound (65). It is crucial to identify and manage potential EDCs in their environments, so appropriate action can be taken to lessen or eliminate their effects.

The screening of potential EDC candidates and the monitoring of known ones, as well as mechanistic studies of endocrine processes, requires modern sophisticated analysis methods and innovative, integrated instrumentation. Traditionally, the endpoints used to determine these chemicals and their effects involve relatively complicated bioassays (competitive binding assays, cell growth assays, and cell- based reporter assays) that are time consuming to perform and include the use of complex biological systems (40, 58, 87). More recently, simpler, non-label sensing methods to monitor protein receptor-EDC interactions have been reported that employ surface plasmon resonance and quartz crystal microbalance techniques (88-90). Relevant to this report, biosensing applications have benefited in recent years from the attributes of modern microelectromechanical systems (BioMEMS) (91). Prominent among MEMS approaches are nanomechanical methods based on microcantilever (MC) transducers. The high sensitivity and widespread availability of inexpensive MCs have generated intense interest in their use as chemical (17, 92, 93) and biological sensors (18, 21, 50, 56, 94). Additionally, MCs can be used with on-chip circuitry and in microcantilever arrays (MCAs) for high throughput, simultaneous differential assays with a very small sensor footprint that potentially can be employed in the field, advantages not fully realized with more traditional sensors.

As discussed in Chapter 1, a MC suitable for biosensing is modified on one side with a suitable receptor phase that has some degree of affinity for the analyte. Specific interactions of the target analytes with that phase cause an apparent surface stress and nanomechanical bending of the MC. The bending may be conveniently monitored using the beam bending technique commonly used in atomic force microscopy. The static

bending (tip deflection, z_{max}) of the MC varies in selectivity and sensitivity due to preferential binding of analyte molecules on the functionalized, active MC surface and is governed by Stoney's equation (14). See equation 4 in Chapter 1.

We demonstrate that detection and screening for EDCs can be accomplished with bioreceptor functionalized MCs. These sensors provide real-time measurements of surface stress changes in the low-to-sub-nanomolar range (50). By exploiting the protein receptor-EDC interaction, as well as antibody-antigen/hapten reactions, we are able to screen for potential EDCs and target specific compounds quickly and without extensive, time-consuming labeling techniques (40, 62, 87). Immobilization of EDC receptor proteins on MCs with a non-specific orientation glutaraldehyde protocol does not appear to appreciably denature the protein or otherwise inhibit interactions with known EDCs and, moreover, allows for sufficient surface stress for sensitive detection. The sensitivity and reversibility afforded by MCs with nanostructured active surfaces, as well as the biological interaction, allows impressive limits of detection (LOD) in this work down to ~$1x10^{-11}$ M, though the thickness of the nanostructured MC surfaces are not optimized in this work (see figures in the Appendix). The EDCs studied herein include various steroids, a plastic component, a synthetic estrogen, and the heavy metal cadmium. Versatile screening of EDCs is accomplished by estrogen receptor-α (ER-α) and estrogen receptor-β (ER-β) protein receptor-based MC systems, which can respond to a variety of EDCs. Conversely, it is demonstrated that a specific estrogenic compound (17-β-estradiol) can be targeted by antibody mediated nanomechanics. To our knowledge, this is the first time estrogen responding receptors have been immobilized on a MC surface for nanomechanical-based sensing.

2.2 Experimental

Experiments were performed using commercially available silicon arrays of MCs having dimensions 400 µm length, 100 µm width, and approximately 1 µm thickness (Mikro Masch Co., Sunnyvale, CA). Chromium, gold, and silver metals deposited on the MCs were obtained from Kurt J. Lesker, Gatewest, and Alfa Aesar Co., respectively, at 99.9% purity. 2-Aminoethanethiolhydrochloride (AET), glutaraldehyde (GA), the salts employed for the preparation of buffer solutions, cadmium chloride, and all other reagents were purchased from Sigma-Aldrich Chemical Co (St. Louis, MO) or Fisher at highest available purity and used as received. The EDCs, diethylstilbestrol (DES), 17-β-estradiol (17-β-ES or beta-ES or β-ES), 17-α-estradiol (17-α-ES or alfa-ES or α-ES), bisphenol A (Bis A), androstenedione, p,p'-dichlorodiphenyldichloroethylene (p,p'-DDE) and protein bovine serum albumin (BSA) were also obtained from Sigma-Aldrich. In addition, 2-OH-estrone was obtained from Steraloids Inc. (Wilton, NH, USA). Monoclonal anti-17-β-estradiol antibody (17-β-ES Ab) (mouse generated to a BSA conjugate of the hapten) was purchased from Biogenesis, Inc. (Kingston, NH, USA). Human recombinant ER-α and ER-β were purchased from Invitrogen Corp. (Carlsbad, CA, USA). Water used to prepare solutions was obtained from a Branstead E-pure water filtration system.

The process of creating nanostructured surfaces on MCs is described in detail elsewhere (49). The cantilevers were first cleaned in a piranha bath (75% H_2SO_4, 25% H_2O_2) for 30 minutes, followed by thorough rinsing in deionized water [Caution: piranha solution reacts violently with organics]. The MCs were then placed into a physical vapor

deposition (PVD) chamber (Cooke Vacuum Products, Model CVE 301, South Norwalk, CT) to be coated on one side with the appropriate metallic films using thermal deposition. To create a nanostructured MC, a thin film (~5nm) of chromium was applied to the surface to act as an adhesion layer followed by a thin film of gold (~15nm). Next, a film consisting of gold and silver was co-deposited. Subsequently, the silver was chemically removed via oxidation from the film ("dealloying") using an aqueous solution of 5 mg/mL $HAuCl_4$ leaving a gold surface with nanosized, colloid-like features. The thickness of the dealloyed gold layer was ~50 nm in these studies.

In these studies, nanostructured MCs were chemically modified by immersion in 1 mM aqueous solution of AET (16 hours) producing a self-assembled monolayer of AET on the cantilever surface. Following thorough rinsing in deionized water, the amino groups were derivatized with the cross linker by immersing the cantilever in a 2% (w/v) solution of GA in water for 3 hours (95). The chemically treated cantilever was allowed to soak in a large volume of water for a few minutes to remove any nonspecifically bound GA on the nanostructured and silicon sides of the cantilevers. Subsequently, immobilization of both the estrogen receptor proteins (α and β) and 17-β-ES Ab was achieved in random orientation by dipping the functionalized cantilevers into 100 mg/L solutions of proteins or antibody in phosphate buffered saline (PBS, 10 mM, pH=7) for 4 hours. During functionalization with ER-α and ER-β, the MCs dipped into the protein samples were kept at 4°C to maintain the ER activity. Both estrogen receptor proteins (α and β) and antibodies were separately immobilized on the functionalized surfaces of different cantilevers from separate arrays. After washing with PBS, the functionalized microcantilevers could be stored in PBS at 4°C until it is used. Although we used an

array of MC, in this study we chemically treated all the cantilevers the same and simply recorded the response of a single randomly chosen MC within an array.

The MC deflection measurements were carried out using the optical beam-deflection technique as depicted in Fig. 8A. The apparatus included a 5 mW diode laser (Coherent Laser Corp., Auburn, CA) operating at 632 nm, a spatial filtering and focusing system, and an in-house built position sensitive optical detector. The output of the detector was displayed and recorded using a SRS 850 DSP lock-in amplifier as a multichannel digital recorder (Stanford Research Systems, Sunnyvale, CA). The signal output is recorded as volts (approximately 1 nm z_{max} per mV output). Data was collected at 1 Hz and then a moving averaging algorithm covering 180 data points was used to generate the figures presented herein. This smoothing did not alter the shape of the true response curves (92).

The cantilever system was mounted inside a ~5 µL volume flow cell made of a 3 cm diameter by 2 cm long Delrin rod that was machined with 1/16 inch diameter input and output holes that meet at 1 cm distance apart at the face of the rod. Narrow bore tubing of 1/16 inch O.D. was slid into the holes up to the rod face and secured with fittings. A semi transparent silicone gasket, which is slightly thicker than the MC chip (~500 µm versus 400 µm), was cut with a scalpel tool to form a ~250 µm wide flow channel between the input/output holes and to tightly hold the MC chip (Fig. 8B). The silicone gasket is sandwiched between the Delrin rod face and a thin quartz window. A Watec CCD camera (Edmund Industrial Optics, Barrington, NJ) was used to image the MC chip in the flow cell. The camera facilitated aligning the focused laser beam to

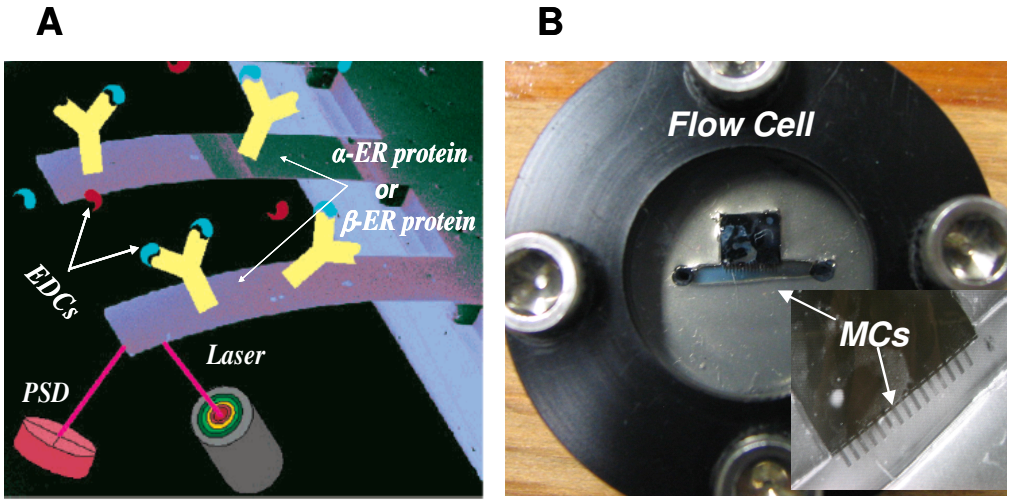

Fig. 8. (A) Micrograph of silicon cantilevers (100 mm x 400 mm x ~1 μm thick) (a linear 16 cantilever array was used in this work). Schematic depiction of the optical detection system and surface-immobilized receptor proteins and antibodies (Y symbols) are included in the figure. (B) Photograph of the delrin flow cell showing the silicone gasket that defines a 250 mm flow channel and holds the MC chip.

reflect off the cantilever tip. Analyte solutions were delivered to the flow cell via a system of vessels connected to three-way valves allowing for switching between different solutions. The gravity-driven flow was generally adjusted to 30 μL/minute by adjusting vessel height.

Most of the EDCs are sparingly soluble in water. Thus, 1×10^{-2}M stock solutions of all EDCs were prepared in pure methanol and then diluted with PBS (10 mM Phosphate Buffer + 10 mM $NaNO_3$, pH = 7.0) to make the desired concentration of each EDC [Caution: because of their potential harmful effects, care must be taken in the handling and disposing of EDC solutions]. PBS was also used as a background solution. MCs mounted in the flow cell were initially allowed to equilibrate in PBS until the signal was stable. For our purposes, tensile and compressive responses involve contraction and expansion of the active MC surface, respectively.

2.3 Results and Discussion

Our work addresses three analysis scenarios. Since hundreds to thousands of potential EDC candidates have been targeted, and the effects of these candidates may be seen in various mixed combinations, there is a pressing need for high throughput EDC screening methods. Because a large number of EDCs exert their effects through estrogen receptor (ER) proteins (97), our studies have focused on the development of MC systems using these proteins as bioreceptor phases to screen for estrogenic compounds. A second scenario involves the targeted detection of known EDCs in environmental samples such as waste treatment streams, feed stocks, etc. wherein target specific bioreceptor phases can be employed. We use cantilevers modified with anti-17-β-ES antibody to

demonstrate the potential utility of MC sensing in this situation. Finally, in comparison to existing methods, we are developing MC systems that may prove to be a quicker, simpler, and less expensive means to detect EDC actions in support of fundamental endocrinology studies.

The promise of our nanomechanical approaches will depend largely on whether adequate levels of sensitivity are reached for EDCs, since they are known to show effects at extremely low concentrations. We have achieved substantial improvements in sensitivity by nanostructuring the active surfaces of MCs by the described dealloying process. In many cases the response enhancement has surpassed the increase in surface area of the active surface (5, 17, 49). The enhancement in bioaffinity response with nanostructuring is discussed and illustrated in the Appendix (see Fig. Appendix-1 and -2).

Conformational changes of MC surface immobilized proteins after binding with analytes may give rise to relatively large cantilever responses (21, 50). Since conformational changes in the ligand binding region of ER proteins give rise to changes in the DNA binding region of the proteins, this system is a good candidate for MC nanomechanical sensing. However, there can be concern that chemical attachment to the MC surface will make binding sites inaccessible or distort the sites such that the natural affinity for ligands will be substantially altered. The results presented below provide strong evidence that at least an appreciable fraction of the immobilized bioreceptors remain active to ligand binding. It is important to note that unlike spectroscopic or simple mass responding sensors, the MC sensor requires transfer of the energy of ligand binding into surface stress. Thus, in the case of the ER proteins, immobilization at the DNA binding sites which change configuration in response to conformation changes in

the ligand binding region, may be desirable. It has been observed that proper orientation of the bioreceptor proteins on the MC surface does not always yield improvements in response (See Table Appendix -1), presumably because of the stress induction response requirement.

Fig. 9A shows the comparison of nanomechanical responses of an ER-β functionalized MC on exposure to 1×10^{-7}M solutions of six different potential EDCs in PBS, illustrating the selective interaction of DES and estradiols over the other EDCs. The relatively slow response kinetics is consistent with prior protein bioreceptor MC work (14, 15) and indicates that the small EDC molecule causes conformational changes in the ER-β (see above) which translates into a large apparent surface stress on the cantilever. The very high binding affinity of ER-β protein for DES followed by 17-β-ES and 17-α-ES have been observed by other researchers (40, 97). Also, we have observed the similar trend in the value of response magnitude for both 1×10^{-7} M and 1×10^{-9} M solutions of these three EDCs. The binding affinity for Bis A is much lower than that of ES (both α and β) and the very low binding affinity for p,p'-DDE and androstenedione are in agreement with previous studies (40, 88, 97). The inset demonstrated the response behavior of ER-β functionalized MC as a function of time for 1×10^{-7}M of DES and Bis A. An exposure time of 10 minutes produced a compressive surface stress (expansion of the active surface) for both the EDCs that reverse when the analyte solution was replaced by background buffer (PBS) solution. The relative magnitude of responses are consistent with prior reports (88-90). In our previous studies, the reversible compressive response is

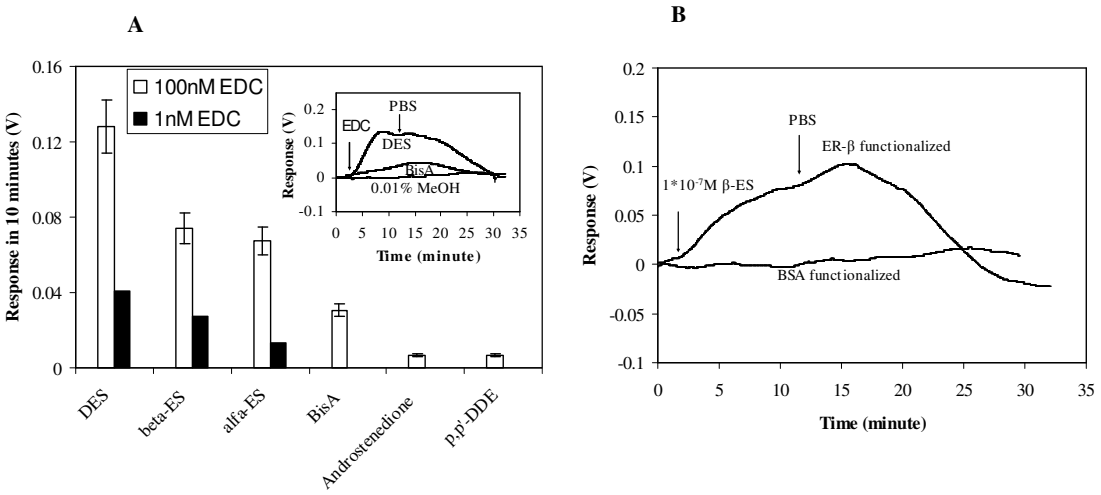

Fig. 9. (A) Comparison of nanomechanical responses of ER-β functionalized MC on exposure to $1x10^{-7}$ M and $1x10^{-9}$ M of several different potential EDCs in PBS illustrating selectivity. The error bar indicates the standard deviation (with CV = 10 %) for three replicate measurements with three different MC arrays functionalized with ER-β at different times using $1x10^{-7}$ M of different EDCs. The inset in (A) provides representative time traces of ER-β functionalized MC on exposure to $1x10^{-7}$ M of two of the EDC analytes, DES and Bis A (arrows denote points of EDC and PBS background in flow cell). (B) Comparison of ER-β to BSA (blank) functionalized MC on exposure to $1x10^{-7}$ M of 17-β -ES in PBS.

also observed for other bioreceptor functionalized dealloyed surfaces whereas similarly functionalized smooth gold MC shows an irreversible compressive response on exposure to the same concentration of analytes (21, 50) (also, see related discussion and Fig. Appendix-1).

Fig. 9B compares the response of specific protein (ER-β) functionalized MC to nonspecific protein (BSA) functionalized MC (blank) on exposure to the same concentration (1×10^{-7} M) of 17-β-ES. A large compressive response was observed due to the binding of 17-β-ES with a MC modified with ER-β protein whereas no response was observed when the same analyte was exposed to the nonbinding protein (BSA) immobilized MC. The fact that our MC system's relative response magnitudes are similar to prior works, and does not show a nonspecific blank response, is critically important and indicates the surface immobilization of the ER-β does not substantially alter its EDC ligand binding function and selectivity. However, it can not be assumed that the surface immobilized receptors will retain the same ligand binding affinity constants as observed in free form.

Studies have shown that there are a number of functional similarities between human ER-α and ER-β, especially in the DNA binding domain (98). However, there are also significant structural differences noted for human ER-α and ER-β and some of the EDCs have differential binding affinity for human ER-α and ER-β (40, 88, 97). Fig. 10A compares the nanomechanical responses of ER-α against ER-β functionalized MCs on exposure to 1×10^{-9}M of three test EDCs, 2-OH-estrone, 17-α-ES, and 17-β-ES. The results in Fig. 10A show that 17-β-ES produce comparable responses with both ER

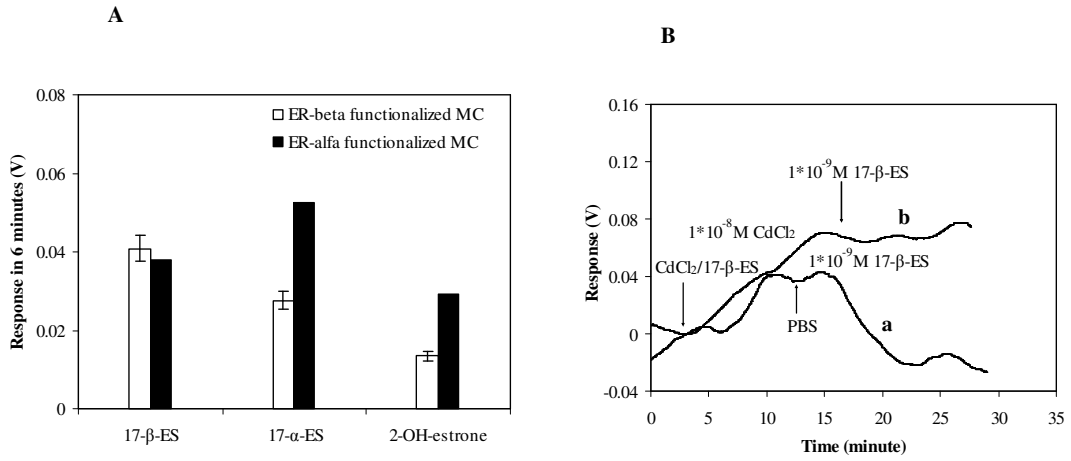

Fig. 10. (A) Comparison of nanomechanical responses of ER-α and ER-β functionalized MCs on exposure to $1x10^{-9}$ M of 2-OH-estrone, 17-α-ES, and 17–β-ES in PBS. The error bar indicates the standard deviation (with CV = 8 %) for three replicate measurements with three different MC arrays functionalized with ER-β at different times using $1x10^{-9}$ M of different EDCs. (B) Response of ER-β functionalized MC to $1x10^{-9}$ M of 17–β-ES; (a) absence and (b) presence of $1x10^{-8}$ M of $CdCl_2$.

proteins indicating that it binds with equal relative affinity to both ER subtypes, which was also observed before (40, 97). The other two EDCs, 2-OH-estrone and 17-α-ES preferentially bind with ER-α producing 2-3 fold greater responses than with ER-β. Greater binding for these EDCs with ER-α than ER-β was also noted by others in a prior report, although by a greater factor than in our work (40). The optical systems used in our prior reports on MC arrays, that were differentially coated with non-bioaffinity receptor phases and optically probed, should transfer well to arrays employing different protein receptor phases for simultaneous multi-bioaffinity measurements based on MCA nanomechanics (99).

Previous studies have shown that heavy metal cadmium activates ER-α through an interaction with the hormone binding domain of the receptor, thereby inhibiting estradiol binding to the receptor (58). Mechanistic studies of hormone agonist or antagonist actions are vital for understanding and controlling the impacts of EDCs in the environment. To demonstrate the potential of the MC nanomechanical sensor in such studies, we sought to determine whether cadmium may also block estradiol binding to ER-β. The response was recorded for a ER-β functionalized MC on exposure to 1×10^{-9}M of 17-β-ES in absence and in presence of 1×10^{-8}M of $CdCl_2$ (Fig. 10B). Initially, in absence of cadmium ion, estradiol showed appreciable compressive response which is reversed upon flushing the cell with background buffer. Subsequently, the same MC upon exposure to 1×10^{-8} M of $CdCl_2$ for 14 minutes produced a large compressive response, most likely indicating the binding of cadmium ion with ER-β protein. Martin and coworkers have shown that the interaction of cadmium with ER-α appears to involve

several amino acids present in the hormone-binding pocket of the receptor, suggesting that the metal may form a coordination complex with the hormone-binding domain (58). Also, it is known that cadmium binds to ER-α with an affinity similar to that of estradiol for the receptor. An injection of 1×10^{-9}M of 17-β-ES for 10 minutes in presence of $CdCl_2$ showed no additional compressive response (Fig. 10B), which provides evidence that the metal ion may also inhibit the binding of 17-β-ES to ER-β protein.

High levels of specificity involving molecular recognition, e.g., antibody-antigen/hapten interactions are generally considered desirable in analytical chemistry. However, inherent to this high level specificity can be a lack of versatility and reversibility. Herein, we have developed a MC based immunosensor using a monoclonal antibody for 17-β-ES for selective and sensitive detection of 17-β-ES in presence of other nonspecific analytes. 17-β-ES has no immunogenicity due to its small molecular size, but antibodies generated to a BSA conjugate are commercially available and we have functionalized dealloyed MCs using this antibody. In our prior work, glutaraldehyde-based immobilization resulted in a cantilever resonance frequency decrease of approximately 30 Hz, indicating less than a femtomole of antibody was immobilized on the functionalized surface of a single MC (21).

Fig. 11 shows the cantilever response as a function of time when exposed to 1×10^{-8}M of 17-β-ES in PBS. The specific interaction of the immobilized antibody with 17-β-ES resulted in a 60 mV compressive response (positive voltage signal), which is likely to occur in similar fashion to the endocrine receptor protein case; i.e. a combined effect of hydrogen bonding and hydrophobic interactions with the hapten cause

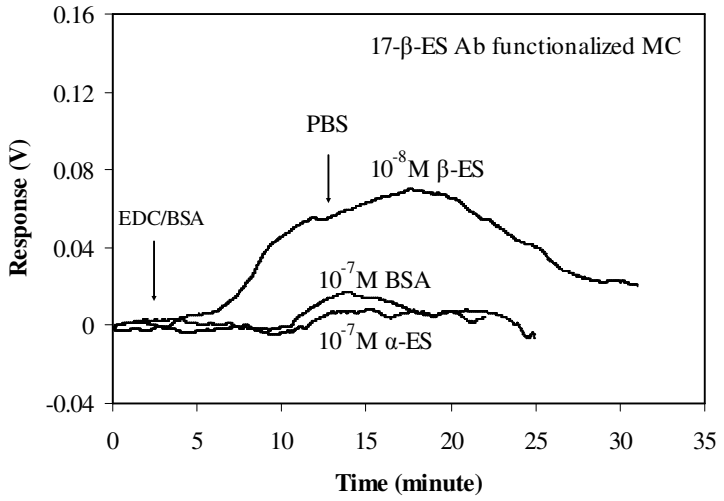

Fig. 11. Nanomechanical responses of an anti-17-β-ES antibody (Ab) functionalized MC to $1x10^{-8}$ M of 17-β-ES in comparison no responses to non-specific analytes 17-α-ES and BSA at higher concentration of $1x10^{-7}$ M.

rearrangement of the conformation of the large antibody biomolecule and an apparent surface stress. It is interesting to see that the response increases even after injection of background buffer which may involve the gradual conformational changes of the antibodies to achieve a more stable conformation or wash out issues with our flow cell. Also, it is interesting to observe that the nanomechanical response of the cantilever produced by the antibody-hapten interaction on the nanostructured surface was easily reversed with the replacement of the 17-β-ES solution by the background buffer (PBS) solution despite the expected very large affinity constants (see "Response characteristics of nanostructured MCs" in the Appendix). In our previous studies (50), we have observed the similar behavior; i.e. antibody functionalized nanostructured surface of MCs are more easily regenerated than similarly functionalized smooth gold surface of MCs. Irreversible response of the smooth gold surface was also observed by other researchers for specific interactions of different antibody-antigen pairs (18, 56, 100). To check for specificity, the same MC was again exposed to one order of magnitude higher concentration (1×10^{-7}M) of BSA (Ab was generated to BSA-hapten conjugate) and 17-α-ES, producing negligible deflection for each potential interferent.

Fig. 12A demonstrates nanomechanical response profiles of ER-β protein functionalized MC to different concentrations of 17-β-ES in the range of 50 pM to 10 nM where the response increases with increasing concentration. The kinetic response of the cantilever after 4 minutes of exposure is plotted against the concentration of 17-β-ES ranging from 50 pM to 100 nM in Fig. 12B. As seen in the figure, the response increased gradually and reached a plateau by 100 nM. The inset in Fig. 12B illustrates a linear

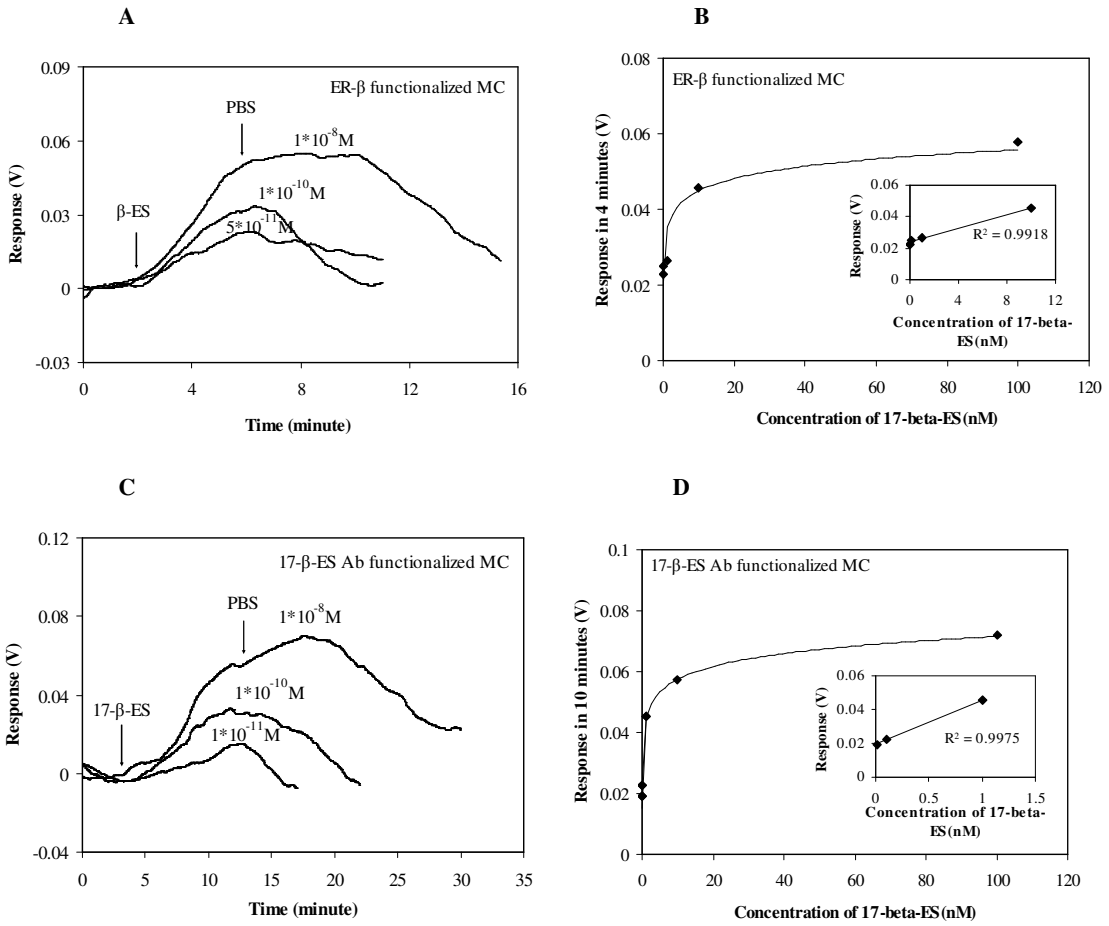

Fig. 12. Concentration based nanomechanical responses of (A) ER-β protein and (C) anti-17-β-ES Ab functionalized MC to different concentrations of 17-β-ES. Net responses to 17-β-ES after 4 minutes and 10 minutes for ER-β protein and anti-17-β-ES Ab, respectively, functionalized MCs are plotted (B & D) over a concentration range from less than $1x10^{-10}$ M (see lowest concentrations in A & C) to $1x10^{-7}$ M. The linear portions of these plots extend over two orders of magnitude in concentration (see inserts in B & D). The first data points in insert B and D correspond to $5x10^{-11}$ M and $1x10^{-11}$ M of 17-β-ES respectively.

dynamic range for more than two orders of magnitude (the first data point corresponds to the lowest concentration of Fig. 12B) in concentration from an approximate LOD less than 50 pM to 10 nM). Similarly, Fig. 12C shows the response profiles of an anti-17-β-ES antibody functionalized cantilever for different concentrations of 17-β-ES in PBS in the range of 1 pM (approximate LOD is somewhat less than this) to 10 nM. The kinetic response of the cantilever after 10 minutes exposure of the antibody functionalized MC is plotted against the antigen concentrations over a range of 1 pM to 100 nM (Fig. 12D). Our current experiment involving optimization of the thickness of the dealloyed surface of the MC may improve the LOD lower than pM level (see the Appendix and Fig. Appendix-2).

Prior work showed that calibration plots are generally linear for two or more orders of magnitude, while coefficients of variation (CVs) for measurements using a given system of MC and molecular-recognition phase are generally 10% or better (17, 21, 50, 92). Our experiments in the detection of 17-β-ES using both the receptor protein (ER-β) and antibody (anti-17-β-ES Ab) showed good measurement reproducibility in the same day tested via three replicate consecutive measurements of a solution of 1×10^{-10}M of 17-β-ES (see Fig. 13). ER-β functionalized MC arrays prepared in different batches showed 8-10% CV values in the detection of different concentrations of 17-β- ES.

To investigate stability, anti-17-β-ES Ab functionalized MC was exposed to 1×10^{-9}M of 17-β-ES at three different periods after storing in PBS at 4°C (2-nd, 4-th, and 8-th day after functionalization), an average value of deflection on day 4 and day 8 were 97% and 76% of the initial response, respectively. Similarly, the stability of

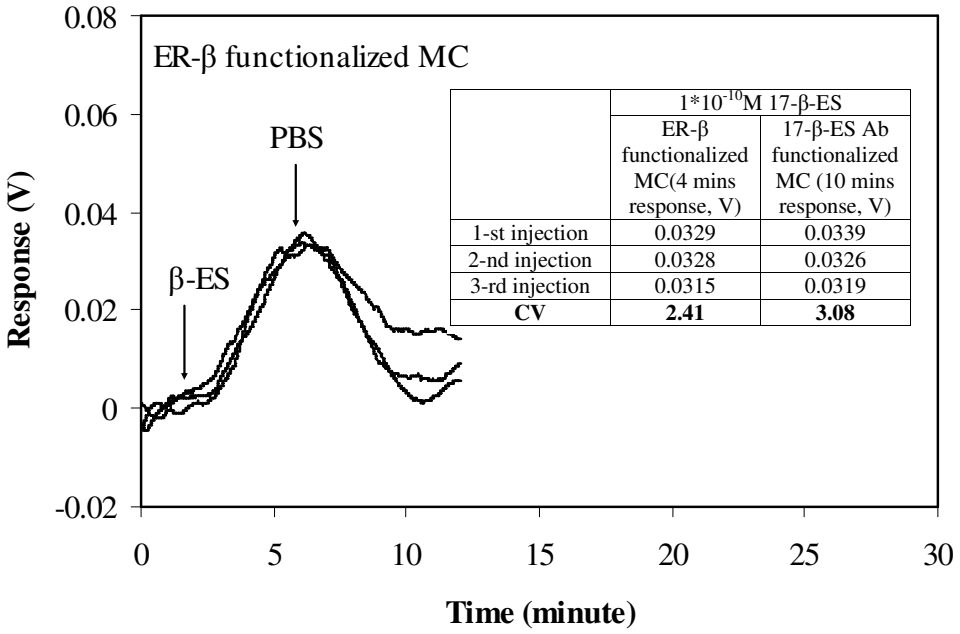

	$1*10^{-10}$M 17-β-ES	
	ER-β functionalized MC(4 mins response, V)	17-β-ES Ab functionalized MC (10 mins response, V)
1-st injection	0.0329	0.0339
2-nd injection	0.0328	0.0326
3-rd injection	0.0315	0.0319
CV	**2.41**	**3.08**

Fig. 13. Nanomechanical responses of ER-β functionalized MC on exposure to $1x10^{-10}$ M 17-β-ES for three replicate injections demonstrating reproducibility in nanomechanical responses where the inset shows the response and CV for three replicate measurements of this EDC using both the receptor protein and the antibody functionalized MCs.

ER-β functionalized MC was studied over periods of 5 days after storing in PBS at 4°C wherein it showed poorer stability; exposure to 1×10^{-9}M of 17-β-ES yielded responses after 3 and 5 days that were 78% and 36% of the initial response, respectively. Also, the stability of ER-functionalized MC was tested at 4°C varying the environment (stored dry versus in PBS). The results showed that the immobilized antibody retained it's functionality for a longer period of time (7-10 days after functionalization) if stored dry at 4°C whereas it can be stored in PBS for near immediate use. Surprisingly, in both of the experiments performed, the response actually increased by a factor of two after one week of dry storage at 4°C.

2.3 Conclusions

In summary, a highly sensitive, biospecific, and reusable biosensor for the detection and screening of EDCs has been developed using nanostructured MCs by exploiting protein receptor-EDC and antibody-EDC interactions. Our results indicate that the interaction of ER protein with different ligands produced different cantilever responses showing the maximum response for the synthetic estrogen DES with the ER-β functionalized MCs followed by estradiols and other EDCs. While receptor proteins provide generalized responses to subclasses of EDCs with impressive LODs, antibodies specific to a particular EDC can be used for specific analyte detection with a linear dynamic range over two orders of magnitude in concentration and about 3% of intra-day RSD. Also, measurements exhibited 10% RSD between different MC arrays functionalized at different times.

Since a single analyte ligand can stimulate changes in multiple receptor proteins and thereby synergistically mediate diverse biochemistry in complex living systems, an integrated analysis tool in a small, inexpensive platform is highly desirable. Thus, future research will involve the development of efficient and reproducible methods to differentially functionalize the cantilevers in arrays with different types of receptor proteins, the resulting chip platforms are expected to provide unique capabilities and exhibit significant biomedical and environmental utility.

Chapter 3 Morphological and Chemical Optimization of Microcantilever Surfaces for Thyroid System Biosensing and Beyond

Chapter 3 is an adaptation of a research article *Analytica Chimica Acta* **2008**, 625, 55-62. In this article protein immobilization conditions were optimized, which includes the gold nanostructured surface, aminoethanethiol and glutaraldehyde conditions, and protein incubation conditions. These optimized conditions were applied to thyroid transport protein functionalization to detect and screen for thyroid disrupting chemicals.

3.1 Introduction

Biomedical, environmental, and many other areas of research rely on biosensors for screening and detecting environmental contaminants that can have detrimental health effects on humans, livestock, and wildlife. The development and optimization of a label-free biosensor based on ligand-induced nanomechanical responses of microcantilevers (MCs) allows for sensitive and selective detection of contaminants from their specific interactions with the biomolecular recognition phase immobilized on the active surface of the MC. Functionalizing only one side of the MC with some receptor phase allows one to measure the static cantilever deflection due to molecular recognition events which generate surface stress. The bare silicon side of the cantilever is relatively passive. This active side binding causes a change in surface stress. The resulting static bending of the MC is governed by Stoney's equation (14). See equation 4 in Chapter 1. Due to the small size of MCs (herein l = 400 μm and t ~1 μm), they exhibit high mass sensitivity

compared to other types of sensors. The widespread availability of inexpensive MCs has generated interest in these transducers as chemical (17, 93, 101-104) and biological (18, 21, 56, 105-111) sensors. Sensitivity is critical in these biosensors due to the ultra-trace concentrations of many contaminants that impact biological systems. Nanostructured MC biosensors allow detection without labels and in a detection range that is applicable for real biological systems (112).

Three key performance metrics are generally significant in biosensing. First, the specificity of the ligand-receptor interaction is important in achieving the selectivity needed to deal with complex biological matrices and, second, high sensitivity is needed to deal with the fact that ultra-trace concentrations of many ligands impact biological systems. Finally, high selectivity and sensitivity must be achieved while maintaining the reversibility that is a base requirement of any true sensor. For a more in depth discussion of these performance metrics see Chapter 1. The nature of the MC surface and the method by which the bioreceptor is immobilized influence these performance metrics and, hence, optimization studies involving these were conducted.

In our previous studies (21, 50), we observed sensitive, reversible bio-nanomechanical responses with MCs that have the active side nanostructured via a dealloying process. Dealloying is accomplished by co-depositing gold and silver onto the MC surface, then removing the silver via oxidation leaving a roughened (granular or porous) gold surface (49). In the initial dealloyed studies, the sensitivity and reversibility was very good, particularly when compared to smooth gold MCs, so until recently we had not fully optimized the dealloying surface treatment step. In this paper, we optimize the dealloyed thickness and gold to silver ratio for a model biological system, anti-

immunoglobulin (anti-IgG)-IgG. The concentration, buffer pH, and incubation time of the immobilization linking chemistry and protein or antibody functionalization conditions were optimized by comparing model systems' responses. By varying these conditions, we demonstrate the reversibility and sensitivity of our bio-functionalized MC sensors and clearly demonstrate the advantages of using nanostructured MCs. Random versus specific antibody/antigen immobilization experiments yield surprising results, which illustrate the importance of optimizing immobilization methods and the unique response characteristics of transducers that rely on the generation of surface stress.

We report for the first time the use of thyroxine binding globulin (TBG), a thyroid transport protein, for sensing thyroid disrupting chemicals (TDCs) under non-optimal and optimal immobilization conditions on MCs. TDCs are a sub-class of endocrine disrupting chemicals (EDCs), which include organohalogen compounds. TDCs can affect the thyroid hormone system at the thyroid gland, the thyroid transport proteins, and the thyroid hormone metabolism (37). Disrupting thyroid activity can occur at different levels and cause many adverse health problems. Traditionally, complex competitive binding assays, like radioligand binding assays, and surface plasmon resonance based inhibition assays have been used to detect TDCs (37, 69). These methods require extensive labeling or complex biological assays. Meerts et al. radioligand binding assay method tested various potential TDCs with L-thyroxine (T4) binding to transthyretin (TTR), a thyroid transport protein, down to 1.95 nM concentration of TDCs (37). The sensitivity of the surface plasmon resonance based inhibition assay of Marchesini et al. with TBG for T4 is 0.7 nM (69). Mikami et al. detected T4 in dietary supplements with absorbance based ELISA and liquid chromatography-mass chromatography (LC/MS).

The LC/MS detection had a lower limit of detection, which was approximately 0.64 μM, than the ELISA method (33). Although not T4 detection, Kerrigan et al compared two types of enzyme-linked immunosorbent assay (ELISA) kits in detecting drugs of abuse, where the lower detection limit is approximately <3.2 nM (32). We optimize a label-free TDC nanomechanical biosensor used to screen various TDCs that shows excellent sensitivity, down to 0.1 nM, and reversibility for the main hormone of the thyroid system, T4. Selectivity patterns in this TDC work (see below) and in prior EDC work (15) are consistent with that appearing in the literature. Thus, the three performance metrics are addressed in this application with optimized MC biosensors providing high selectivity, sensitivity, and reversibility.

3.2 Experimental

Experiments were performed using commercially available silicon arrays of MCs having dimensions 400 μm length, 100 μm width, and approximately 1 μm thickness (Mikro Masch Co., Sunnyvale, CA). Chromium, gold, and silver metals deposited on the MCs were obtained from Kurt J. Lesker, Gatewest, and Alfa Aesar Co., respectively, at 99.9% purity. 2-Aminoethanethiolhydrochloride (AET), 4-aminothiophenol (ATP), glutaraldehyde (GA), the salts employed for the preparation of buffer solutions and all other reagents were purchased from Sigma-Aldrich Chemical Co (St. Louis, MO) or Fisher at highest available purity and used as received. The proteins human immunoglobulin G (hIgG, reagent grade), anti-hIgG (Fc specific) antibody produced in goat (anti-hIgG Ab), TBG from human plasma, L-thyroxin, biotin A, anti-biotin antibody

produced in goat, and Protein A were also obtained from Sigma-Aldrich. Water used to prepare solutions was obtained from a Branstead E-pure water filtration system.

The process of creating nanostructured surfaces on MCs is described in detail elsewhere (49). The cantilevers were first cleaned in a piranha bath (75% H_2SO_4, 25% H_2O_2) for 30 minutes, followed by thorough rinsing in deionized water [*Caution*: piranha solution reacts violently with organics]. The MCs were then placed into a physical vapor deposition (PVD) chamber (Cooke Vacuum Products, Model CVE 301, South Norwalk, CT) to be coated on one side with the appropriate metallic films using thermal deposition. To create a nanostructured MC, a thin film (5 to 10 nm) of chromium was applied to the surface to act as an adhesion layer followed by a thin film of gold (~15 nm). Next, gold and silver were co-deposited to the desired film thickness. In most cases the deposition rates for the two metals were set to create a 50:50 alloy, but in this study 40:60 and 60:40 ratios were also tested for effects on MC performance. The deposition rate and film thickness were monitored using a quartz crystal microbalance. Subsequently, the silver was chemically removed via oxidation from the film (dealloying) with an aqueous solution of 5 mg/mL $HAuCl_4$ leaving a gold surface with nano-sized, colloid-like features. The thickness of the dealloyed gold layer was varied from 25 to 200 nm, but it was ~150 nm in most of these studies.

In these studies, nanostructured MCs were chemically modified by immersion in aqueous solution of AET, or in one study ATP, (concentration and time of incubation with the thiol compounds were varied to get the optimum kinetic response of the protein functionalized MC) producing a self-assembled monolayer (SAM) of AET/ATP on the cantilever surface. Following thorough rinsing in deionized water, the amino groups

were derivatized with the cross linker by immersing the cantilever in a solution of GA (95) where concentration and pH of the GA solution as well as the time of incubation were varied to optimize the conditions of functionalization. The chemically treated cantilever was allowed to soak in a large volume of water/phosphate buffered saline (10 mM pH 8 PBS) for a few minutes to remove any nonspecifically bound GA on the nanostructured and silicon sides of the cantilevers. Subsequently, immobilization of anti-hIgG Ab in random orientation was optimized by dipping the pre-functionalized cantilevers into different concentrations of antibody solutions in PBS varying the incubation time. For the orientation studies, 0.5 mg/mL of hIgG antigen (Ag) or anti-hIgG antibody (Ab) was immobilized directly on the functionalized dealloyed surface of the cantilevers. The MCs were functionalized by 1mM AET (1 hour incubation) and 1% GA (3 hours incubation). The Ag or Ab was immobilized for an hour. Immobilization of Ab and Ag (0.5 mg/mL) anchored in oriented manner was performed by immersing AET-GA pre-functionalized microcantilevers (optimized conditions) in 0.5 mg/mL protein A solution in 10 mM pH 7 PBS for one hour and then functionalized with Ag or Ab in the same manner mentioned above. After washing with PBS, the functionalized microcantilevers are stored in PBS at 4°C until it is used or until the next day for the best performance. Although we used a MC array in this study, we chemically treated the array and recorded the response of a single randomly chosen MC.

The MC deflection measurements were carried out using the optical beam-deflection technique as described previously (17). The apparatus included a 5 mW diode laser (Coherent Laser Corp., Auburn, CA) operating at 635 nm, a spatial filtering and focusing system, and an in-house built position sensitive optical detector (Fig. 2). The

whole microcantilever sensor system was mounted on vibration-free High Performance Table Top (Newport Corp., CA). The output of the detector was displayed and recorded using a SRS 850 DSP lock-in amplifier as a multichannel digital recorder (Stanford Research Systems, Sunnyvale, CA). The signal output is recorded as volts (approximately 1 nm z_{max} per mV output). Data was collected at 1 Hz and then a moving averaging algorithm usually covering 32 data points was used to generate the figures presented herein. This smoothing did not alter the shape of the true response curves (92).

The MC system was mounted inside a ~5µL volume flow cell made of a 2 cm diameter by 2 cm long Delrin rod that was machined with 1/16 inch diameter input and output holes that meet at 1 cm distance apart at the face of the rod (15). Narrow bore tubing of 1/16 inch O.D. was slid into the holes up to the rod face and secured with fittings. A semi transparent silicone gasket, which is slightly thicker than the MC chip (~500 µm versus 400 µm), was cut with a scalpel tool to form a ~250 µm wide flow channel between the input/output holes and to tightly hold the MC chip. The silicone gasket is sandwiched between the Delrin rod face and a thin quartz window. A Watec CCD camera was used to image the MC chip in the flow cell (Fig. 8). The camera facilitated aligning the focused laser beam to reflect off the cantilever tip (Edmund Industrial Optics, Barrington, NJ). Analyte solutions were delivered to the flow cell via a system of vessels connected to three-way valves allowing for switching between different solutions or via an injection valve controlled by a syringe pump (orientation studies). The flow rate was generally adjusted to 100 µL $minute^{-1}$.

Solutions of hIgG were made with PBS (10 mM Phosphate Buffer + 10mM $NaNO_3$, pH 7). PBS was also used as a background solution. The pH of PBS solution was

checked before experiments using an Orion SA 520 pH meter (Thermo Orion, Beverly, MA). MCs mounted in the flow cell were initially allowed to equilibrate in PBS until the signal was stable. For our purposes, tensile and compressive responses involve contraction and expansion of the active MC surface, respectively.

3.3 Results and Discussion

Our work focuses on five optimization aspects for biofunctionalized MCs. The optimized functionalization steps include dealloyed thickness and metal ratio, the incubation time and concentration for AET, the buffer pH, concentration, and incubation time for GA and two model proteins, and the orientation of proteins. We applied these optimized conditions to TBG immobilization for detecting and screening TDCs and thyroid hormones. We compared the responses of TBG functionalized MCs under optimal versus non-optimal biofunctionalization conditions. Our developing MC biosensors, in support of fundamental endocrinology studies, may prove to be a quicker, simpler, and less expensive method to detect TDCs compared to existing methods.

Enhancement of sensitivity in biosensing is important due to the small concentrations of ligands that often stimulate or impair receptor proteins. We have substantially improved the sensitivity of MC biosensors by nanostructuring the active surfaces of the MC by the described dealloying process. In some cases the response enhancement has surpassed the increase in surface area of the active surface (5, 17, 49). The bioaffinity response was enhanced with previous nanostructured surface techniques, but the current optimization allows for responses to be further enhanced.

Fig. 14 shows the comparison of MC responses by varying the thickness of 50 gold :50 silver dealloyed surface with immobilized anti-hIgG exposed to 0.05 mg mL^{-1} of hIgG in PBS. This figure demonstrates increased response with varying thicknesses with the best enhancement afforded by 150 nm dealloyed. A trend is observed for greater response with increasing dealloyed thickness until a drop in response when the thickness reaches 200 nm. This trend may be a result of apparent increasing surface area. With the increasing thickness and surface area, the $\Delta\sigma$ term in the Stoney equation (eq 4) is expected to increase as well (92). While $\Delta\sigma$ is increasing, the stiffness due to changes in the Young's modulus and cantilever thickness (note Et^2 in the denominator) is most likely increasing with dealloyed thickness. These two terms oppose one another according to eq 4, resulting in an optimal dealloyed thickness for best MC performance (Fig. 14). The inset in the figure shows three responses for immobilized anti-hIgG on 50 nm dealloyed on exposure to 0.05 mg/mL hIgG in PBS. The experiments do not reach equilibrium because we purposefully inject analyte for a brief period of time. The time scale of response is determined by the kinetics of the protein-analyte binding and that interaction is translated to cantilever surface stress. Rearrangement of the immobilized protein occurs when analyte molecules, which include antigen and small molecule analyte solutions, interact with the protein. This relatively slow rearrangement leads to MC surface stress. MC biosensor response time depends on factors such as the kinetics of the protein interaction as well as the rearrangement of the immobilized protein upon analyte binding. It is worth noting that operating in this non-equilibrium mode enhances reversibility (see the figure).

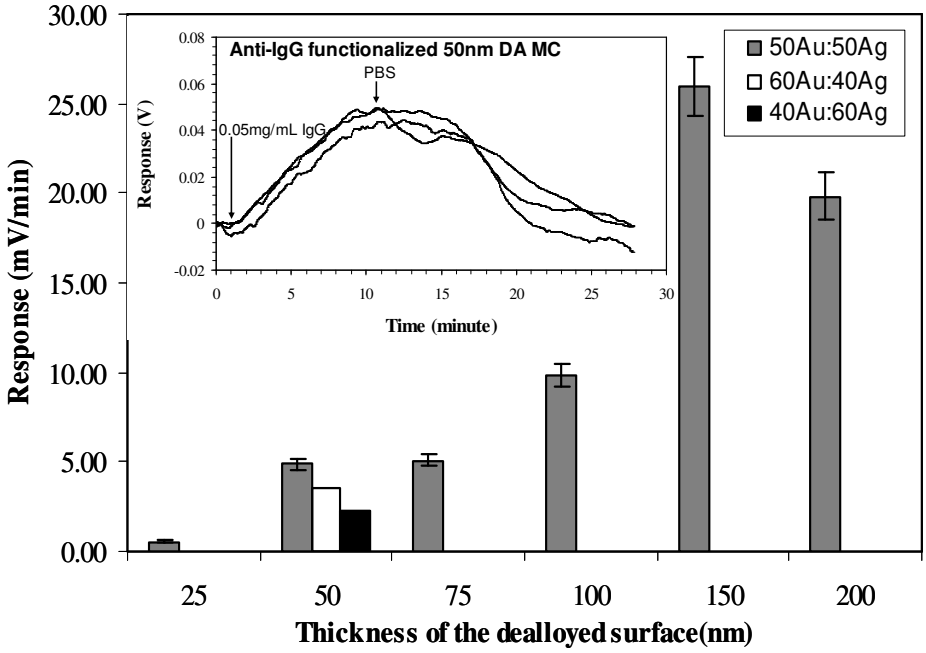

Fig. 14. Comparison of responses of anti-hIgG Ab functionalized DA MCs with different thicknesses of the DA layers on exposure to 0.05 mg/mL of hIgG in 10 mM pH 7 PBS. The error bar indicates the standard deviation (with CV = 6.5%) for three replicate measurements with the same MC. The insert provides three response profiles of anti-hIgG Ab functionalized MC on exposure to 0.05 mg/mL hIgG for 50 nm thick DA (arrows denote points of introducing hIgG solution and PBS background into the flow cell). Three different composite ratios for gold and silver were compared for a 50 nm DA layer which were functionalized with anti-hIgG Ab and exposed to 0.05 mg/mL hIgG.

Fig. 14 also compares anti hIgG Ab functionalized 50 nm dealloyed MC responses varying the gold to silver ratio, which comprises the dealloyed, with the latter removed via oxidation with $HAuCl_4$. Three different composites were studied (40:60, 50 :50, and 60 :40 gold : silver) with immobilized anti-hIgG subsequently exposed to hIgG. The best response is observed from the 50:50 gold :silver system. This ratio appears to allow for the optimal porosity of the gold when the silver is removed while maintaining a stable metal surface.

Concern arises when immobilizing proteins that the chemical attachment of the protein will cause the protein binding sites to distort or be blocked. This problem would not allow the benefit of the natural antibody/antigen or hapten affinity binding. Our previous studies have provided evidence that an appreciable portion of the protein binding sites remain functional after immobilization (15, 20, 50). In this work, we optimized the immobilization steps so that we obtain an enhanced bioaffinity response.

The initial linking chemistry step exposes the nanostructured dealloyed surface to AET producing a self-assembled monolayer. A comparison of AET and ATP was performed. AET and ATP have similar terminal groups, but different carbon backbones or structures. AET consists of a two carbon chain, whereas ATP has a rigid aromatic ring. The aromatic ring makes the molecule larger than AET, which could hinder unwanted crosslinking with two adjacent GA groups. However, this did not prove to be beneficial in terms of enhanced responses in this work. Fig. 15 compares bioaffinity (anti-hIgG-hIgG) responses on 150 nm dealloyed by varying concentration and time of incubation for AET. The inset shows a representative trace of an anti-hIgG Ab functionalized MC exposed to 0.05 mg/mL hIgG with a 1 hour incubation in a 1 mM

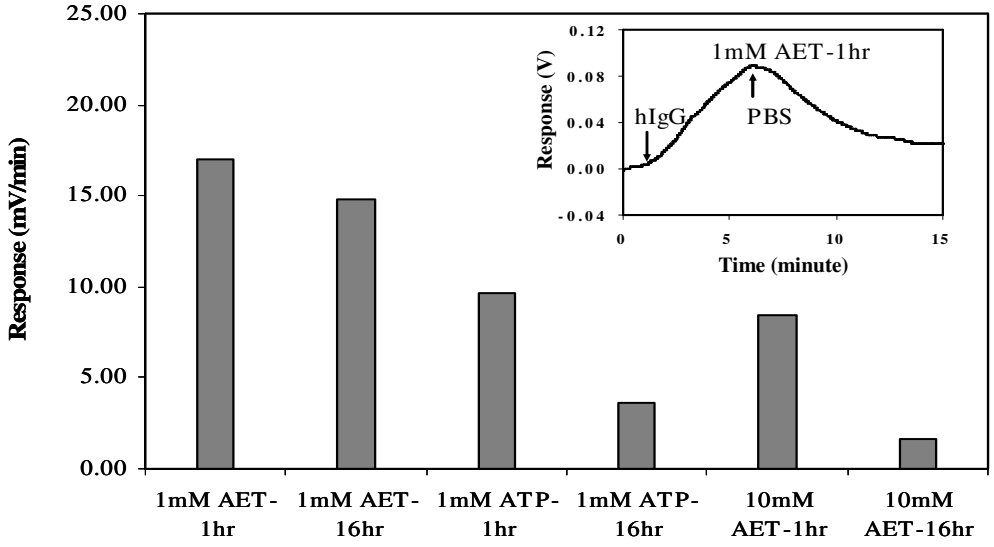

Fig. 15. Nanomechanical responses of anti-hIgG Ab functionalized 150 nm DA MCs on exposure to 0.05mg/mL hIgG in PBS. The concentration and time of incubation with AET solution were varied. The insert shows a representative response profile of anti-hIgG Ab immobilized on 150 nm DA MC exposed to 0.05 mg/mL hIgG with 1 mM AET (1 hour incubation) functionalization. The arrows denote points of introducing hIgG solution and PBS background in the flow cell, respectively.

AET solution. The best response was observed when conditions were 1 mM AET for 1 hour. This also shows that AET achieves a better anti-hIgG-hIgG nanomechanical response than ATP under the same conditions.

The amino groups from the AET were derivatized with a cross-linker by immersing the MC in a GA solution. GA acts as a linker for the immobilized antibodies or proteins to the surface. It is generally accepted that reactions between the carbonyl group of GA and the amino functions of the protein take place yielding a Schiff base (113). Terumichi et al. have previously reported that the activity of enzyme increased by using alkaline-treated GA, suggesting alkaline treated GA may act as a crosslinker in a manner different from the generally accepted Schiff base formation reaction (114). A possible mechanism may involve the additional reaction of an amino group to the double bond in the aldol condensate of GA (115). So, in these studies, GA was functionalized in both pH 7 and pH 8 PBS varying the concentrations and time of incubation to compare the responses of Ab functionalized MCs in different conditions. Antibodies and proteins are not appreciably denatured by GA immobilization (56). Fig. 16 shows immobilized anti-hIgG Ab responses upon exposure to 0.05 mg/mL hIgG with varying GA concentration, pH, and incubation time. The optimal GA conditions are 1% GA in 10 mM 8 pH PBS for 3 hours. These optimized conditions are relatively minor changes from our established conditions for AET and GA. A representative response profile for the anti-hIgG-hIgG system is shown in the insert for MC treatment in 2% GA in 10 mM pH 8 PBS with an incubation time of 3 hours. For all of the GA optimization experiments the AET was under optimal conditions.

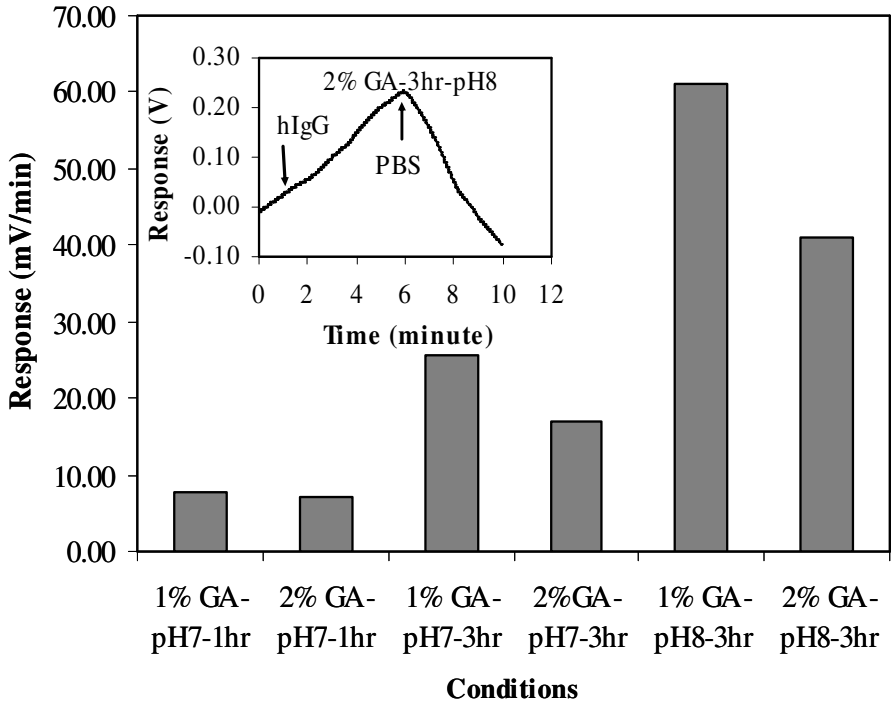

Fig. 16. Comparison of responses of anti-hIgG Ab functionalized 150 nm DA MCs on exposure to 0.05 mg/mL hIgG in PBS at different conditions of GA functionalization. The concentration, pH and time of incubation with GA solution were varied. The insert shows a representative trace of anti-hIgG Ab immobilized on a 150 nm DA MC which was functionalized with a 2% GA solution in 10 mM pH 8 PBS for 3 hours. The arrows denote points of introducing hIgG solution and PBS background in the flow cell, respectively.

Antibody-antigen interactions involving high specificity is a desirable characteristic for biosensors. Biofunctionalized MCs exploit this interaction often resulting in high sensitivity and selectivity. The antibody has an inherent selectivity for various antigens. Our prior work showed that calibration plots are generally linear for two or more orders of magnitude, while coefficients of variation (CVs) for measurements using a given system of MC and biological molecular-recognition phase are generally 10% or better (15, 21, 50). For endocrine disrupting chemical sensing, we have demonstrated CVs of 2.4% and 3.1% for triplicate replicate consecutive intra-day injections of 17-β-estradiol with estrogen receptor β and 17-β-estradiol antibody (15). Our immunosensor for human interleukin-1 β (HILI-β) Ab on exposure to HILI-β antigen showed a CV of 10% of triplet replicate intra day injections (50). In stereoselective detection, we have shown detection of chiral amino acids with antibody immobilized MCs with excellent same day reproducibility (CV=2%) (9). Our previous studies illustrate the reproducibility of the nanomechanical biosensor which we utilized and optimized for these experiments. Biosensor problems can arise from a lack of reversibility due to high affinity. We have developed a MC-based immunosensor that allows the antibody-antigen interaction to be reversed with the replacement of antigen with background buffer. This reversibility on the nanostructured surface has been observed in our previous work as well (15, 50).

To compare optimization conditions for protein immobilization we choose two common model systems for study, anti-hIgG-hIgG and anti-biotin-biotin. hIgG is a antibody with a molecular weight of approximately 150,000 Da, while biotin is considered a small molecule (hapten) with a molecular weight of 244 g/mol (116). hIgG

is the most common class of immunoglobulin and provides the majority of antibody based immunity (69), while biotin is a common water soluble vitamin (116). These systems were chosen due to their differences in size, low cost, and their common use in biosensor applications.

Fig. 17 compares anti-biotin and anti-hIgG interaction when exposed to 0.05 mg/mL biotin or hIgG under various immobilized antibody concentrations and incubation times. The best conditions for both anti-biotin and anti-hIgG were observed for 0.5 mg/mL protein solution for 1 hour on 150 nm dealloyed. When a protein is not readily available at this high of a concentration, then a less concentrated solution can be used with a longer incubation time, although depending on protein stability a shorter incubation time may be required. The AET and GA were also under optimal conditions for these protein optimization experiments. The inset shows a representative response profile for the optimized conditions of 0.5 mg/mL anti-hIgG with a 1 hour incubation time exposed to 0.05 mg/mL hIgG.

We also report receptor orientation studies using a MC sensor system. Earlier work demonstrated that simple physical adsorption of protein on MCs did not provide stable receptor phases and that some form of stronger attachment is needed (102, 103). Thus, the covalent attachment of protein receptors via AET and GA chemistry was pursued and optimized as described above. However, most proteins including hIgG contain randomly distributed lysine residues which lead to multiple attachment sites, resulting in random orientation on the surface (117). While stability is required and will benefit from multiple points of attachment, distortion of the receptor can diminish ligand-receptor binding and thus effecting both sensitivity and selectivity. In addition, the

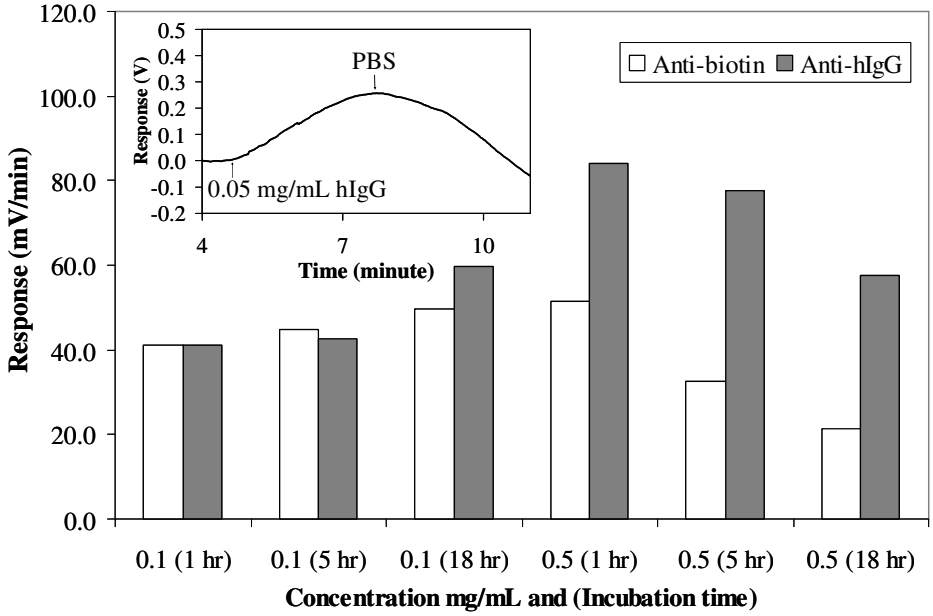

Fig. 17. Comparsion of responses of anti-hIgG and anti-biotin functionalized 150 nm DA MCs on exposure to 0.05 mg/mL hIgG in PBS and 0.05 mg/mL biotin D in PBS. The concentration of protein and incubation time were varied. The insert shows the response of 0.5 mg/mL anti-hIgG with a 1 hr incubation on 150 nm DA MC exposed to 0.05 mg/mL hIgG in PBS. The arrows denote points of introducing hIgG solution and PBS background into the flow cell, respectively.

ligand receptor site can be surface confined and not available to the ligand. Fig. 18 provides a graphic depiction of a hIgG (Ag) and anti-hIgG (Ab) system with both species used as the receptor in separate experiments, with the other protein acting as the ligand. For this system the binding sites of the Ab resides in the two Fab portions and the Fc portion of the Ag represents the epitope for the monoclonal Ab. The figure also depicts the use of Protein A as an orientation linker that is specific for the Fc portion of the hIgG molecule (Ab or Ag).

In Fig. 18A, randomly functionalized MCs with Ag gave 225 mV reversible compressive stress responses on exposure to anti-hIgG (0.05 mg/mL) in 10 mM pH 7 PBS. Note that some of the surface immobilized Ag are depicted not properly oriented with the Fc portion easily accessible to the Ab. When the Ag is properly oriented with Protein A linkage the response increases to 420 mV (Fig. 18B), whereas when random orientation is performed using immobilized Ab (Fig. 18C) and exposure to Ag, (0.05 mg/mL) in 10 mM pH 7 PBS, the response is less (115 mV) for the same Ab-Ag pair. The most surprising result occurs when the Ab is properly oriented with Protein A (Fig. 18D) resulting in a minuscule 15 mV signal when exposed to the Ag. These results while surprising, were repeatable, and in agreement with our previously obtained results under non-optimized conditions (15), but are contrary to other reports (50, 111, 112). Factors to consider are that the immobilized species is monovalent in the case of the Ag while bivalent in the case of the Ab, such that each species may have specific preferred surface binding sites. Nanomechanical responses are generated from surface stress and are not strictly mass dependent. Although only a cartoon depiction we purposely show the

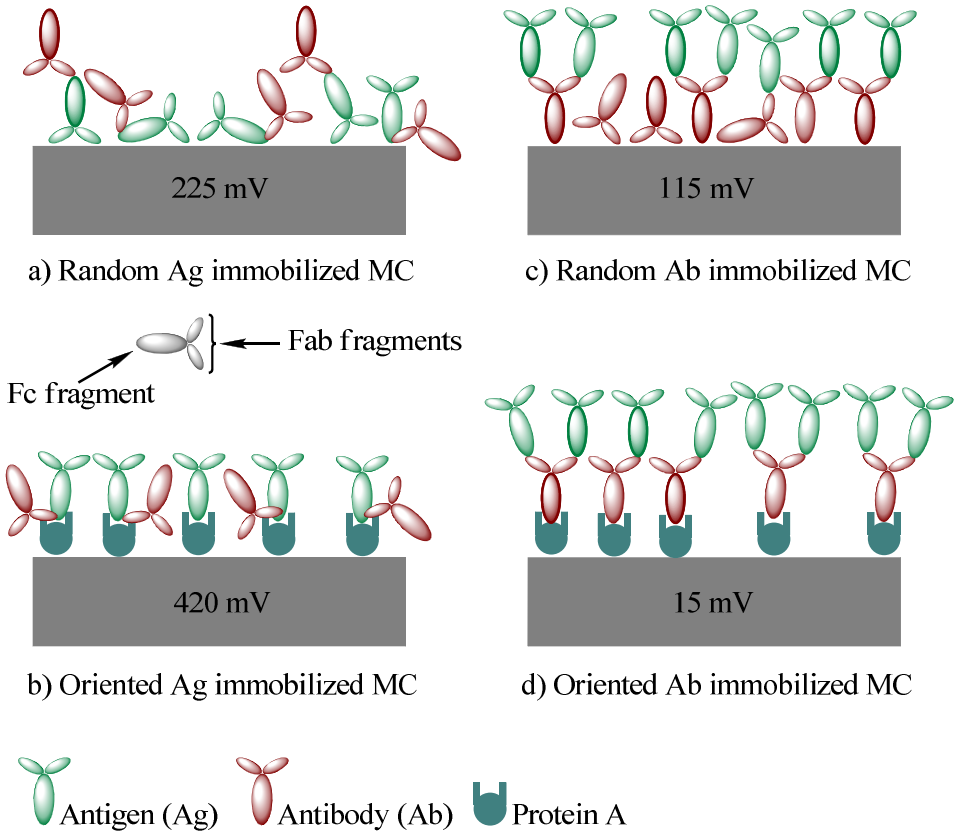

Fig. 18. Left two pictures represent 0.5 mg/mL hIgG (Ag) immobilized in random (A) (no protein A attached) and oriented (B) (0.5 mg/mL protein A) manner on 150 nm DA MCs. Right two pictures visualize 0.5 mg/mL anti-hIgG (Ab) immobilized (functionalized) in random (C) (no protein A attached) and oriented (D) (0.5 mg/mL protein A) manner on 150 nm DA MCs. Functionalized MCs were exposed for 10 min to 0.05 mg/mL anti-hIgG (Ab) – (A) and (B), and hIgG (Ag) – (C) and (D) in 10 mM pH 7 PBS, respectively. All voltage responses are average of two experiments.

highest loading of surface for the system that generated the smallest response (Fig. 18D). That is the case where minimal steric issues arise, but the smallest amount of ligand binding energy is transferred to the surface of the MC (note the protein mass between the surface and the binding site). Conversely, in the case of the largest signal (Fig. 18B) Ag and Ab are competing for similar portions of the surface bound receptor (Protein A). It is clear that optimal conditions are influenced by the nuances of the biosystem involved and one should guard against over generalizations on the best methods for immobilization.

Applying these optimized nanomechanical sensing conditions to the real life application of detecting TDCs should allow for enhanced sensitivity, which is crucial due to the small concentrations of contaminants that can adversely affect the body. TDCs can modulate the thyroid system leading to disturbances in hormone status and thyroid gland processes. Screening for all potential TDCs or EDCs is a major challenge since the list of known compounds is ever expanding. This marks the importance of the development of a real-time, highly sensitive, label-free biosensor.

Fig. 19A illustrates the use of a TBG functionalized MC for the detection of four compounds, which include potential TDCs and natural hormones. In human plasma, TBG is the major thyroid transport protein for T4. It is responsible for 75% of the T4 binding activity. TTR, another thyroid transport protein in human plasma, carries ~20% of T4 (69). TBG has a slightly higher binding affinity for T4 than TTR. TBG and TTR may bind with different structural characteristics of the T4 molecule, which indicates their unique T4 binding properties (41). Previous studies have shown that TBG and TTR have different binding affinities with various environmental contaminants (41, 69, 118).

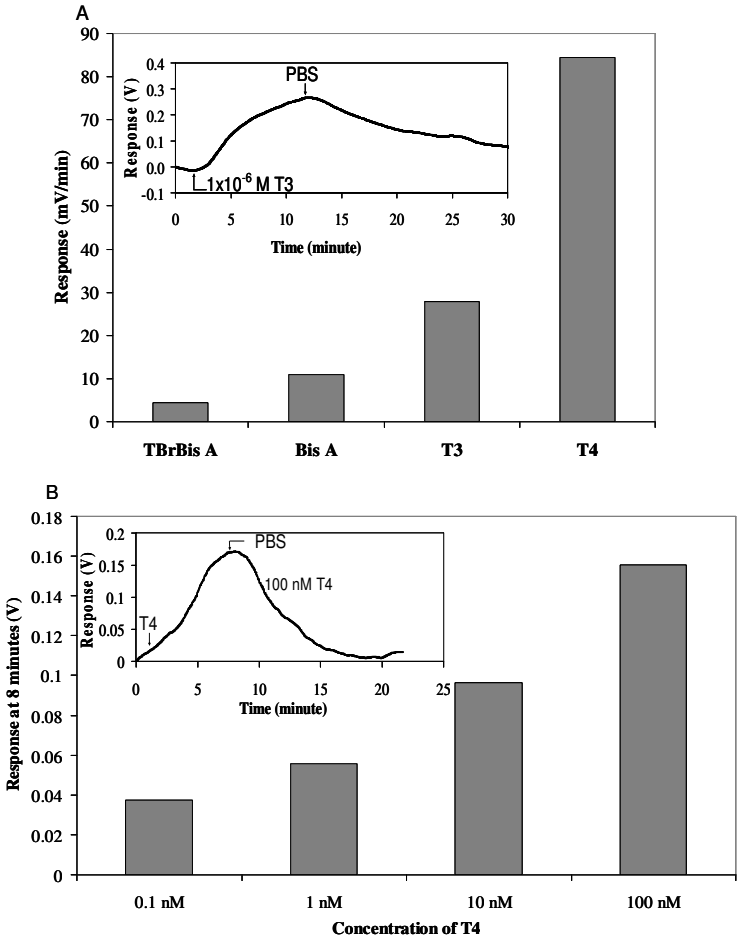

Fig. 19. (A) TBG shows different selectivity towards various TDCs: comparison of responses of TBG functionalized DA MCs on exposure to $1x10^{-6}$ M solutions of four different potential TDCs in 10 mM pH 8.5 PBS. The insert provides a representative response profile for immobilized TBG exposed to T3. (B) Concentration-based nanomechanical responses of TBG protein functionalized MC to different concentrations of T4. Net responses to T4 at 8 minutes for TBG functionalized MCs are plotted over a concentration range of $1x10^{-10}$ M to $1x10^{-7}$ M.

We choose to study TBG's interaction with contaminants, as well as natural hormones. Two naturally occurring hormones include T3 and T4, where T4 is the main hormone of the human thyroid system. T4 is also one of the top 200 most widely prescribed pharmaceuticals in the United States, so it is present in the environment and inadvertent exposure is possible, like many other pharmaceuticals, thus it is a potential TDC as well (105). Comparison of nanomechanical responses of TBG functionalized MC on exposure to 1 x 10^{-6} M solutions of four different potential TDCs in PBS is shown in the Fig. 19A. This figure shows that TBG exhibits selectivity toward T4 compared to the other TDCs. The high affinity of TBG for T4 followed by T3 then Bis A and TBrBis A has been observed by other researchers (105). This similarity demonstrates that the immobilization of TBG does not significantly alter the TDC ligand binding function and selectivity. The inset demonstrates the response behavior of TBG functionalized MC as a function of time for exposure to 1 x 10^{-6} M T3. During the optimization study some of the TDC experiments were performed under partially optimized conditions.

Fig. 19B compares the response of TBG functionalized MC to different concentrations of T4. The net responses to T4 at 8 minutes time are plotted. A 4 hour incubation time was used here due to the stability of TBG. The T4 concentration extends over a range of 4 orders of magnitude with sub nanomolar sensitivity. TBG functionalized MCs under optimal conditions yielded over 400% more response than non-optimized conditions.

In the present work, we have optimized a highly sensitive, label-free nanomechanical biosensor and applied these optimized conditions to detect TDCs with a thyroid transport protein. Optimizing the nanostructured surface, linking chemistry, and

protein functionalization conditions demonstrates the reversibility and sensitivity of our MC biosensors, which are critical aspects of any biosensor. The optimized sensors allow for screening and detecting various contaminants that may adversely affect the thyroid system. The protein immobilization process takes less than one day and our results provide strong evidence that at least an appreciable fraction of protein ligand binding sites remain active. These two factors are important in creating nanomechanical biosensors.

Further studies will apply these optimized conditions into creating differential MCAs (i.e., multiple receptors on a single array) for biosensing. The development of MCAs functionalized with multiple protein receptors is expected to have utility that extends beyond simply being novel nanomechanical sensor arrays. Significant to the differential MCA approach is the possible synergy between the effects of different small molecules (drugs, pollutants, hormones) on the responses of different immobilized receptors in determining holistic biomedical impacts. Thus, a novel bioassay tool that can simultaneously probe many such systems in a small, low volume, inexpensive and disposable platform is highly desirable and represents to a future direction of this work.

Chapter 4 Microcantilever-based Nanomechanical Studies of the Orphan Nuclear Receptor PXR

4.1 Introduction

Humans are exposed to harmful chemicals and contaminants each day. It is essential that these toxins are removed or detoxed from the body. These foreign compounds or xenobiotics, which include environmental toxins, endogenous hormones, steroids, pharmaceuticals, and dietary supplements, trigger a line of defense mechanisms within the body. The family of cytochrome P450 enzymes are the main xenobiotic defenders for mammals. These enzymes include four families of cytochrome P450 monooxygenases: CYP1, CYP2, CYP3, and CYP4 (76). Cytochrome P4503A4 (CYP3A4), a critical member of our defense system, makes the removal of many unwanted xenobiotics possible (77). CYP3A4 and it's isoforms are highly involved in pharmaceutical metabolism, playing a significant role in metabolizing approximately 50% of drugs used today (84, 119). When xenobiotic ligands bind to a specific nuclear hormone receptor, the interaction transcriptionally activates CYP3A4 (78). In 1998, a novel orphan human nuclear receptor was identified and termed pregnane X receptor (PXR), steroid and xenobiotic receptor (SXR), pregnane activated receptor (PAR), and NR1I2 (72-75). Herein, we choose to use the term PXR.

PXR is an orphan nuclear receptor that displays broad ligand specificity and is expressed mainly in the liver and intestine (82). Orphan receptors do not have specific

identified hormones and can be utilized in the search for unknown hormones through reverse endocrinology (77). PXR's promiscuity makes it unlike most other types of hormone receptors, which are highly selective to their specific hormone. PXR is activated by a broad array of structurally diverse xenobiotics (79). This wide activation range is possible is due to a unique ligand binding domain (LBD) or pocket, which can expand to fit a variety of sized ligands. PXR's LBD has two β strands that are not present in other nuclear receptors and that allow it's expansion (80). This flexible, hydrophobic LBD allows PXR to be activated by a diverse range of synthetic and naturally occurring chemicals making it an ideal candidate to serve as a xenobiotic sensor (82).

Importantly, PXR is activated by numerous pharmaceuticals with diverse properties, functions, and structures and controls the expression of genes that are vital to pharmaceutical metabolism (81, 83). PXR activation mediates transcription of CYP enzymes, including CYP3A, and many other enzymes and transporters within the body (82). CYP enzymes are considered drug metabolizing enzymes (76). Since, PXR activation allows for regulation and expression of CYP3A this interaction is critical to drug metabolism (77). CYP3A processes drugs and endogenous chemicals through oxidative, peroxidative, and reductive metabolism. CYP3A4 also oxidizes cholesterol to 4β-hydroxycholesterol, a major circulating oxysterol, which is important in many biological processes (119). Pharmaceutical metabolism and interaction is vital to monitor and prevent drug-drug interactions. Drug-drug interactions can occur when co-administered drugs alter the efficacy of one another. This usually occurs when one drug increases or decreases the metabolism of another (84, 85). Contaminants could modify

drug concentrations in vivo and skew the prescribed therapeutic dose. These cases could lead to fatal consequences.

High throughput, sensitive screening and detection of xenobiotics are critical to determine harmful toxins and possible drug-drug interactions. A highly sensitive, inexpensive, and rapid sensor utilizing the nuclear receptor PXR has been developed and is demonstrated within. Recently, biosensors based on nanomechanical microcantilevers (MCs) have been used to detect and screen for many harmful environmental contaminants using estrogen and thyroid receptors (15, 20). The high sensitivity and widespread availability of inexpensive MCs has generated intense interest in their use as chemical and biological sensors (17, 18, 21, 50, 56, 92-94, 104, 109). Additionally, MCs can be used with on-chip circuitry and in microcantilever arrays (MCAs) for high throughput and simultaneous differential assays and bioaffinity studies with a very small transducer footprint that potentially could be employed in the field.

A MC suitable for biosensing is modified on one side with some receptor phase that has some degree of affinity for the analyte. By exploiting PXR's affinity for a diverse range of ligands, we are able to screen for xenobiotics and target specific compounds quickly and without extensive, time-consuming labeling techniques and cell preparation (39, 43, 79, 81, 120). Specific interactions of the target analytes with that phase cause an apparent surface stress and nanomechanical bending that may be conveniently monitored based on the beam bending technique commonly used in atomic force microscopy. The static bending (tip deflection, z_{max}) of the MC varies in selectivity and sensitivity due to preferential binding of analyte molecules on the functionalized,

active MC surface and is governed by Stoney's equation (14). See equation 4 in Chapter 1.

We demonstrate that detection based on nanomechanics for pharmaceuticals and endocrine disrupting chemicals (EDCs) can be accomplished with functionalized MCs. These measurements provide real-time measurements of surface stress changes in the low-to-sub-nanomolar range (50). Sensitivity is critical when nanomechanical biosensing is performed due to the ultra-trace concentrations of many xenobiotics that can impact biological systems. Nanostructured MC biosensors allow detection without labels and in a detection range that is applicable for real biological systems (112). PXR immobilized on a nanostructured MC surface provides sensitive and reversible detection of various pharmaceuticals and environmental contaminants or EDCs. To our knowledge, this is the first time the orphan nuclear receptor PXR has been immobilized on a MC surface. Due to PXR's LBDs unique nature we saw interesting results in our concentration studies with rifampicin as well as surprising responses when utilizing different tagged receptors.

4.2 Experimental

Experiments were performed using commercially available silicon arrays of MCs having dimensions 400µm length, 100µm width, and approximately 1µm thickness (Mikro Masch Co., Sunnyvale, CA). Chromium, gold, and silver metals deposited on the MCs were obtained from Kurt J. Lesker, Gatewest, and Alfa Aesar Co., respectively, at 99.9% purity. 2-Aminoethanethiolhydrochloride (AET), glutaraldehyde (GA), the salts employed for the preparation of buffer solutions, and all other reagents were purchased from Sigma-Aldrich Chemical Co (St. Louis, MO) or Fisher at highest available purity

and used as received. The EDCs, phthalic acid, nonylphenol and bisphenol A were also obtained from Sigma-Aldrich. The pharmaceuticals, rifampicin, pregnenolone-16α-carbonitrile (PCN), and 3-methylcholanthrene (3-MC) were purchased from Sigma Aldrich. Glutathione-s-transferase (GST)-tagged human PXR was purchased from Invitrogen (Carlsbad, California). 6-histidine (6-HIS)-tagged human PXR was generously provided by Astra Zeneca. Ovalbumin was purchased from Sigma Aldrich. Water used to prepare solutions was obtained from a Branstead E-pure water filtration system.

The process of creating nanostructured surfaces on MCs is described in detail elsewhere (49). The cantilevers were first cleaned in a piranha bath (75% H_2SO_4, 25% H_2O_2) for 30 minutes, followed by thorough rinsing in deionized water [Caution: piranha solution reacts violently with organics]. The MCs were then placed into a physical vapor deposition (PVD) chamber (Cooke Vacuum Products, Model CVE 301, South Norwalk, CT) to be coated on one side with the appropriate metallic films using thermal deposition. To create a nanostructured MC, a thin film (~ 5nm) of chromium was applied to the surface to act as an adhesion layer followed by a thin film of gold (~15nm). Next, a film consisting of gold and silver was co-deposited. Subsequently, the silver was chemically removed via oxidation from the film ("dealloying") using an aqueous solution of 5 mg/mL $HAuCl_4$ leaving a gold surface with nanosized, colloid-like features. The thickness of the dealloyed gold layer was ~100 or ~150 nm in these studies. Chapter 1 and Chapter 3 provide more information on the background of nanostructured surfaces and optimized dealloyed conditions.

Nanostructured MCs were chemically modified by immersion in 1mM aqueous solution of AET for one hour producing a self-assembled monolayer of AET on the cantilever surface. Following thorough rinsing in deionized water, the amino groups were derivatized with the cross linker by immersing the cantilever in a 1% (w/v) solution of GA in pH 8 10 mM phosphate buffered saline (PBS) for three hours (95, 115). The chemically treated cantilever was allowed to soak in a large volume of water for a few minutes to remove any nonspecifically bound GA on the nanostructured and silicon sides of the cantilevers. Subsequently, immobilization of both the PXR nuclear receptor and the ovalbumin was achieved in random orientation by dipping the functionalized cantilevers into 100 mg/L solutions of receptor or protein in phosphate buffered saline (PBS, 10mM, pH=7) for four hours. During functionalization with PXR, the MCs dipped into the receptor samples were kept at 4°C to maintain activity. Both PXR and ovalbumin were separately immobilized on the functionalized surfaces of different cantilevers from separate arrays. After washing with PBS, the functionalized microcantilevers could be stored in PBS at 4°C until it is used.

The MC deflection measurements were carried out using the optical beam-deflection technique. The apparatus included a 5 mW diode laser (Coherent Laser Corp., Auburn, CA) operating at 632 nm, a spatial filtering and focusing system, and an in-house built position sensitive optical detector (Fig. 2). The output of the detector was displayed and recorded using a SRS 850 DSP lock-in amplifier as a multichannel digital recorder (Stanford Research Systems, Sunnyvale, CA). The signal output is recorded as volts (approximately 1 nm z_{max} per mV output). Data was collected at 1 Hz and then a moving averaging algorithm covering 180 data points was used to generate the figures

presented herein. This smoothing did not alter the shape of the true response curves (92). Chapter 1 provides more information on the static bending setup.

The cantilever system was mounted inside a ~5μL volume flow cell made of a 3 cm diameter by 2 cm long Delrin rod that was machined with 1/16 inch diameter input and output holes that meet at 1 cm distance apart at the face of the rod. Narrow bore tubing of 1/16 inch O.D. was slid into the holes up to the rod face and secured with fittings. A semi transparent silicone gasket, which is slightly thicker than the MC chip (~500μm versus 400μm), was cut with a scalpel tool to form a ~250 μm wide flow channel between the input/output holes and to tightly hold the MC chip. The silicone gasket is sandwiched between the Delrin rod face and a thin quartz window. A Watec CCD camera (Edmund Industrial Optics, Barrington, NJ) was used to image the MC chip in the flow cell (Fig. 8). The camera facilitated aligning the focused laser beam to reflect off the cantilever tip. Analyte solutions were delivered to the flow cell via a system of vessels connected to three-way valves allowing for switching between different solutions. The gravity-driven flow was generally adjusted to 100 μL/minute by adjusting vessel height.

Many of the pharmaceuticals and EDCs are sparingly soluble in water. Thus, 1×10^{-2}M stock solutions of all EDCs and some pharmaceuticals were prepared in pure methanol and then diluted with PBS (10mM Phosphate Buffer + 10mM $NaNO_3$, pH = 7.0) to make the desired concentration of each analyte [Caution: because of their potential harmful effects, care must be taken in the handling and disposing of EDC and pharmaceutical solutions]. PCN pharmaceutical stock solution was prepared in acetone. PBS was also used as a background solution. MCs mounted in the flow cell

were initially allowed to equilibrate in PBS until the signal was stable. For our purposes, tensile and compressive responses involve contraction and expansion of the active MC surface, respectively.

4.3 Results and Discussion

Our studies focus on developing MC systems utilizing the nuclear receptor PXR as the immobilized bioreceptor phase. We demonstrate that our immobilization process does not appreciably denature the PXR. The magnitude based response order for PXR activators is maintained when compared to well-established assays. With these PXR active analytes, PXR selectivity is demonstrated when compared to a similarly sized immobilized protein. The assay magnitude based response order is also maintained when PXR is exposed to EDCs. Reproducibility and sensitivity is illustrated using a potent PXR activator, rifampicin. To demonstrate the translation of receptor-ligand binding into MC surface stress, we compare receptor tag size and amino acid residue makeup of two tags, glutathione S-transferase (GST) and 6-histidine (6-HIS) tag. Our developing PXR MC biosensor, in support of fundamental nuclear receptor studies, may prove to be a quick, less expensive method for EDC screening and possible drug-drug interaction predictions.

Sensitivity enhancement in biosensing is key due to the small concentrations of ligands that can activate nuclear receptors. By nanostructuring the active MC surface, we are able to substantially improve the sensitivity, which has in many cases surpassed the increase in surface area (5, 17, 49). The initial “dealloying” of the MC surface provides a

greater surface area for nuclear receptor immobilization, which leads to an enhancement in sensitivity.

Fig. 20 compares the responses of a PXR functionalized MC when exposed to three analytes in PBS. This figure illustrates that $1x10^{-6}$ M rifampicin is the most potent PXR activator in this group. Our experiments in the detection of rifampicin using the nuclear receptor, PXR, showed good measurement reproducibility in the same day tested via three replicate consecutive injections of $1x10^{-6}$ M solution (see Fig. 20 inset). Coefficients of variation (CVs) for measurements using a given system of MC and molecular-recognition phase are generally 10% or better (15, 17, 21, 50, 92). The relatively slow response kinetics is comparable to prior biosensor MC experiments (15, 21, 50). This provides strong evidence that the ligands interact with the LBD causing conformational changes in the immobilized PXR, which translates into a large apparent surface stress on the cantilever. The high binding affinity of human PXR for rifampicin followed by PCN has been observed by other researchers (39, 43, 72, 73, 121, 122). Although 3-MC is predicted to have a low binding energy to the LBD of human PXR (123), it has been shown to be activated by members of the cytochrome P450 family of enzymes, which include activating CYP1A1/2 enzymes (124-126). The magnitude response order of rifampicin > PCN > 3-MC is what we expected from the literature. In our previous studies, the reversible compressive response is also observed for other bioreceptor functionalized dealloyed surfaces whereas smooth gold MC shows an irreversible compressive response on exposure to the same concentration of analytes (21, 50).

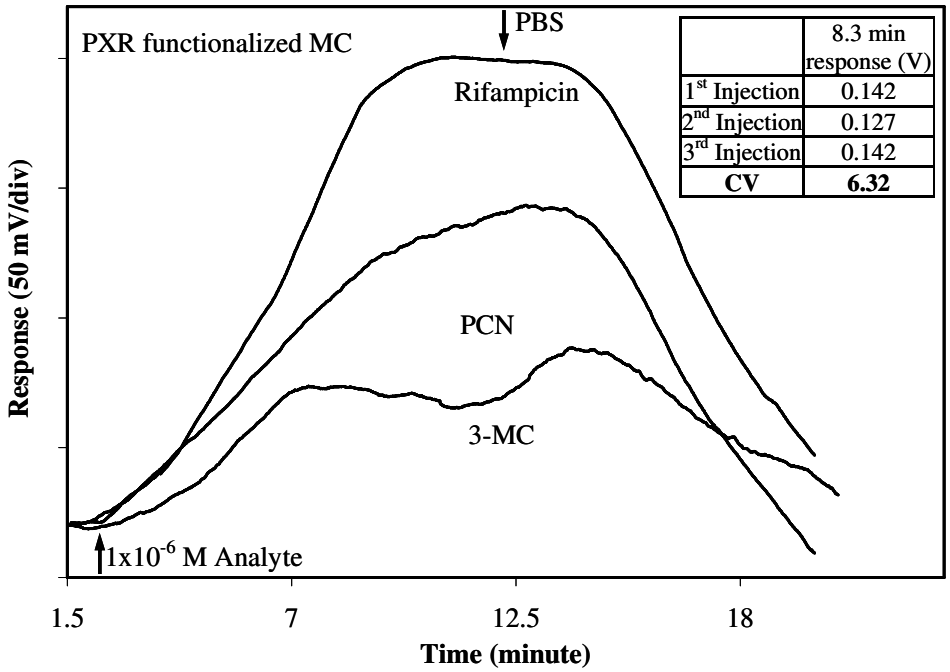

	8.3 min response (V)
1st Injection	0.142
2nd Injection	0.127
3rd Injection	0.142
CV	**6.32**

Fig 20. Comparison of nanomechanical responses of PXR functionalized MC on exposure to $1x10^{-6}$ M of rifampicin, PCN, and 3-MC in PBS. Inset shows CV for three replicate injections of $1x10^{-6}$ M rifampicin with PXR functionalized MC.

Fig. 21 inset compares the response of specific protein (PXR) functionalized MC to nonspecific protein (ovalbumin) functionalized MC (blank) on exposure to the same concentration ($1x10^{-6}$ M) of rifampicin. A large compressive response was observed due to the binding of rifampicin with a MC modified with PXR receptor whereas no response was observed when the same analyte was exposed to the nonbinding protein (ovalbumin) immobilized MC. It is important to note that our system does not show a nonspecific blank response. This indicates that the surface immobilization procedure does not significantly alter the PXR's LBD function and selectivity. However, it can not be assumed that the surface immobilized receptors will retain the same ligand binding affinity as observed in free form. Fig. 21 compares the specific and non-specific response magnitude of $1x10^{-6}$ M rifampicin, PCN, and 3-MC to immobilized PXR and ovalbumin (blank).

EDC exposure could be adverse even at very small concentrations (62). EDCs can alter or inhibit the function of the endocrine system by binding to estrogen receptors, which are part of the nuclear receptor superfamily (40, 58, 71). Studies have shown that the nuclear receptor PXR binds to certain EDCs with different affinities (31, 127). Fig. 22 shows the nanomechanical response magnitude of PXR functionalized MCs on exposure to $1x10^{-6}$ M EDCs, phthalic acid, nonylphenol, and bisphenol A. The response magnitude order of PXR with these three EDCs is similar to prior work with phthalic acid > nonylphenol and with relatively no response or a very low response to bisphenol A (127). After MC exposure to EDCs, we injected $1x10^{-6}$ M rifampicin, a potent PXR activator, for comparison. As predicted, the rifampicin caused a large compressive response when compared to the EDCs (see inset).

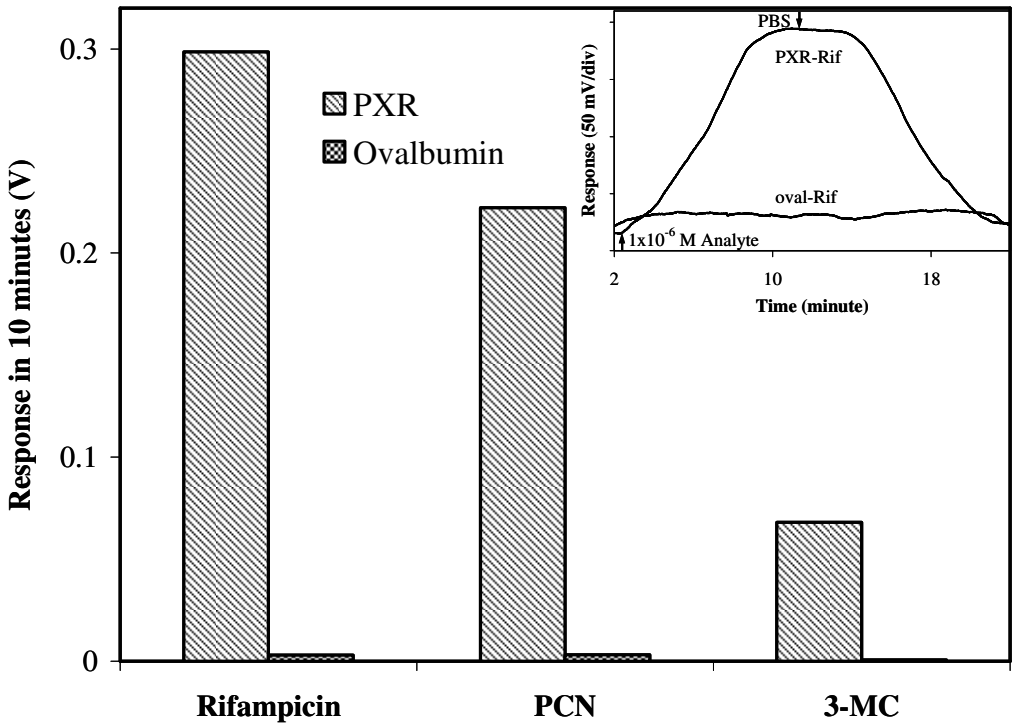

Fig 21. Comparison of nanomechanical responses of PXR and ovalbumin functionalized MCs exposed to $1x10^{-6}$ M rifampicin, PCN, and 3-MC in PBS. Inset shows representative traces of ovalbumin and PXR functionalized MCs on exposure to $1x10^{-6}$ M rifampicin in PBS.

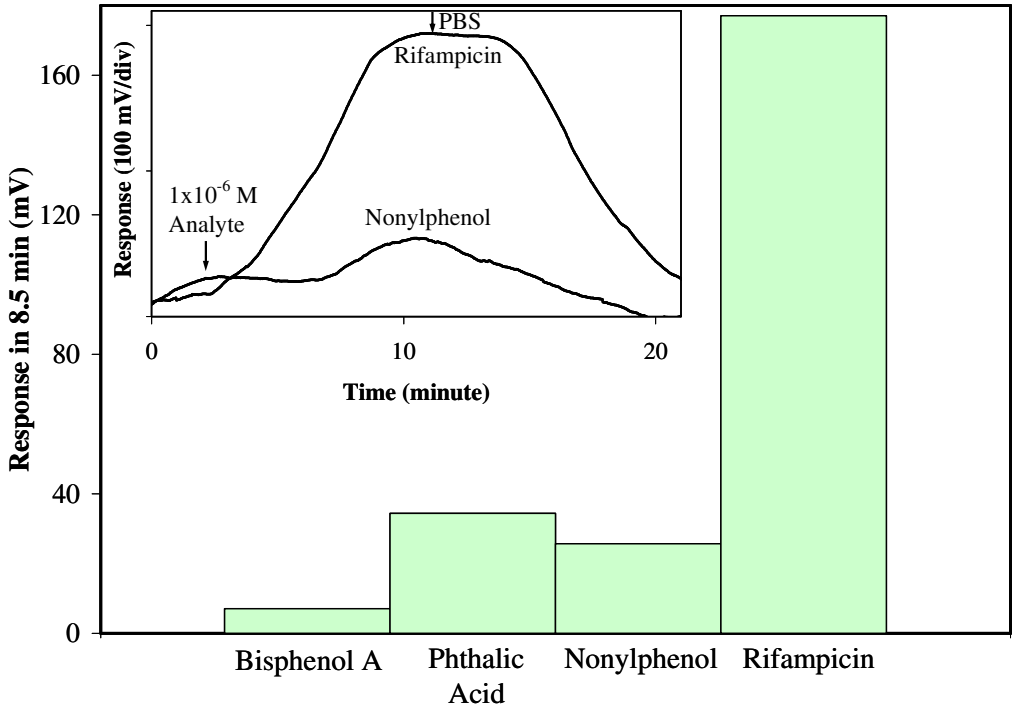

Fig 22. Comparison of response magnitudes in 8.5 min of PXR functionalized MC on exposure to $1x10^{-6}$ M analytes in PBS, which include three EDCs. The inset shows representative responses of PXR functionalized MC exposed to $1x10^{-6}$ M nonylphenol and rifampicin.

Fig. 23A demonstrates nanomechanical response profiles of PXR receptor functionalized MC to different concentrations of rifampicin in the range of 0.1 nM to 1 μM where the response increases with increasing concentration. The response magnitude does not increase as significantly as expected with increasing concentration. This may be due to the structural flexibility of the LBD. The expansion of the LBD size to accommodate for rifampicin's large size could have an effect on the interaction's translation to MC surface stress. Rifampicin is one of the largest known ligands for PXR at 823 Da (81). It is also possible that once ligand binding rearrangement of the PXR occurs, the protein does not quickly or completely reassume its original conformation (renature) upon ligand removal. The kinetic response of the cantilever at 6.7 minutes of exposure is plotted against concentration of rifampicin in Fig. 23B. As illustrated in the figure, the response increased gradually and reached a plateau by 100 nM. The inset in Fig. 23B shows a linear dynamic range for two orders of magnitude (the first data point corresponds to the lowest concentration in Fig. 23B 0.1 nM) in concentration.

In our current functionalization procedure, the protein is immobilized on the MC surface with GA without excessive denaturing of the protein (55). This is accomplished by the aldehyde groups in the GA reacting with lysine residues in the receptor (54). This makes the number and location of the lysine residues that make up the protein or receptor important to our random immobilization process. The tags on the PXR LBD allows for the purification of the receptor. The amino acids present in the tag and their location could be beneficial or detrimental to our MC receptor functionalization. GST-tagged human PXR LBD from Invitrogen has a calculated molecular weight of

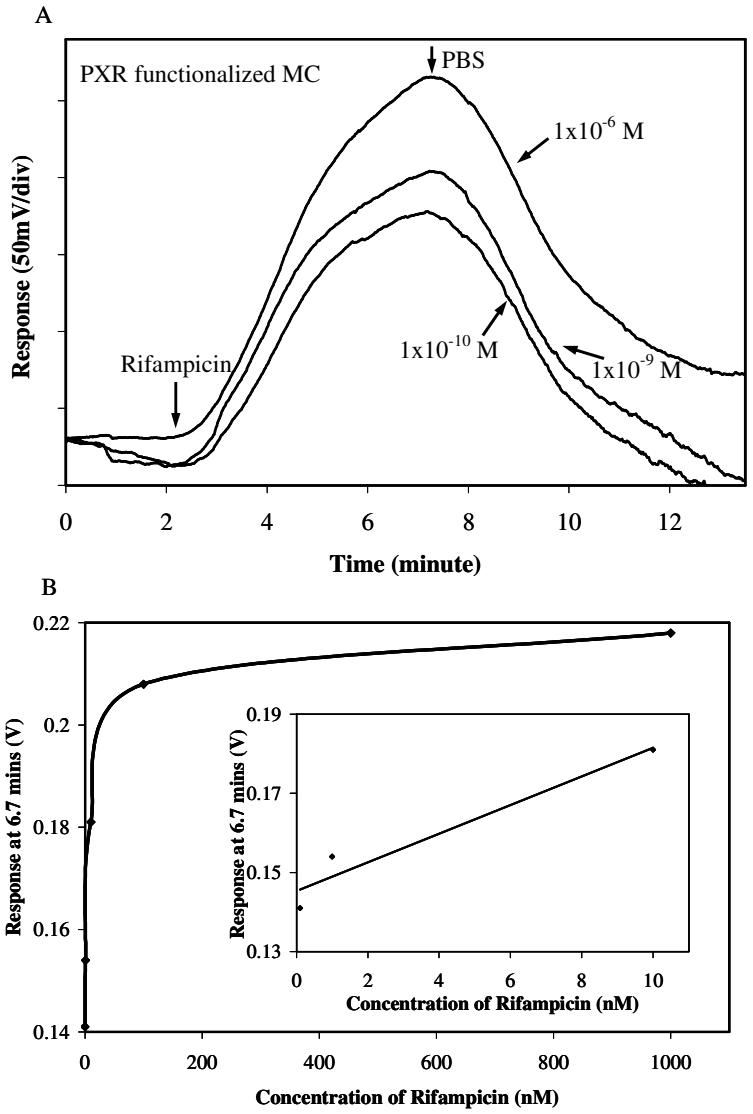

Fig. 23. (A) Concentration-based nanomechanical responses of PXR functionalized MC to different concentrations of rifampicin in PBS over the range $1x10^{-10}$ to $1x10^{-6}$ M. (B) Responses to rifampicin at 6.7 min for PXR are plotted over a concentration range from $1x10^{-10}$ M to $1x10^{-6}$ M, respectively.

64.70 kDa. The approximate molecular weight of human PXR LBD is 37.35 kDa, which leads to the calculated molecular weight for the GST-tag to be 27.35 kDa. The GST-tag and the PXR LBD have similar molecular weights in this case. The 6-HIS-tag on the Astra Zeneca LBD PXR is approximately 2524 Da and contains no lysine residues. The GST-tag contains an estimated 21 lysine residues, depending on which version of the GST was used in the preparation. 6-HIS-tagged PXR LBD was not bound to the surface by the tag, but by the nuclear receptor itself, where as the much larger GST-tag could have been the component bound on the MC surface. Fig. 24A compares the responses of 6-HIS-tagged LBD PXR and GST-tagged LBD PXR upon exposure to $1x10^{-6}$ M rifampicin. The 6-HIS-tagged LBD PXR gives a large compressive response whereas the GST-tagged LBD PXR shows no response. This indicates that the GST-tag may be bound to the surface and could have the PXR too far from the surface. This distance from the surface may not allow the conformational change upon ligand binding to translate efficiently to measureable surface stress. The very small, lysine deficient 6-HIS-tag requires the receptor to be surface bound and could easily transfer conformational change to the MC surface. This is illustrated through a schematic in Fig. 24B.

In summary, a sensitive, selective, and reusable biosensor for the study of PXR activating chemicals has been developed using nanostructured MCs. Our results indicate that the interaction of LBD PXR with various ligands produced different cantilever responses showing the maximum response for the antibiotic rifampicin. PXR functionalized MCs showed responses to rifampicin in concentrations down to $1x10^{-10}$ M.

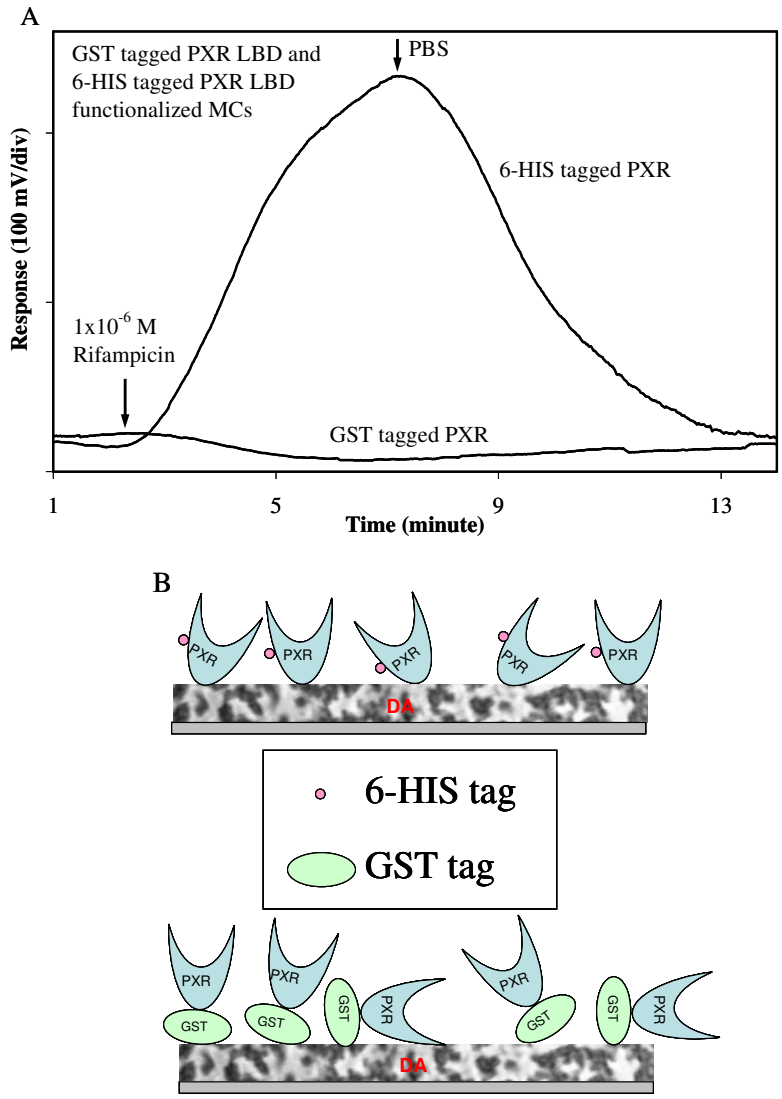

Fig 24. (A) Comparison of 6-HIS tagged PXR LBD (AZ) and GST tagged PXR LBD (Invitrogen) on exposure to $1x10^{-6}$ M rifampicin in PBS. (B) Schematic depiction of 6-HIS tagged PXR and GST tagged PXR immobilized on DA MC surface. Demonstrates the space between the DA and the PXR LBD depending on the tag.

Dissimilarity in tag size and residue makeup also indicate differences in receptor-ligand binding translation into MC surface stress.

Chapter 5 Summary

The development of biosensors is critical to understanding complex biological processes and pathways in the body. Understanding these processes can make it easier to determine where, when, and possibly why diseases start and how they move through the body. Since trace concentrations of contaminates can cause debilitating health problems, screening and detection of these compounds may be crucial to lessening or eliminating them from the environment. The research presented in this work utilized biofunctionalized MC sensors to study contaminate interaction with various receptors. Chapter 2 presented estrogen receptor and antibody studies on various EDCs. Nanostructured MCs were functionalized with two subtypes of estrogen receptor, ER-α and ER-β, then exposed to naturally occurring and synthetic potential EDCs. ER-α and ER-β showed different responses to each EDC, which followed the response magnitude order of more established bioassays. An EDC specific antibody was immobilized on DA MCs which responded with high sensitivity and selectivity to the specific EDC and showed very little interaction with non-specific ligands. These studies help demonstrate that immobilizing bioreceptors on the MC surface allow the receptor to maintain some of it's ligand binding capabilities and it's ability to distinguish between various ligands.

Chapter 3 focused on optimizing DA morphology and chemical immobilization of proteins. The nanostructured surface and the chemical linking of the protein to the MC can influence the sensitivity, selectivity, and reversibility of the biofunctionalized MC sensor. Optimizing the MC surface and immobilizing conditions may help improve the MC biosensor performance. The dealloying parameters, which include thickness and

metal ratio, were initially optimized with the model test system, anti-IgG-IgG. Proteins are chemically immobilized with a SAM of AET and GA linkage. Chemical linking conditions were optimized including concentration, pH, and reaction time by testing with the same model test system as the DA. Protein incubation time and conditions were optimized with two model test systems, which are anti-IgG-IgG and anti-biotin-biotin. This was to include large ligands and small ligands, which are called haptens. The optimized conditions for the model test system, anti-IgG-IgG, are as follows: 50 Au: 50 Ag 150 nm DA, 1 mM aqueous solution of AET with a 1 hour reaction time, 1% GA solution in 10 mM PBS pH 8 with a 3 hour reaction time, 0.5 mg/mL anti-IgG in 10 mM PBS pH 7 with an incubation time of 1 hour. The optimized and non-optimized conditions were applied to detecting TDCs with the thyroid transport protein, TBG. The selectivity pattern for various TDCs followed the response magnitude patterns established by other researchers' studies. Surprising results were obtained when performing orientation studies with protein A on anti-IgG and IgG functionalization, indicating that specific orientation of the immobilized protein may not always yield better responses than randomly orientated immobilized proteins.

Chapter 4 studied EDC and pharmaceutical interactions with the orphan nuclear receptor PXR. PXR plays an important role in metabolizing endogenous compounds to remove them from the body. Immobilizing PXR onto the nanostructured MC surface allowed for the study of ligand interaction with PXR's LBD. PXR functionalized MC interaction with the antibiotic rifampicin, a known PXR activator, was studied. Pharmaceutical and chemical interaction was studied with PXR and also a similarly sized non-specific protein, ovalbumin, to show the selectivity of the interactions. PXR

functionalized MCs were also exposed to EDCs, which demonstrated that the response magnitude order for the EDCs is similar to prior assay studies. The tag size and residue makeup was studied on immobilized PXR to illustrate the importance of receptor conformational change upon ligand binding translating into MC surface stress.

Coefficients of variation (CVs) for measurements using a given system of MC and biological molecular-recognition phase are generally 10% or better (15, 20, 21, 50). The immunosensor for human interleukin-1 β (HILI-β) Ab on exposure to HILI-β antigen showed a CV of 10% of triplet replicate intra day injections (50). In stereoselective detection, we have shown detection of chiral amino acids with antibody immobilized MCs with excellent same day reproducibility (CV=2%) (9). For endocrine disrupting chemical sensing, we have demonstrated CVs of 2.4% and 3.1% for triplicate replicate consecutive intra-day injections of 17-β-estradiol with estrogen receptor β and 17-β-estradiol antibody (15). ER-β functionalized MC arrays prepared in different batches showed 8-10% CV values in the detection of different concentrations of 17-β- ES.

To investigate stability, anti-17-β-ES Ab functionalized MC was exposed to 1×10^{-9} M of 17-β-ES at three different periods after storing in PBS at 4°C (2-nd, 4-th, and 8-th day after functionalization), an average value of deflection on day 4 and day 8 were 97% and 76% of the initial response, respectively. Similarly, the stability of ER-β functionalized MC was studied over periods of 5 days after storing in PBS at 4°C wherein it showed poorer stability; exposure to 1×10^{-9} M of 17-β-ES yielded responses after 3 and 5 days that were 78% and 36% of the initial response, respectively. Also, the

stability of ER-functionalized MC was tested at 4°C varying the environment (stored dry versus in PBS). The results showed that the immobilized antibody retained it's functionality for a longer period of time (7-10 days after functionalization) if stored dry at 4°C whereas it can be stored in PBS for near immediate use. Surprisingly, in both of the experiments performed, the response actually increased by a factor of two after one week of dry storage at 4°C. LBD PXR functionalized MC on exposure to intra-day triplicate sequential injections of $1x10^{-6}$ M rifampicin showed a CV of 6.32%. In general, good reproducibility is seen for bioreceptor functionalized nanostructured MCs.

The research presented in this work is the beginning of creating complex bioarray sensors that can better mimic biological systems. The promise of creating label-free bioarrays comprised of nuclear receptors and antibodies to study their simultaneous interactions with contaminants and pharmaceuticals with real-time measurement could be an important step to better understanding some biological pathways. A bioarray could help in studying contaminate-drug and drug-drug interactions, which is critical in pharmaceutical development and contaminate screening. Bioarrays may also be useful in studying mixtures of analytes, yielding information about specific interactions with receptors and may show that competitive interactions could occur in our system. Future work could also involve studying the aspects of analyte saturation of the immobilized receptor and this saturation effect on receptor recovery upon buffer introduction.

References

1. Binnig, G.; Quate, C. F.; Gerber, C. *Phys. Rev. Lett*. **1986**, 56, 930-933.
2. Alexander, S.; Hellemans, L.; Marti, O.; Schneir, J.; Elings, V.; Hansma, P. K. *J. Appl. Phys*. **1989**, 65, 164-167.
3. Thundat, T; Warmack, R. J.; Chen, G.Y.; Allison, D. P. *Appl. Phys. Lett*. **1994**, 64, 2894-2903.
4. Barnes, J. R.; Stephenson, R. J.; Welland, M. E.; Gerber, C.; Gimzewski, J. K. *Nature* **1994**, 372, 79-81.
5. Sepaniak, M.; Datskos, P.; Lavrik, N.; Tipple, C. *Anal. Chem*. **2002**, 568A-575A.
6. Lavrik, N. V.; Sepaniak, M. J.; Datskos, P. G. *Rev. Sci. Instrum.* **2004**, 75, 2229-2253.
7. Sauerbrey, G. Z. *Phys*. **1959**, 155, 206-222.
8. Wohltjen, H.; Dessy, R. *Anal. Chem*. **1979**, 51, 1458-1464.
9. Yan, X.; Ji, H.; Thundat, T. *Curr. Anal. Chem.* **2006**, 2, 297-307.
10. Campbell, G. A.; Mutharasan, R. *Anal. Sci*. **2005**, 21, 355-357.
11. Gupta, A.; Akin, D.; Bashir, R. *Appl. Phys. Lett*. **2004**, 84, 1976-1978.
12. Dareing, D. W.; Tian, F.; Thundat, T. *Ultramicroscopy* **2006**, 106, 789-794.
13. Israelachvili, J. *Intermolecular and Surface Forces*, 2nd ed.; Academic Press: San Diego, 1991.
14. Stoney, G. G. *Proc. R. Soc. London, Ser. A*, **1909**, 82, 172-177.
15. Dutta, P.; Hill, K.; Datskos, P. G.; Sepaniak, M. J. *Lab Chip* **2007**, 7, 1184-1191.
16. Lavrik, N. V.; Tipple, C. A.; Sepaniak, M. J.; Datskos, P. G. *Biomed. Microdevices* **2001**, 3, 35-44.
17. Tipple, C. A.; Lavrik, N. V.; Culha, M.; Headrick, J.; Datskos, P.; Sepaniak, M. J. *Anal. Chem*. **2002**, 74, 3118-3126.
18. Grogan, C.; Raiteri, R.; O'Connor, G. M.; Glynn, T. J.; Cunningham, V.; Kane, M.; Charlton, M.; D. Leech *Biosens. Bioelectron.* **2002**, 17, 201-207.
19. Chapman, P. J.; Long, Z.; Datskos, P. G.; Archibald, R.; Sepaniak, M. J. *Anal. Chem.* **2007**, 79, 7062-7068.
20. Hill, K.; Dutta, P.; Zareba, A.; Eldridge, M. L.; Sepaniak, M. J. *Anal. Chim. Acta* **2008**, 625, 55-62.
21. Dutta, P.; Tipple, C. A.; Lavrik, N. V.; Datskos, P. G.; Hofstetter, O.; Sepaniak, M. J. *Anal. Chem*. **2003**, 75, 2342-2348.
22. Schultz, J. S.; Taylor, R. F. *Handbook of Chemical and Biological Sensors*. Institute of Physics Publishing: Bristol, 1996.
23. Hauptmann, P. *Sensors: Principles and Applications*. Carl Hanser Verlag and Prentice Hall: Munich and Hertfordshire, 1991.
24. Nelson, J. M.; Griffin, E. G. *J. Am. Chem. Soc*. **1916**, 38, 1109-1115.
25. Hughes, W. S. *J. Am. Chem. Soc*. **1922**, 44, 2860-2866.
26. Janata, J. *Principles of Chemical* Sensors. Plenum Press: New York, 1989.
27. Janata, J.; Bezegh, A. *Anal Chem* **1988**, 60, 62R-74R.
28. Fireman-Shoresh, S.; Popov, I.; Avnir, D.; Marx, S. *J. Am. Chem. Soc*. **2005**, 127, 2650-2655.

29. Xu, C.; Ng, S. C.; Chan, H. S. O. *Langmuir* **2008**, 24, 9118-9124.
30. Trojanowicz, M.; Kaniewska, M. *Electroanalysis* **2009**, 21, 229-238.
31. Masuyama, H.; Suwaki, N.; Tateishi, Y.; Nakatsukasa, H.; Seqawa, T.; Hiramatsu, Y. *Mol. Endocrinol.* **2005**, 19, 1170-1180.
32. Kerrigan, S.; Phillips, W. H. *Clin. Chem*. **2001**, 47, 540-547.
33. Mikami, E.; Ohno, T.; Matsumoto, H.; Sekita, S. *Journal of Health Science* **2003**, 49, 547-550.
34. Meulenberg, E. P.; Peelen, G. O. H.; Lukkien, E.; Koopal, K. Intern. *J. Environ. Anal. Chem.* **2005**, 85, 861-870.
35. Schneider, C.; Schöler, H. F.; Schneider, R. J. *Anal. Chim. Acta* **2005**, 551, 92-97.
36. Friguet, B.; Chaffotte, A. F.; Djavadi-Ohaniance, L.; Goldberg, M. E. *J. Immunol. Methods* **1985**, 77, 305-319.
37. Meerts, I. A. T. M.; Van Zanden, J. J.; Luijks, E. A. C.; Van Leeuwen-Bol, I.; Marsh, G.; Jakobsson, E.; Bergman, A.; Brouwer, A. *Toxicol. Sci*. **2000**, 56, 95-104.
38. Olsson, R. A.; Davis, C. J.; Gentry, M. K.; Vomacka, R. B. *Anal. Biochem.* **1978**, 85, 132-138.
39. Jones, S. A.; Moore, L. B.; Shenk, J. L.; Wisely, G. B.; Hamilton, G. A.; McKee, D. D.; Tomkinson, N. C. O.; LeCluyse, E. L.; Lambert, M. H.; Willson, T. M.; Kliewer, S. A.; Moore, J. T. *Mol. Endocrinol.* **2000**, Vol 14, 27-39.
40. Kuiper, G. G. J. M.; Lemmen, J. G.; Carlson, B.; Corton, J. C.; Safe, S. H.; Van Der Saag, P. T.; Van Der Burg, B.; Gustafsson, *J. Endocrinology* **1998**, 139, 4252-4263.
41. Lans, M. C.; Spiertz, C.; Brouwer, A.; Koeman, J. H. *Eur. J. Pharmocol. Environ. Toxicol. Pharm.* **1994**, 270*,* 129-136.
42. Jones, S. A.; Moore, L. B.; Wisely, G. B.; Kliewer, S. T. *Methods Enzymol. Cytochrome P450 Part C* **2002**, 357, 161-170.
43. Moore, L. B.; Parks, D. J.; Jones, S. A.; Bledsoe, R. K.; Consler, T. G.; Stimmel, J. B.; Goodwin, B.; Liddle, C.; Blanchard, S. G.; Willson, T. M.; Collins, J. L.; Kliewer, S. A. *J. Biol. Chem.* **2000**, 275, 15122-15127.
44. Ohno, K.; Fukushima, T.; Santa, T.; Waizumi, N.; Tokuyama, H.; Maeda, M.; Imai, K. *Anal. Chem*. **2002**, 74, 4391-4396.
45. Ito, Y.; Fujita, S.; Kawazoe, N.; Imanishi, Y. *Anal. Chem*. **1998**, 70, 3510-3512.
46. Wild, D. , Ed. *The Immunoassay Handbook*, 2nd ed.; Nature Publishing Group: New York, 2001.
47. Nelson, D. L.; Cox, M. M. *Principles of Biochemistry*, 4th ed.; W. H. Freeman and Company: New York, 2005.
48. Kohler, G.; Milstein, C. *Nature* **1975**, 256, 495-497.
49. Lavrik, N. V.; Tipple, C. A.; Sepaniak, M. J.; Datskos, P. G. *Chem. Phys. Lett.* **2001**, 336, 371-376.
50. Dutta, P.; Sanseverino, J.; Datskos, P. G.; Sepaniak, M. J. *NanoBiotechnology* **2005**, 1, 237-244.

51. Cass, T.; Ligler, F. S., Ed. *Immobilized Biomolecules in Analysis*. Oxford University Press: New York, 1998.
52. Nuzzo, R. G.; Allara, D. L. *J. Am. Chem. Soc*. **1983**, 105, 4481-4483.
53. Margel, S. J. *Polym. Sci. Polym. Chem. Ed*. **1984**, 22, 3521-3533.
54. Walt, D. R.; Agayn, V. I. *Trends Anal. Chem.* **1994**, 13, 425-430.
55. Hopwood, D.; Allen, C. R.; McCabe, M. *Histochemical Journal* **1970**, 2, 137-150.
56. Wu, G.; Datar, R. H.; Hansen, K. M.; Thundat, T.; Cote, R. J.; Majumdar, A. *Nat. Biotechnol*. **2001**, 19, 856-860.
57. Messina, M. J.; Persky, V.; Setchell, K. D. R.; Barnes, S. *Nutr. Cancer* **1994**, 21, 113-131.
58. Stoica, A. S.; Katzenellenbogen, B. S.; Martin, M. B. *Mol. Endocrinol.* **2000**, 14, 545-553.
59. Moriarty, K.; Kim, K. H.; Bender, J. R. *Endocrinology* **2006**, 147, 5557-5563.
60. Murdoch, F. E.; Gorski, J. *Mol. Cell Endocrinol*. **1991**, 78, C103-C108.
61. Greco, T. L.; Duello, T. M.; Gorski, J. *Endocrine Reviews* **1993**, 14, 59-71.
62. Kuramitz, H.; Natsui, J.; Sugawara, K.; Itoh, S.; Tanaka, S. *Anal. Chem*. **2002**, 74, 533-538.
63. Xue, N.; Xu, X.; Jin, Z. *Chemosphere* **2005**, 61, 1594-1606.
64. Sonnenschein, C.; Soto, A. M. J. *Steroid Biochem. Biol*. **1998**, 65, 143-150.
65. EPA website, Endocrine Disruptor Screening Program, www.epa.gov/oscpmont/oscpendo/index.htm
66. Robbins, J.; Edelhoch, H. *Werner's The Thyroid.* Lippincott: Philadelphia, 1986.
67. Schreiber, G. J. *Endocrinol*. **2002**, 175, 61-73.
68. Camerman, N.; Camerman, A. *Proc. Natl. Acad. Sci*. **1972**, 69, 2130-2131.
69. Marchesini, G. R.; Meulenberg, E.; Haasnoot, W.; Mizuguchi, M.; Irth, H. *Anal. Chem*. **2006**, 78, 1107-1114.
70. Brouwer, A.; Ahlborg, U. G.; Van den Berg, M.; Birnbaum, L. S.; Boersma, E. R.; Bosveld, B.; Denison, M. S.; Gray, L. E.; Hagmar, L.; Holene, E. *Eur. J. Pharmacol.* **1995**, 293, 1-40.
71. Mangelsdorf, D. J.; Thummel, C.; Besto, M.; Herrlich, P.; Schütz, G.; Umesono, K.; Blumberg, B.; Kastner, P.; Mark, M.; Chambon, P.; Evans, R. M. *Cell* **1995**, 83, 835-839.
72. Bertilsson, G.; Heidrich, J.; Svensson, K.; Åsman, M.; Jendeberg, L.; Sydow-Bäckman, M.; Ohlsson, R.; Postlind, H.; Blomquist, P.; Berkenstam, A. *Proc. Natl. Acad. Sci.* **1998**, 95, 12208-12213.
73. Blumberg, B.; Sabbagh, Jr., W.; Juguilon, H.; Bolado, Jr., J.; van Meter, C. M.; Ong, E. S.; Evans, R. M. *Genes Dev.* **1998**, 12, 3195-3205.
74. Kliewer, S. A.; Moore, J. T.; Wade, L.; Staudinger, J. L.; Watson, M. A.; Jones, S. A.; McKee, D. D.; Oliver, B. B.; Willson, T. M.; Zetterström, R. H.; Perlmann, T.; Lehmann, J. M. *Cell* **1998**, 92, 73-82.
75. Nuclear Receptors Nomenclature Committee, **1999**.

76. Nelson, D. R.; Koymans, L.; Kamataki, T.; Stegeman, J. J.; Feyereisen, R.; Waxman, D. J.; Waterman, M. R.; Gotoh, O.; Coon, M. J.; Estabrook, R. W.; Gunsalus, I. C.; Nebert, D. W. *Pharmacogenetics* **1996**, 6, 1-42.
77. Kliewer, S.A.; Lehmann, J. M.; Willson, T. M. *Science* **1999**, 284, 757-760.
78. Zhang, J.; Kuehl, P.; Green, E. D.; Touchman, J. W.; Watkins, P. B.; Daly, A.; Hall, S. D.; Maurel, P.; Relling, M.; Brimer, C.; Yasuda, K.; Wrighton, S. A.; Hancock, M.; Kim, R. B.; Strom, S.; Thummel, K.; Russell, C. G.; Hudson, Jr., J. R.; Schuetz, E. G.; Boguski, M. S. *Pharmacogenetics* **2001**, 11, 555-572.
79. Watkins, R. E.; Wisely, G. B.; Moore, L. B.; Collins, J. L; Lambert, M. H.; Williams, S. P.; Willson, T. M.; Kliewer, S. A.; Redinbo, M. R. *Science* **2001**, 292, 2329-2333.
80. Moore, L. B.; Maglich, J. M.; McKee, D. D.; Wisely, B.; Willson, T. M.; Kliewer, S. A.; Lambert, M. H.; Moore, J. T. *Mol. Endocrinol.* **2002**, 16, 977-986.
81. Chrencik, J. E.; Orans, J.; Moore, L. B.; Xue, Y.; Peng, L.; Collins, J. L.; Wisely, G. B.; Lambert, M. H.; Kliewer, S. A.; Redinbo, M. R. *Mol. Endocrinol.*, **2005**, 19, 1125-1134.
82. Zhou, C.; Verma, S.; Blumberg, B. *Nuclear Receptor Signaling* **2009**, 7, 1-21.
83. Kliewer, S. A.; Goodwin, B.; Willson, T. M. *Endocrine Reviews* **2002**, 23, 687-702.
84. Michalets E. L. *Pharmacotherapy* **1998**, 18, 84-112.
85. Moore, J. T.; Kliewer, S. A. *Toxicology* **2000**, 153, 1-10.
86. Watkins, R. E.; Maglich, J. M.; Moore, L. B.; Wisely, G. B.; Noble, S. M.; Davis-Searles, P. R.; Lambert, M. H.; Kliewer, S. A.; Redinbo, M. R. *Biochemistry* **2003**, 42, 1430-1438.
87. Sanseverino, J; Gupta, R. K.; Layton, A. C.; Patterson, S. S.; Ripp, S. A.; Saidak, L; Simpson, M. L.; Schultz, T. W.; Sayler, G. S. *Appl. Environ. Microbiol.* **2005**, 71, 4455-4460.
88. Asano, K.; Ono, A.; Hashimoto, T.; Inoue, T.; Kanno, J. *Anal. Sci*. **2004**, 20, 611-616.
89. Carmon, K. S.; Baltus, R. E.; Luck, L. A. *Anal. Biochem.* **2005**, 345, 277-283.
90. Murata, M; Gouda, K.; Yano, S.; Kuroki, T.; Suzutani, T.; Katayama, Y. *Anal. Sci*. **2003**, 19, 1355-1357.
91. Chemical Specificity for BioMEMS Sensing Session, Gordon Conference, Connecticut College, New London, CT, June 25-30, 2006.
92. Dutta, P.; Chapman, P. J.; Datskos, P. G.; Sepaniak, M. J. *Anal. Chem.* **2005**, 77, 6601-6608.
93. Berger, R.; Delamarche, E.; Lang, H. P.; Gerber, C.; Gimzewski, J. K.; Meyer, E.; Guntherodt, H. J. *Science* **1997**, 276, 2021-2024.
94. Shekhawat, G.; Tark. S. H.; Dravid, V. P. *Science* **2006**, 311, 1592-1595.
95. Premkumar, J. R.; Lev, O.; Marks, R. S.; Polyak, B.; Rosen, R.; Belkin, S. *Talanta* **2001**, 55, 1029-1038.
96. Crews, D.; Willingham, E.; Skipper, J. K. *Quart. Rev. Biol*. **2000**, 75, 243-260.
97. Zhu, B. T.; Han, G. H., Shim, J. Y.; Wen, Y.; Jiang, X. R. *Endocrinology* **2006**, 147, 4132-4150.
98. Nilsson, S.; Gustafsson, J. A. *Crit. Rev. Biochem. Mol. Biol*. **2002**, 37, 1-28.

99. Senesac, L.; Dutta, P.; Datskos, P. G.; Sepaniak, M. J. *Anal. Chim. Acta* **2006**, 558, 94-101.
100. Zhang, J.; Ji, H. F. *Anal. Sci.* **2004**, 20, 585-587.
101. Headrick, J. J.; Sepaniak, M. J.; Lavrik, N. V.; Datskos, P. G. *Ultramicroscopy* **2003**, 97, 417-424.
102. Raiteri, R.; Butt, H. J.; Grattarola, M. *Electrochim. Acta* **2000**, 46, 157-163.
103. Lang, H. P.; Baller, M. K.; Berger, R.; Gerber, C.; Gimzewski, J. K.; Battison, F. M.; Fornaro, P.; Ramseyer, J. P.; Meyer, E.; Guntherodt, H. J. *Anal. Chim. Acta* **1999**, 393, 59-65.
104. Thundat, T.; Wachter, E. A.; Sharp, S. L.; Warmack, R. J. *Appl. Phys. Lett*. **1995**, 66, 1695-1697.
105. Wee, K. W.; Kang, G. Y.; Park, J.; Kang, J. Y.; Yoon, D. S.; Park, J. H.; Kim, T. S. *Biosens. Bioelectron* **2005**, 20, 1932-1938.
106. Cherian, S.; Gupta, R. K.; Mullin, B. C.; Thundat, T. *Biosens. Bioelectron*. **2003**, 19, 411-416.
107. Alvarez, M.; Calle, A.; Tamayo, J.; Lechuga, L. M.; Abad, A.; Montoya, A. *Biosens. Bioelectron*. **2003**, 18, 649-653.
108. Hansen, K. M.; Ji, H. F.; Wu, G.; Datar, R.; Cote, R.; Majumdar, A.; Thundat, T. *Anal. Chem*. **2001**, 73, 1567-1571.
109. Fritz, J.; Baller, M. K.; Lang, H. P.; Rothuizen, H.; Vettiger, P.; Meyer, E.; Guntherodt, H.; Gerber, C.; Gimzewski, J. K., *Science* **2000**, 288, 316-318.
110. Moulin, A. M.; O'Shea, S. J.; Welland, M. E. *Ultramicroscopy* **2000**, 82, 23-31.
111. Raiteri, R.; Nelles, G.; Butt, H. J.; Knoll, W.; Skladal, P. *Sensor Actuat. B-Chem*. **1999**, B61, 213-217.
112. Mahalik, N. P., Ed. *Micromanufacturing and Nanotechnology*; Springer: Germany, 2006.
113. De Melo, J. V.; Bello, M. E.; De Azevedo, W. M.; De Souza, J. M.; Diniz, F. B. *Electrochim. Acta* **1999**, 44, 2405-2412.
114. Terumichi, N.; Masahiro, I. *Chem. Pharm. Bull* **1989**, 37, 2463-2466.
115. Park, S. W.; Kim, Y. I.; Chung, K. H.; Hong, S. I.; Kim, S. W. *React. Funct. Polym*. **2002**, 51, 79-92.
116. Law, B., Ed. *Immunoassay: A Practical Guide;* Taylor & Francis: London, 1996.
117. Brogan, K. L.; Wolfe, K. N.; Jones, P. A.; Schoenfisch, M. H. *Anal. Chim. Acta* **2003**, 496, 73-80.
118. Cheek, A. O.; Kow, K.; Chen, J.; McLachlan, J. A. *Environ. Health Persp*. **1999**, 107, 273-278.
119. Guengerich, F. P. *Cytochrome P450: Structure, Mechanism, and Biochemistry*, 3rd ed.; Plenum Publishers: New York, 2005.
120. Shukla, S. J.; Nguyen, D.; MacArthur, R.; Simeonov, A.; Frazee, W. J.; Hallis, T. M.; Marks, B. D.; Singh, U.; Eliason, H. C.; Printen, J.; Austin, C. P.; Inglese, J.; Auld, D. S. *Assay and Drug Development Technologies* **2009**, 7, 143-169.

121. Staudinger, J. L., Goodwin, B.; Jones, S. A.; Hawkins-Brown, D.; MacKenzie, K. I.; LaTour, A.; Liu, Y.; Klaassen, C. D.; Brown, K. K.; Reinhard, J.; Willson, T. M.; Koller, B. H.; Kliewer, S. A. *Proc. Natl. Acad. Sci.* **2001**, 98, 3369-3374.
122. Yeung, E. Y. H.; Sueyoshi, T.; Negishi, M.; Chang, T. K. H. *Drug Metab. Dispos.* **2008**, 36, 2270-2276.
123. Kortagere, S.; Chekmarev, D.; Welsh, W. J.; Ekins, S. *Pharm. Res.* **2009**, 26, 1001-1011.
124. Li, A. P. *Drug Metab. Dispos.* **2009**, 37, 1598-1603.
125. Abdelrahim, M.; Ariazi, E.; Kim, K.; Khan, S.; Barhoumi, R.; Burghardt, R.; Liu, S.; Hill, D.; Finnell, R.; Wlodarczyk, B.; Jordan, V. C.; Safe, S. *Cancer Res*. **2006**, 66, 2459-2467.
126. Jackson, J. P.; Kabirov, K. K.; Kapetanovic, I. M.; Lyubimov, A. *Chem.-Biol. Interact*. **2009**, 179, 263-272.
127. Masuyama, H.; Suwaki, N.; Tateishi, Y.; Nakatsukasa, H.; Segawa, T.; Hiramatsu, Y. *Mol. Endocrinol.* **2000**, 14, 421-428.

Appendix: Development of a Nanomechanical Biosensor for Analysis of Endocrine Disrupting Chemicals

Experimental

Aminoethanethiolhydrochloride (AET), glutaraldehyde (GA), the salts employed for the preparation of buffer solutions, and all other reagents were purchased from Sigma-Aldrich Chemical Co (St. Louis, MO) or Fisher at highest available purity and used as received. The proteins human immunoglobulin G (hIgG, reagent grade), protein A, and anti- human IgG were also obtained from Sigma-Aldrich.

Smooth gold (40nm) and dealloyed (50nm, 100nm, and 200nm) MCs were prepared (See Cantilever Modification in the main text) and functionalized with anti-human IgG antibody. Random functionalization (without protein A) of both the anti-human IgG antibody and human IgG was achieved by dipping the AET and GA functionalized MCs (see the Cantilever Modification under Experimental section in the main text) into 50mg/L solutions of protein in 10 mM phosphate buffered saline (PBS, pH 7) for 5 hours. Oriented functionalization (with protein A) was performed as follows. Initially, the AET and GA functionalized cantilevers were dipped into 100mg/L solutions of protein A in PBS for 1 hour, washed with PBS for several times and then the protein A functionalized cantilevers were dipped into 50mg/L solutions of anti-human IgG/human IgG in PBS for 5 hours. Both proteins were separately immobilized on the functionalized surfaces of different cantilevers from different microcantilever arrays.

Results and Discussion

Response characteristics of nanostructured MCs

Fig. Appendix-1 shows comparison of bending responses of antibody functionalized nanostructured MC to similarly functionalized smooth gold MC using anti human IgG antibody. When the nanostructured MC, functionalized with anti human IgG antibody was exposed to 50mg/L of human IgG, specific interaction of antibody-antigen exhibited 480mV (~380nm) cantilever tip deflection that corresponds to a compressive surface stress change. Upon flushing the cell with background buffer, the response was reversed. Conversely, similarly functionalized MC with a smooth gold surface shows a largely irreversible compressive response on exposure to the same concentration of human IgG; which was also observed by other researchers for specific interactions of different antibody-antigen pairs (See references 18, 56, and 100). When comparing a smooth to a nanostructured MC surface, 50nm dealloyed gold coating increases MC response by roughly a factor of two. In some prior applications not involving bioaffinity functionalized MC, the nanostructuring resulting in as much as 2-3 orders of magnitude enhancements in chemi-mechanical responses (References 17 and 49 show direct comparisons of dealloyed versus smooth gold surfaces) for both self-assembled monolayers and thin films of responsive phases. Some of this enhancement in response has been attributed to increased surface area for the nanostructured surfaces.

The reversibility of response for the nanostructured MC, despite very high sensitivity (see Figure 11 for example), is surprising and counter to the expected large

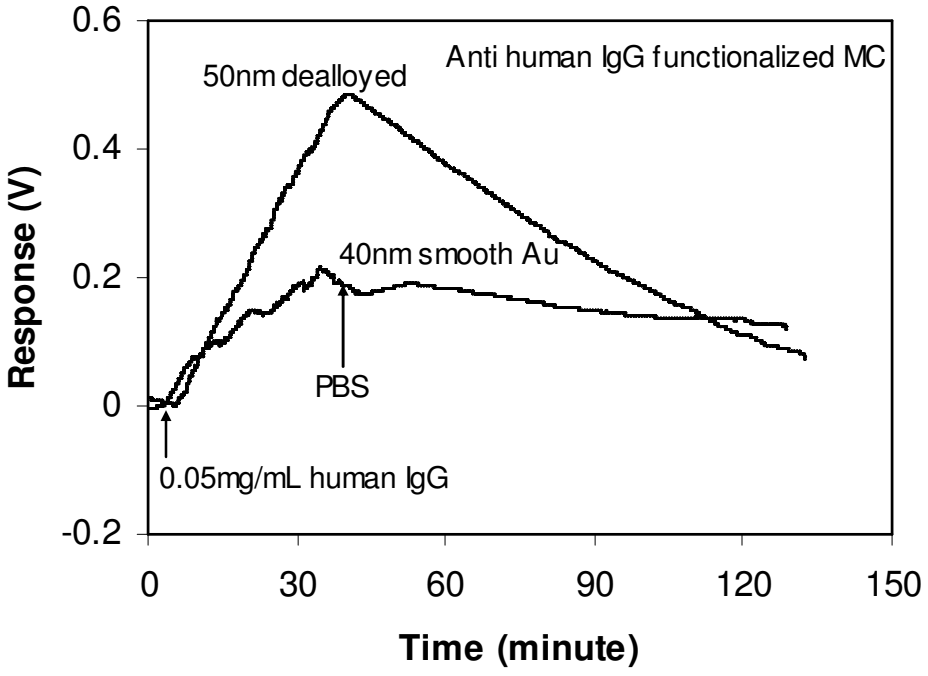

Fig. Appendix-1. Comparison of bending signals of anti human IgG antibody functionalized nanostructured (dealloyed) MC to similarly functionalized smooth gold MC.

affinity constants. The morphology and chemical nature of these two types of MC surfaces are not the same and perhaps chemical attachment of the bioreceptor in the dealloyed case shows a decrease in affinity constants that is compensated by the inherent larger responses of the large surface area nanostructured MC. It is also worth noting that we do not allow the establishment of equilibrium upon exposure to analyte (sampling only occurs for several minutes before we return to buffer flow). Long term exposure to the sample may not show the same reversibility. In any event, the fortuitous nature of high sensitivity with reversibility is a unique and valuable attribute of our bioaffinity nanomechanical sensing approach.

Concurrent with the studies described in the main text, we performed some optimization studies involving the dealloying process. Fig. Appendix-2 demonstrates the responses of anti human IgG antibody functionalized dealloyed MCs with different thicknesses of the dealloyed surfaces. On exposure to 0.05mg/mL of hIgG in 10 mM pH7 PBS for 10 minutes, antibody functionalized MCs showed increased response with increasing thickness of the dealloyed MCs. The response of the antibody functionalized 100nm and 200nm dealloyed MCs are 2.5 and 5 fold greater, respectively, than the response of the similarly functionalized 50nm dealloyed MCs. The work with EDC receptors was performed with the thinner 50nm dealloyed layer, thus even greater sensitivity than is demonstrated in the main text for EDC detection may be possible.

Random and Oriented functionalization of antibody and antigen

Both oriented and randomly functionalized MCs with anti human IgG or human IgG showed reversible compressive stress responses (expansion of the active surface) on

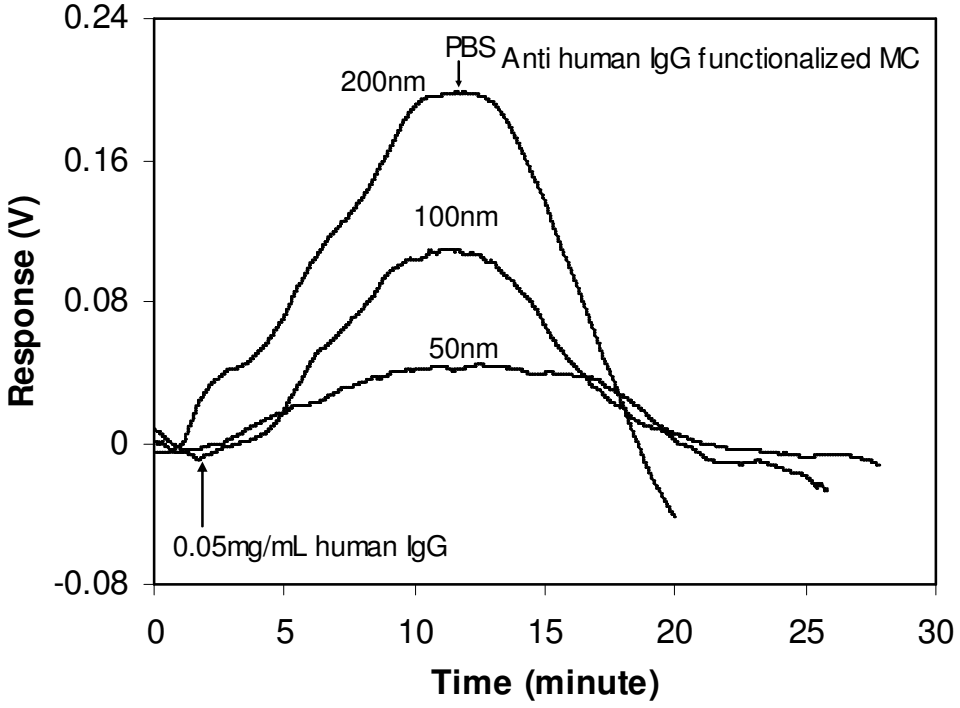

Fig. Appendix-2. Response of anti human IgG antibody functionalized nanostructured (dealloyed) MC with different thicknesses of the dealloyed surfaces on exposure to 0.05 mg/mL of human IgG in 10 mM pH 7 PBS.

exposure to different concentrations of human IgG (0.001mg/mL) or anti human IgG (0.05mg/mL) in PBS. It is interesting to observe that the random functionalization shows a three times larger response than the oriented case when the cantilever is functionalized with anti human IgG antibody. Conversely, when MC is functionalized with human IgG, oriented functionalization shows greater response than the random one when exposed to the antibody (See Table Appendix-1). These two different experiments demonstrate that proper orientation of bioreceptor proteins on the MC surface do not always yield improvements in response, presumably because of the stress induction response requirement (i.e. conformational changes upon analyte binding are important but depending on the nature of the linkage to the MC surface this conformational change may not translate into a large apparent surface stress). Note that both this specific monoclonal antibody and the protein A (the protein A may act in some cases as a spacer that reduces the induction of stress) are specific for the Fc portion of the IgG protein. Because of these complications, affinity constants determined by the nanomechanical approach would only be apparent ones and of only minor significance.

	Antibody functionalized MC	Antigen functionalized MC
	0.001mg/mL human IgG (5 mins response) (V)	0.05mg/mL anti human IgG (5mins response) (V)
With Protein A	0.043	0.518
Without Protein A	0.126	0.321

Table Appendix-1. Comparison of the response of antibody and antigen functionalized MC on exposure to antigen/antibody with random (without Protein A) and oriented (with Protein A) functionalization.

Vita

Kasey Lauren Hill was born in Gainesville, GA on June 22nd, 1982. She was raised in Hoschton, GA. She graduated from Jackson County Comprehensive High School, Jefferson, GA in 2000. She then earned her B.S. in Chemistry in 2004 from North Georgia College and State University, Dahlonega, GA. In May 2010, Kasey will graduate with a Ph.D. in Analytical Chemistry. She will then begin a postdoctoral appointment at Pennington Biomedical Research Center in Baton Rouge, LA.